POTENTIAL ENVIRONMENTAL AND HEALTH RISKS FROM NANOPARTICLES AND III-V MATERIALS USED IN SEMICONDUCTOR MANUFACTURING

by

Chao Zeng

A Dissertation Submitted to the Faculty of the

DEPARTMENT OF CHEMICAL AND ENVIRONMENTAL ENGINEERING

In Partial Fulfillment of the Requirements

For the Degree of

DOCTOR OF PHILOSOPHY

WITH A MAJOR IN ENVIRONMENTAL ENGINEERING

In the Graduate College

THE UNIVERSITY OF ARIZONA

2017

THE UNIVERSITY OF ARIZONA

GRADUATE COLLEGE

As members of the Dissertation Committee, we certify that we have read the dissertation prepared by Chao Zeng, entitled *Potential Environmental and Health Risks from Nanoparticles and III-V Materials Used in Semiconductor Manufacturing,* and recommend that it be accepted as fulfilling the dissertation requirement for the Degree of Doctor of Philosophy.

_____ Date: (12/01/2016)

Reyes Sierra-Alvarez

_____ Date: (12/01/2016)

Farhang Shadman

_____ Date: (12/01/2016)

Jim A. Field

_____ Date: (12/01/2016)

Joan E. Curry

Final approval and acceptance of this dissertation is contingent upon the candidate's submission of the final copies of the dissertation to the Graduate College.

I hereby certify that I have read this dissertation prepared under my direction and recommend that it be accepted as fulfilling the dissertation requirement.

_____ Date: (12/01/2016)

Dissertation Director: Reyes Sierra-Alvarez

_____ Date: (12/01/2016)

Dissertation Director: Farhang Shadman

STATEMENT BY AUTHOR

This dissertation has been submitted in partial fulfillment of the requirements for an advanced degree at the University of Arizona and is deposited in the University Library to be made available to borrowers under rules of the Library.

Brief quotations from this dissertation are allowable without special permission, provided that an accurate acknowledgement of the source is made. Requests for permission for extended quotation from or reproduction of this manuscript in whole or in part may be granted by the head of the major department or the Dean of the Graduate College when in his or her judgment the proposed use of the material is in the interests of scholarship. In all other instances, however, permission must be obtained from the author.

SIGNED: Chao Zeng

ACKNOWLEGEMENTS

First I would like to express my deepest appreciation to my advisors: Prof. Reyes Sierra, Prof. Farhang Shadman and Prof. Jim Field. It has been an honor working with these professionals. The door to Prof. Sierra's office was always open whenever I ran into a trouble of my experiment or had questions about my research plan. I really appreciate her patience and persistent help. Prof. Field has the big picture of our research in mind while also pays attention to the details of each experiment. I've learnt a lot from him about research planning and scientific writing. Prof. Shadman is an expert in environmentally benign semiconductor manufacturing. He taught me a lot about how to correlate fundamental researches with applications and how to use our knowledge into practices. This dissertation would not have been possible without the guidance of my mentors.

I would also like to thank Prof. Joan E. Curry for being in my committee, I have learnt a lot in her classes. I am thankful to Prof. Scott Boitano for his training and support of my experiments using RTCA testing system.

I would like to acknowledge Dr. Lila Otero González for her guidance during my first year of this research. I would like to give my gratitude to Adrian Alvarez Gonzalez, Emily Orenstein and Chi H. Nguyen who have collaborated with some of my work and all my colleagues in our research group. They are all my friends and good teachers.

Finally, I would like to thank all my family and my special gratitude to my parents, Weiming Zeng and Juying Fan. No matter physically how far we are from each other, I never feel I am away from my family. We are and will always be together.

TABLE OF CONTENTS

LIST OF FIGURES

LIST OF TABLES

ABSTRACT

Nanoparticles (NPs) have unique electronic, optical and chemical properties due to the extreme small size. Engineered nanoparticles (ENPs) are intentionally produced for desired applications, with specific properties related to shape, size, surface properties and chemistry. Nano-sized silica (SiO_2), alumina (Al_2O_3) and ceria (CeO_2) are three important ENPs with large production and wide applications. One of the principal uses of these ENPs is in chemical and mechanical planarization (CMP), a key process applied to polish wafers when fabricating integrated circuits in semiconductor manufacturing, in which SiO_2, Al_2O_3 and CeO_2 NPs are used as abrasive particles in CMP slurries. CMP generates large amounts of waste effluents containing high levels of ENPs. Some ENPs have been proven to be able to cause toxicity to microorganisms and higher life forms, including humans. Therefore, there are concerns about the potential risks that ENPs may pose to the natural environment and human health. In addition, III-V materials like indium arsenide (InAs) and gallium arsenide (GaAs) are increasingly used in electronic and photovoltaic devices. Besides ENPs, the waste streams from III-V manufacturing also contain dissolved and particulate materials removed from III-V films during CMP. Arsenic is one of the most notorious contaminants that has been widely studied, while only very limited ecotoxicity information is available for gallium and indium. Finally, since ENPs have high surface area, it is very likely they will interact with the soluble species (such as arsenic ions) in CMP wastewater. Therefore, it is of great importance to understand whether the interactions between these materials could alter their fate and toxicity. The objective of this work is to investigate the potential environmental and health risks from the ENPs and III-V materials used in semiconductor manufacturing. To this end, the physical, chemical and toxicological characterization of ENPs used in CMP was performed (*Chapter 3*). Furthermore, the fate and transport of the most used ENP, SiO_2, in porous media was studied (*Chapter 4*). In addition, acute toxicity of As(III), As(V), In(III) and Ga(III) species was evaluated using different bioassays (*Chapter 5*). Finally, the cytotoxicity of ENPs used in CMP slurries to human lung bronchial epithelial cells was evaluated using an impedance based real time cell analysis (RTCA) assay (*Chapter 6*).

In *Chapter 3*, four model slurries containing ENPs including colloidal silica (c-SiO_2), fumed silica (f-SiO_2) cerium oxide (CeO_2) and aluminum oxide (Al_2O_3) were characterized for their physical, chemical and toxicological properties. Ecotoxicity of these slurries to the marine

bacterium, *Aliivibrio fischeri,* was evaluated by measuring its bioluminescence activity as a function of the ENP concentration dosed. The results showed that f-SiO_2 and CeO_2 were not toxic at concentrations up to 700 and 1000 mg/L, respectively. On the other hand, c-SiO_2 and Al_2O_3 were inhibitory only at very high concentrations (> 600 mg/L). At about 1300 mg/L, c-SiO_2 and Al_2O_3 led to 37.6% and 28.4% decrease of cell activity after 30 min exposure, respectively. The inhibitory effect from c-SiO_2 was related to additives in the slurry. In summary, the results indicate that these slurries are not likely to cause acute toxicity at environmentally relevant concentrations.

The potential risks from ENPs are dependent on their fate and transport in the environment. In *Chapter 4*, the transport and abatement of SiO_2 NPs was studied through laboratory scale column experiments. Synthetic fluorescent core-shell SiO_2 NPs (83 nm) were used to facilitate NP traceability. Three widely used filtering materials, *i.e.,* sand, anthracite and granular activated carbon (GAC), were used as porous media. Sand showed very poor capacity for the filtration of SiO_2 NPs due to its limited surface area and high concentration of negative surface charge. In addition, the stability and transport of SiO_2 NP was strongly dependent on the ionic strength of the solution. High ionic strength led to NP agglomeration and facilitated SiO_2 NP retention, while low ionic strength resulted in release of captured NPs from the sand bed. Compared to sand, anthracite and GAC showed higher efficiency for SiO_2 NP capture. The superior capacity of GAC was primarily due to its porous structure and high surface area. A process model was developed to simulate NP capture in the packed bed columns and determine fundamental attraction parameters. This model provided an excellent fit to the experimental data. Taken together the results obtained indicate that GAC is an interesting material for SiO_2 NPs filtration.

With the increasing usage of III-V materials, there are concerns about the ecological threats posed by III-V ions released during semiconductor manufacturing and from disposal of decommissioned electronic devices. In *Chapter 5*, the acute toxicity of As(III), As(V), In(III) and Ga(III) species was evaluated using different bioassays, including three microbial assays, testing for methanogenic activity, O_2 uptake and bioluminescence inhibition of marine bacterium *A. fischeri*. Acute toxicity to the freshwater crustacean *Daphnia magna* was also tested. The results showed that In(III) and Ga(III) were generally not toxic or only mildly toxic in all assays, while both As(III) and As(V) showed strong inhibitory effects on different microbial activities (methanogenic and bioluminescence). The toxicity of these ions was strongly dependent on the bioassay target. For In(III) and Ga(III), *D. magna* was the most sensitive organism with 50% lethal

concentrations (LC_{50}) of 57.4 and 237.0 mg/L, respectively. On the other hand, As(III) and As(V) were particularly toxic to methanogens. The 50% inhibitory concentrations (IC_{50}) of both species were about 1.5mg/L. Mixed aerobic heterotrophic culture was highly resistant to all four ions and O_2 uptake by the aerobes was not affected in the tested concentrations. Overall, the results indicate that the ecotoxicity of In(III) and Ga(III) is much lower than that of the As species. This finding is important in filling the knowledge gap regarding the ecotoxicology of In and Ga.

Besides ecotoxicity, ENPs and III-V materials in CMP effluents could also pose a threat to human health. In *Chapter 6,* the cytotoxicity of CMP slurries to human bronchial epithelial cells (16HBE14o-) was assessed using a novel impedance based real time cell analyzer (RTCA). Cell death and detachment was observed in assays supplied with high concentrations of c-SiO_2 and f-SiO_2 NPs ($\geq$ 250 mg/L). On the other hand, CeO_2 and Al_2O_3 slurries were not inhibitory at concentrations up to 1250 mg/L. In addition, since CMP wastewater generated during the planarization of III-V films contains a mixture of ENPs and soluble III-V species, it is important to understand whether the interactions between these materials could alter their fate and toxicity. As(III) toxicity to human lung cells in the presence and absence of CeO_2 NPs was evaluated using the RTCA assay. Exposure to As(III) (0.5 mg/L) for 48 h resulted in 81.3% inhibition of cell viability and proliferation, while cell inhibition decreased to only 13.0% when As(III) was dosed together with sub-toxic levels of CeO_2 NPs (250 mg/L). This detoxification effect was mainly due to As(III) adsorption onto CeO_2 NPs. When the NPs were added, the soluble arsenic concentration was reduced significantly from 0.5 mg/L to 0.03 mg/L. This work demonstrates that adsorption of As(III) on CeO_2 NPs can lower As(III) concentration in the solution and reduce its bioavailability and subsequently result in As(III) detoxification.

In conclusion, this dissertation indicates that the ENPs (SiO_2, CeO_2 and Al_2O_3) used in semiconductor industry are not expected to cause acute toxicity to the natural environment and human health under environmentally relevant concentration (< 1 mg/L). Among the soluble III-V species, In(III) and Ga(III) showed no or mild acute inhibitory effects in different bioassays even at comparatively high concentration. However arsenic species are highly toxic to various important microbial populations in the environment and human cells. The results showed that arsenic could induce toxic effects under current discharge limit set for semiconductor industry. Finally, we demonstrated that the adsorption of As(III) on CeO_2 NPs can lower the concentration of soluble As(III) and subsequently resulted in As(III) detoxification.

CHAPTER 1 INTRODUCTION

1.1 Engineered nanoparticles

1.1.1 Definition and applications of engineered nanoparticles

Nanomaterials (NMs) are defined as materials with one dimension less than 100 nm. Within this group of materials, nanoparticles (NPs) are materials with at least two dimensions between 1 to 100 nm [1]. NPs are normally classified into different categories including carbonaceous NPs (fullerene, carbon nanotubes), zero-valent metals (Fe^0, Ag^0), metal oxides (TiO_2, Fe_2O_3, Al_2O_3, CeO_2), quantum dots (QD) and organic polymers. Because of the extreme small sizes, NPs have very high surface to volume ratio, which results in significantly enhanced reactivity. Therefore, NMs have unique electronic, optical and chemical properties compared to their bulk counterpart with same composition [1, 2]. Due to these novel characteristics, different NPs are intentionally produced for desired applications, which are known as engineered NPs (ENPs). So far ENPs have been developed for biological (biological labels, drug delivery), environmental (contaminant remediation) and industrial (heat transfer, food industry, personal care products) applications [3, 4]. As reported, the global production of ENPs is estimated to be more than 10^7 tons per year [5]. Now there are more than 1300 commercial products containing ENPs are available in market and this number is constantly increasing [4].

Nano-sized silica (SiO_2), alumina (Al_2O_3) and ceria (CeO_2) are three important ENPs. The global production of SiO_2, Al_2O_3 and CeO_2 NPs has been estimated to be from 35000 to >200000, 7500 to <10000, and 82500 to >2400000 metric tons per year, respectively [5, 6]. These NPs are used in a variety of applications. For example, SiO_2 is used in cosmetics, printer toners, construction materials biomedical imaging and drug delivery; Al_2O_3 is used in production of tires, paper, catalyst, polymers and personal care products; CeO_2 is used in catalyst, fuel additives and medical applications. In addition, one primary application of these ENPs is chemical and mechanical planarization (CMP), which is covered in the latter sections.

1.1.2 Environmental fate of ENPs

Wastewater treatment plants (WWTPs) play an important role in controlling the release of ENPs to aquatic or terrestrial environments. A WWTP normally contains the following treatment processes: preliminary treatment (bar screens, grit chamber) is a step designed to remove coarse materials and grit; primary treatment (sedimentation tanks) uses simple mechanical and physical processes to achieve partial removal of suspended solids and organic matter; secondary treatment (activated sludge, trickling filter) uses biological processes to substantially degrade organic matters; tertiary treatment (granular or membrane filtration, disinfection) is designed to further improve the effluent quality before it is discharged to the receiving environment.

Among these steps, secondary treatment processes play an important role in NP removal. Gómez-Rivera et al. [7] reported 96.7% of total CeO_2 NP was removed in lab-scale activated sludge treatment. Westerhoff et al. [8] studied the fate of TiO_2 NP in 10 full-scale municipal WWTPs and found biological treatment processes were significant in trapping NPs in biomass, which can then be removed through sedimentation or via filtration. ENPs can also be removed during filtration processes applied in the tertiary treatment. Novel microfiltration and nanofiltration systems have shown some promising results in ENP treatment [8, 9]. On other hand, studies have also shown conventional granular media filtration could be used as cost-effective method for ENP treatment [10]. So far different porous media (e.g. sand, glass beads, granular activated carbon, diatomaceous earth) have been used to study their capacity on ENP retention [10-13]. These studies show the removal efficiency is highly related to the physiochemical properties of the NPs and porous media; aqueous conditions like pH, ionic strength also play an important role in NP transport.

Even though the majority of ENPs can be removed in WWTPs, they are not enough for preventing the release of a range of ENPs into the environment. Soil systems is very important in controlling the fate of ENPs released into the environment as it is a distinguished system with the presence of a heterogeneous mixture of gas, liquid and solid phases. Therefore, soil system can receive ENPs in the forms of waste gas, discharged water and solid residues [14]. Obviously, soil is one of the most common porous media. As a result, understanding the transport of ENPs in porous media is also important in predicting their fate in the natural environment [15].

1.1.3 Toxicity of ENPs

The continuously growing market and expanding application of ENPs has also raised concerns about their potential health and environmental risks. So far lot of work has been done to study their toxic effects using different assays. Studies show there are several common mechanisms are responsible for toxicity induced by NPs (Fig. 1-1). Firstly, dissolution of toxic ions is an important factor lead to toxicity from some metal oxides like ZnO, and AgO. The toxicity of these NPs is mainly due to the release of highly toxic Zn^{2+} and Ag^{+} cations under environmental and biological conditions favor NP dissolution [16-18]. Another mechanism that can lead to nanotoxicity is oxidative stress resulting from reactive oxygen species (ROS). In biological systems, cells can generate ROS when they are exposed to environmental stress. NPs, as foreign materials, have large surface area and high reactivity, therefore they are believed to be able to induce considerable ROS species such as superoxide anion, hydroxyl radical and hydrogen peroxide [19]. Most cells can neutralize a certain amount of ROS through glutathione redox system, however, when their concentration becomes too high the defense system will be overwhelmed and lead to various negative effects such as cell and DNA damage [19-21]. So far a lot of studies have shown a wide range of ENPs (including fullerenes, carbon nanotubes and metal oxides) are capable of induce ROS [22-26]. Therefore, oxidative stress is recognized as one of the most important mechanisms causing nanotoxicity. Finally, ENPs can also cause toxic effects by other mechanisms such as alterations of cellular morphology, disruption of cell membranes, lipid peroxidation and genotoxicity [19, 20, 27].

After their release, ENPs can be exposed to the environment and human beings, therefore, there is an urgent need to understand their ecotoxicity and effects on human beings. Ecotoxicity form ENPs has been widely investigated. Studies show different ENPs are toxic to bacteria (Gram positive and Gram negative), aquatic and marine organisms (both unicellular and animals like fish), plants and mammals [1, 2, 18, 28]. Effect of NPs on human health has been evaluated through different *in vitro* and *in vivo* studies [29, 30] and some of these materials (like NiO NP and asbestos) are proven carcinogens. Fig. 1-2 summarizes the affected organs and associated diseases related to human exposure to NPs. The respiratory system is one of the main entries that can provide access to NPs into human body. NPs can also gain access into body through skin. For example, TiO_2 NPs are often used in sunscreens, they may enter body through hair follicles and wounds

[31]. In addition, NPs can gain access into body through ingestion directly or indirectly (by consuming plants or animals have accumulated NPs). More importantly, NPs seem to be able to translocate and access to different organs once have entered the body [20]. Therefore, there are studies focusing on NP bioaccumulation and toxicity to certain organs (liver, spleen, kidney). From the known mechanism of toxicity at cellular level one can speculate the possible damage NPs could cause in certain parts of the body, but the full mechanisms for in vivo toxicity are not clear and need further investigation [30].

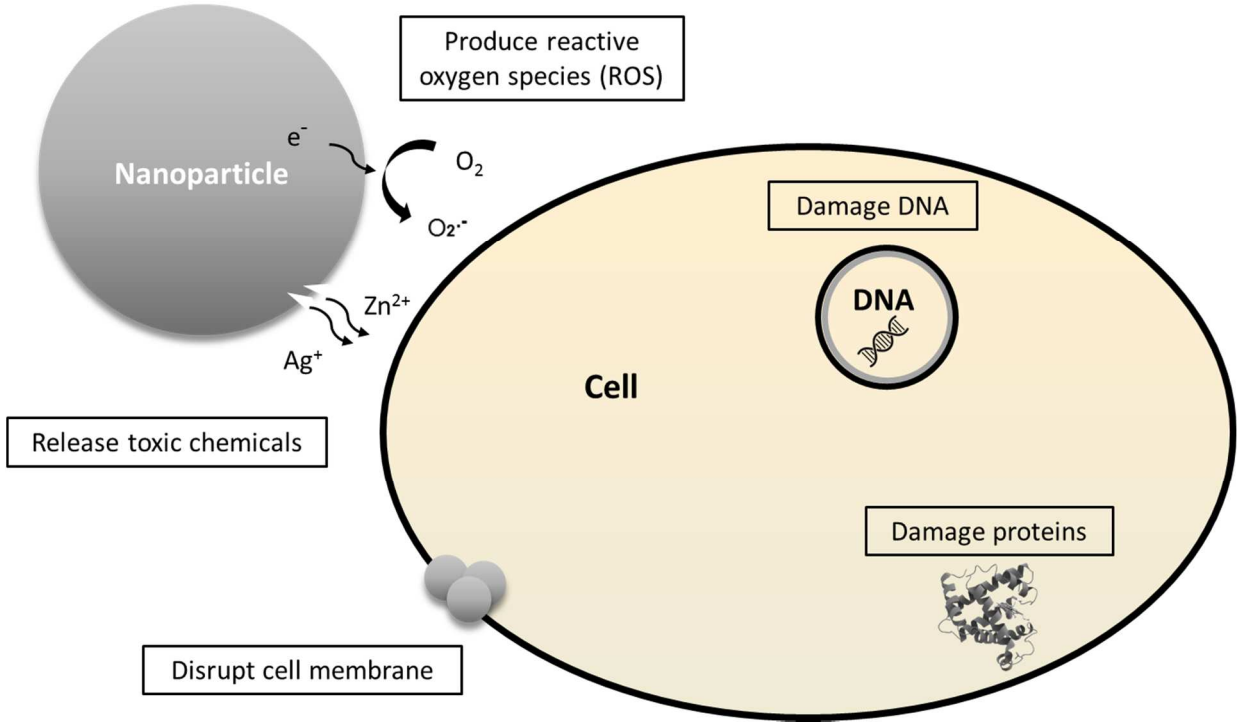

Fig. 1-1. Possible mechanisms that are responsible from toxicity induced by nanoparticles.

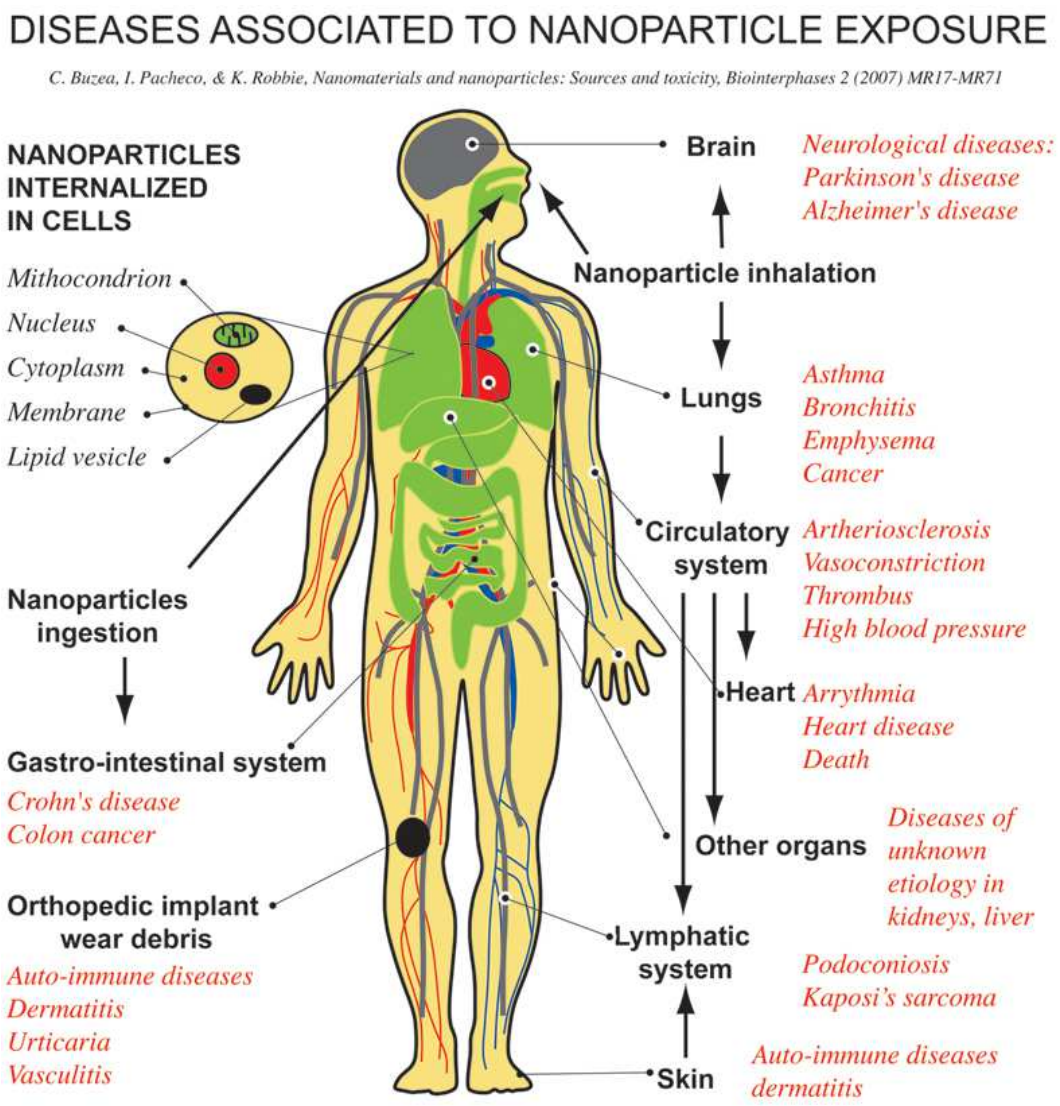

Fig. 1-2. Schematics of the pathways of nanoparticles to human body, the affected organs and associated diseases [29].

1.2 Potential environmental and health risks from semiconductor industry

1.2.1 Application and toxicological effects of III-V materials

III-V compounds such as gallium arsenide (GaAs), indium arsenide (InAs) and indium phosphide (InP) are a group of materials commonly used in semiconductor industry. These materials exhibit many interesting electrical and optical properties like high electron mobility, low power

requirement and promising thermoelectric power generation [32-34]. Because of these novel properties, III-V materials are used in a variety of applications, including light emitting diodes, laser diodes, solar cells, biosensors and microcircuits [35, 36]. GaAs is the second most common semiconductor material widely used in microelectronics [37]. Compared to silicon, GaAs has wider band gap and the electron mobility is about 6 times higher than that of silicon [38]. InAs is another III-V compound used in a wide variety of electronic and optoelectronic devices. It has been reported that the demand for Ga and In has increased significantly during the past 30 years [39, 40]. The world primary production of Ga in 2014, estimated at 440 metric tons, was four times higher than in 2010 [41]. On the other hand, In is under the label of near critical elements by U.S. Department of Energy due to its increasing usage in LCD televisions and for smartphones [42].

The extensive application of III-V materials may contribute to the release of hazardous material from manufacturing activities or through corrosion of decommissioned electronic devices. Arsenic is one of the most notorious contaminants and a well known carcinogen. Studies show As toxicity is closely related to its species. Generally speaking, inorganic As species are more toxic than organic forms to living organisms [43-45]; also, trivalent arsenic is more inhibitory than pentavalent arsenic. The toxicity of As(III) is related to its high affinity for sulfhydryl groups of biomolecules [46]. The formation of these bonds leads to inhibition of crucial enzymatic functions within the cells [44]. On the other hand, As(V) toxicity is the result of its potential for phosphate replacement. Consequently, it inhibits enzymes that use phosphate and uncouples ATP formation, ultimately results in depleting of cell energy [47]. Compared with arsenic, there is much less available information about gallium and indium toxicity. So far most of the studies have focused on their hazardous effects on human health due to occupational exposure to particulate Ga and In containing materials [48-51]. For example, Cummings et. al studied occupational exposure to In compounds was associated with different lung diseases such as pulmonary alveolar proteinosis. Only very limited number of studies have evaluated their ecotoxicity [52-54].

Solubility is an important factor that could affect the ecotoxicity of In and Ga. Fig. 1-3 and Fig. 1-4 show the solubility of Ga and In under different pH, based on thermodynamic calculations [55]. Ga are soluble under acidic and basic conditions, while it has the lowest solubility at pH around 4.2. The theoretical solubility at neutral pH (6-8) is about 70 μg/L. As for In, the predominant species under natural pH is $In(OH)_3$ (solubility constant, $K_{sp} = 1.3 \times 10^{-34}$) [40]. Theoretically, only about 10 μg/L of In is soluble under this condition. From these theoretical

prediction, In and Ga would be insoluble in the most natural and biological conditions. This could have a large impact on their transport and bioavailability. During metal processing or semiconductor manufacturing, chelating agents (e.g. citrate) are used to complex with Ga and In and keep them soluble in the aqueous phase [56].

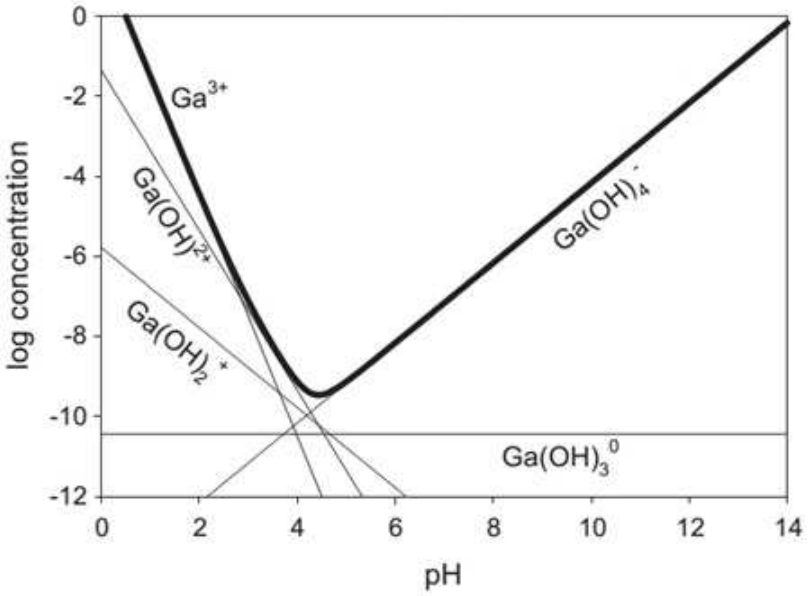

Fig. 1-3. Gallium solubility (in mole/L) in respect with pH at 25°C [55].

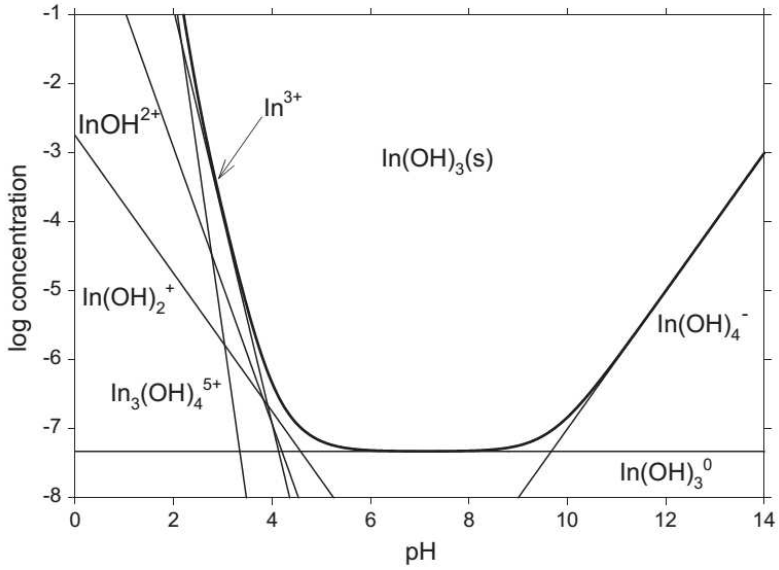

Fig. 1-4. Indium solubility (in mole/L) in respect with pH at 25°C [55].

1.2.2 Potential risks from III-V materials and ENPs used in semiconductor manufacturing

A principal use of ENPs is chemical and mechanical planarization (CMP), a key process applied to polish wafers when fabricating integrated circuits in semiconductor manufacturing [57-60]. Fig. 1-5 shows a scheme of typical CMP process. This process is applied to remove unwanted materials on wafers and create a flat and smooth surface on which integrated circuitry layers are built. As the name implies, in this process, the removal of excess materials and surface planarization is accomplished by synergistic combination of chemical and mechanical actions. SiO_2, Al_2O_3 and CeO_2 NPs (particle size from 20 to 200 nm) are used as abrasive particles in CMP slurries [61]. It has been reported ENPs used for semiconductor manufacturing accounted for 60% of the $1 billion market for nanomaterials in 2005 [62]. CMP slurries also contains other additives like buffers, complexing agents, oxidizers, corrosion inhibitors and surface active organics [57, 58, 63].

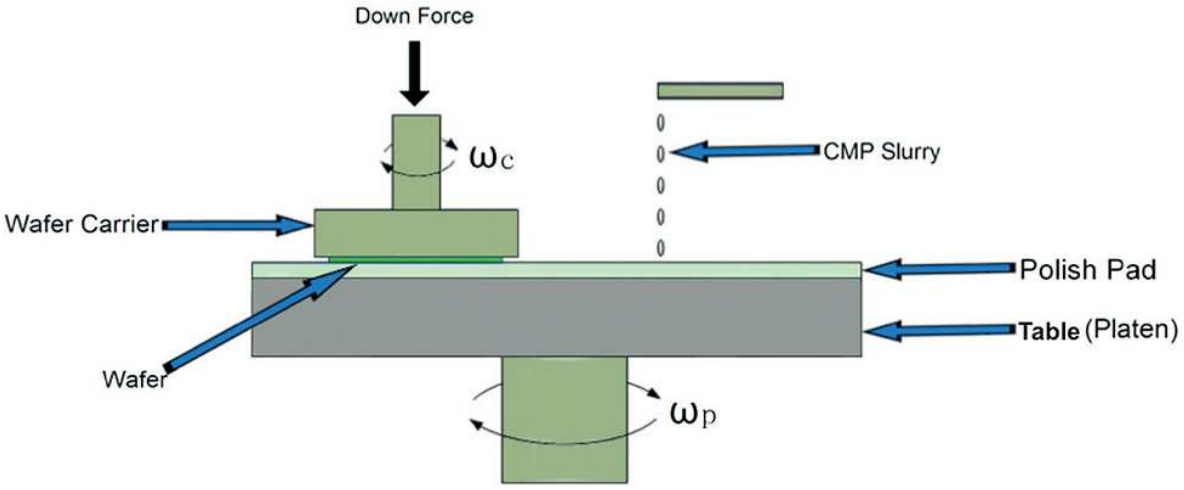

Fig. 1-5. Operation of chemical and mechanical planarization [60].

Semiconductor industry is a "thirsty" business that requires huge amount of water and ultra-pure water. Consequently, it is also an industry could generate high volumes of wastes. A typical wafer production step may cost 0.2 to 0.8 L of CMP slurry, 1 to 2 L rinse water as well as more than 5 L of pad cleaner and rinse water during its production [60]. The total quantity of wastewater generated in CMP process is estimated in the order of 10 L or more per wafer [60]. The waste stream from CMP contains original slurry, dissolved and particulate materials removed from the wafer during this process.

The concentrations of ENPs in CMP wastewater are estimated in the range from 50 mg/L to 8.5 g/L [64, 65]. Although some regulations regulated water qualities (such as turbidity, total suspended solids) can reduce the release of CMP NPs, there are no regulations specifically about the discharges of these NPs generated from semiconductor industry. Therefore, there are concerns about if these NPs could impose threats to the natural environment and human health. High levels of arsenic and other hazardous materials in the waste stream require treatment prior the discharge to meet the regulations. In the United States, the arsenic discharge limits for effluents produced by facilities manufacturing electronic components are 2.09 mg/L as one-day maximum and 0.83 mg/L as 30-day average concentration [66]. However, there have no current regulatory limits for In and Ga discharge. So there is a need to understand their potential health and environmental risks.

The wastewater from CMP process contains both III-V ions and ENPs (which have high surface area and reactivity). Therefore, interactions between these materials will occur in CMP waste stream, which could change their surface property, and subsequently affect their fate and toxicity. Adsorption of III-V ions on CMP NPs could alter their toxicity in different ways as shown in Fig. 1-6. On one hand, it could lower the toxicity of soluble toxicants. For example, both CeO_2 and Al_2O_3 NPs have high affinity for As adsorption [67, 68]. This process could significantly reduce the concentration of soluble (or bioavailable) As species and consequently led to detoxification effects. On the other hand, it is also possible that the interaction between CMP NPs and III-V ions could enhance their toxic effects based on two mechanisms. It is known that some NPs could act as "Trojan horse", which facilitate the transport of adsorbed materials into cells, the following release of toxicant could then result in cytotoxicity. Hu et al. [69] verified the accumulation of As(V) on Fe_2O_3 and Al_2O_3 NPs and the uptake of these transformed NPs could significantly enhance the toxicity of As(V). In summary, in order to understand the potential environment and health risks from semiconductor industry, we should not only consider the toxicity from CMP NPs or III-V materials themselves, but also the interactions between these materials.

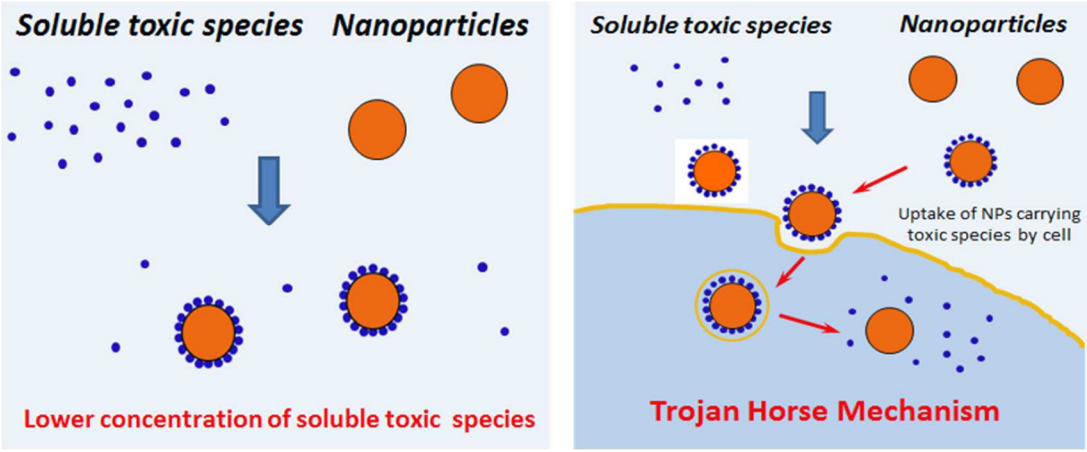

Fig. 1-6. Adoption of III-V ions onto nanoparticles that could alters their properties.

1.3 Acronym list

ζ potential	Zeta-potential
APTES	(3-Aminopropyl) triethoxysilane
As	Arsenic
CFB	Collagen/fibronectin/bovine serum albumin
CGM	Controlled growth medium
CI	Cell index
CMP	Chemical and mechanical planarization
DI water	Deionized water
DLS	Dynamic light scattering
DLVO	Derjaguin-Landau-Verwey-Overbeek
DOC	Dissolved organic carbon
EDL	Electrical double layer
ENMs	Engineered nanomaterials
ENPs	Engineered nanoparticles
EPA	Environmental Protection Agency

Ga	Gallium
GaAs	Gallium arsenide
GAC	Granular activated carbon
GaInAs	Gallium indium arsenide
IC_{20}	20% inhibition concentration
IC_{50}	50% inhibition concentration
IC_{80}	80% inhibition concentration
ICP-OES	Inductively coupled plasma-optical emission spectroscopy
IEP	Isoelectric point
In	Indium
InAs	Indium arsenide
ISO	International Organization for Standardization
LC_{20}	20% lethal concentration
LC_{50}	50% lethal concentration
LC_{80}	80% lethal concentration
LCD	Liquid crystal displays

LED	Light emitting diodes
MEM	Minimum essential medium
NCI	Normalized cell index
NM	Nanomaterial
NP	Nanoparticle
OAS	Osmotic adjusting solution
OECD	Organization for Economic Co-operation and Development
PSD	Particle size distribution
PV	Pore volume
QD	Quantum dots
RAS	Return activated sludge
ROS	Reactive oxygen species
RTCA	Real time cell analyzer
SEM	Scanning electron microscopy
TEM	Transmission electron microscopy
TOC	Total organic carbon

WWTP	Wastewater treatment plant

CHAPTER 2 OBJECTIVES

2.1 Aim

The objectives of this research were to investigate the physicochemical and toxicological characteristics of engineered nanoparticles used in semiconductor manufacturing and evaluate the potential health and environmental risk from III-V semiconductor materials. Furthermore, the interaction between CMP nanoparticles and III-V ions and its effect on their toxicity was also studied in this work.

2.1.1 Specific objectives

1. To investigate the physical, chemical and *in vitro* toxicological properties of SiO_2, CeO_2 and Al_2O_3 NPs using model CMP slurries.

2. To study the transport and abatement of SiO_2 NPs in different porous media including sand, anthracite and granular activated carbon (GAC).

3. To assess the ecotoxicity of ionic As(III), As(V), Ga(III) and In(III) species potentially released from III-V semiconductor materials, using different bioassays.

4. To investigate the cytotoxicity of SiO_2, CeO_2 and Al_2O_3 ENPs used in CMP slurry to human lung cells using the RTCA system.

5. To investigate the adsorption of As(III) onto CeO_2 NPs and its effect on As(III) toxicity to human lung cells using the RTCA system.

CHAPTER 3 PHYSICAL, CHEMICAL AND *IN VITRO* TOXICOLOGICAL CHARACTERIZATION OF NANOPARTICLES USED IN CHEMICAL AND MECHANICAL PLANARIZATION

3.1 Abstract

The physical, chemical and toxicological characterization of engineered nanoparticles (ENPs) used in chemical mechanical planarization (CMP) was investigated. Model slurries containing colloidal silica (c-SiO_2), fumed silica (f-SiO_2) cerium oxide (CeO_2) and aluminum oxide (Al_2O_3) obtained from a commercial CMP vendor were tested for their concentration, particle size and zeta-potential. Their effect on bioluminescence activity of *Aliivibrio fischeri* was also evaluated. These ENPs were stable in the suspension with high positive of negative zeta potentials at the working pH. The hydrodynamic diameters measured by dynamic light scattering were 46.0 ± 0.2 nm, 168.1 ± 3.5 nm, 132.0 ± 0.1 nm and 124.6 ± 2.3 nm for c-SiO_2, f-SiO_2, CeO_2 and Al_2O_3, respectively. These NPs were not or only mildly toxic to *A. fischeri*: f-SiO_2 and CeO_2 were not toxic at concentrations up to 700 and 1000 mg/L, respectively; c-SiO_2 and Al_2O_3 were inhibitory only at very high concentration (> 600 mg/L). At about 1300 mg/L, c-SiO_2 and Al_2O_3 led to 37.6% and 28.4% inhibition on cell activity after 30 min exposure, respectively. Inhibitory effect from c-SiO_2 was found related to the additives used in the suspension. In addition, the stability of ENP suspensions in the bioassay medium was evaluated by measuring their particle size and ζ-potential. The results show the ENPs were not stable in the testing medium, especially for CeO_2 and Al_2O_3, particle aggregation and sedimentation was observed. After 30 min, only 6.5% and 15.4% of total CeO_2 and Al_2O_3 were remained in the suspension, which may lower their bioavailability and toxicity. In summary, the results show these ENPs are not likely to cause acute toxicity at relevant concentrations in the environment.

This chapter has been published.
D. Speed, P. Westerhoff, R. Sierra-Alvarez, R. Draper, P. Pantano, S. Aravamudhan, K.L. Chen, K. Hristovski, P. Herckes, X.Y. Bi, Y. Yang, C. Zeng, L. Otero-Gonzalez, C. Mikoryak, B.A. Wilson, K. Kosaraju, M. Tarannum, S. Crawford, P. Yi, X.T. Liu, S.V. Babu, M. Moinpour, J. Ranville, M. Montano, C. Corredor, J. Posner, F. Shadman, Physical, chemical, and in vitro toxicological characterization of nanoparticles in chemical mechanical planarization suspensions used in the semiconductor industry: towards environmental health and safety assessments, Environ Sci-Nano 2 (2015) 227-244.

3.2 Introduction

Chemical mechanical planarization (CMP) was first invented in IBM in the early 1980s for achieving desired performance goals of modern microprocessor and memory chips [59]. Since then it has become one of the most important semiconductor processes applied to planarize a variety of materials. As the name indicates, in CMP process, the removal of materials and planarization is accomplished by synergistic combination of chemical and mechanical actions with slurries containing different chemical reagents and abrasives [58, 59]. Engineered nanoparticles (ENPs) such as silica (SiO_2), ceria (CeO_2) and alumina (Al_2O_3) with the size of 50 -200 nm are commonly used as abrasives in CMP [58, 59, 70-73]. It has been reported that CMP processes may account for 40% of ultrapure water consumption in semiconductor manufacturing plant and, consequently, large amount of wastewater would be generated [65]. CMP wastewater typically contains high concentrations (50-500 mg/L) of particles [3]. There are some regulations controlling wastewater discharge for semiconductor industry, such as turbidity and total suspended solids, could reduce the release of CMP NPs. However, so far, there are no regulations specifically about these NPs generated from semiconductor industry. Compared with their bulk counterparts, the extremely small size gives NPs unique properties that could not only favors their applications but also induce novel toxic effects [21, 64]. Therefore, there are concerns about the release of these NPs and their potential risks towards natural environment and human health.

SiO_2, CeO_2 and Al_2O_3 NPs are generally believed to be comparatively innocuous, but their toxicity is largely depending on the specific toxicity assay being used (e.g. exposure time, organism used and end point of toxic effect) [74-82]. Toxicity from NPs is also closely related to their own characterization such as particle size and dispersion state [83]. For example, NPs with smaller particles size would facilitate their transport in environmental and biological systems; also, there are studies show NPs with small particle size are more likely to induce the productions of reactive oxygen species (ROS) and cause toxic effects [84]. Therefore, in order to understand the fate and potential environmental risks from CMP NPs it is of great importance to understand their physical and chemical characterization.

In this study, the physical, chemical and toxicological properties of ENPs in CMP suspensions were characterized. Four models slurries including colloidal silica (c-SiO_2), fumed silica (f-SiO_2) cerium oxide (CeO_2) and aluminum oxide (Al_2O_3) were acquired from a major

commercial slurry manufacturer [60]. The concentration, particle size distribution and zeta-potential (ζ-potential) of these ENPs were determined. One bioassay was performed to evaluate their ecotoxicity, in which inhibition of bioluminescence activity in the marine bacterium, *Aliivibrio fischeri* (formerly known as *Vibrio fischeri*) was tested. The Microtox acute toxicity assay is widely used by municipalities and industries worldwide as standard methods to test the toxicity of chemicals and effluent streams, and both methods are accepted by organizations such as the U.S. Environmental Protection Agency (U.S. EPA), the Organization for Economic Co-operation and Development (OECD), and the International Organization for Standardization (ISO).

3.3 Materials and methods

3.3.1 CMP slurries

Four industry relevant model slurries, including c-SiO_2, f-SiO_2, CeO_2 and Al_2O_3 were used in this study. According to the manufacturer, these slurries are with the simplest formulation to generate a stable suspension of ENPs. c-SiO_2 and f-SiO_2 slurries were prepared in acetic acid and potassium hydroxide; there is no additives reported for CeO_2 slurry; Al_2O_3 slurry was provided with dilute nitric acid. Other key characteristics reported by the manufacturer are summarized in Table 3-1.

3.3.2 Particle size and zeta potential measurements

The particle size distribution (PSD) and ζ-potential measurements were performed using a ZetaSizer Nano ZS (Malvern, Inc., Sirouthborough, MA, USA). Dynamic light scattering (DLS) method was applied for PSD measurements; ζ-potential was determined using Smoluchowski equation. In this study, the refractive index values applied for SiO_2, CeO_2 and Al_2O_3 were 1.47, 1.83 and 1.76, respectively.

3.3.3 Si, Al, Ce concentration measurements

All samples (1 mL) were first digested with 10 mL different solutions with one microwave assisted digestion system (MARS 5, CEM Corporation, Matthews, NC, USA). SiO_2 samples were digested

using 1% HF (10 mL); Al_2O_3 with 3.7% HCl (10 mL); CeO_2 with 70% HNO_3 (8 mL) and 30-32% H_2O_2 (2 mL). Al_2O_3 and CeO_2 were digested 30 min at 151°C (25 min ramp time) with a power level of 1600 W. SiO_2 samples were digested at 120°C for 45 min (25 min ramp time). After digestion, the samples were diluted with DI water and then HNO_3 (2% v/v) solution was added to acidify the samples. The concentration of Si, Al and Ce species was determined by inductively coupled plasma optical emission spectroscopy (ICP-OES, Optima 2100 DV, Perkin-Elmer, Waltham, MA, USA) at a wave length of 251.611, 396.153 and 413.764 nm, respectively.

3.3.4 Additives and pH determination

Nitrate (NO_3^-) and nitrite (NO_2^-) were determined using suppressed conductivity ion chromatography with a Dionex IC-3000 system (Sunnyvale, CA, USA) fitted with a Dionex IonPac AS18 analytical column (4 × 250 mm) and an AG18 guard column (4 × 50 mm). During each run, the eluent (KOH, 15 mM) was used for 20 min.

Dissolved organic carbon (DOC) was analyzed by a Shimadzu TOC-VCSH TOC analyzer. Before measurement, the aqueous samples were first filtered through 0.025 μm membrane filters (Millipore).

Potassium was measured by ICP-OES at a wavelength of 766.490 nm.

The pH values of the samples were determined by a VWR SB20 pH meter.

3.3.5 Microtox acute toxicity test

Microtox is an *in vitro*, metabolic inhibition test system uses a strain of naturally luminescent marine bacterium named *A. fischeri* that produce light as byproduct of cellular respiration. These bacteria are very sensitive to a wide range of different toxins, and the toxicity of certain toxicant can be recognized by the loss of luminescence level that results from cellular activity inhibition.

In this study, Microtox M500 analyzer was used to conduct the experiment. Microtox reagent (*A. fischeri*) was purchased from Modern Water Inc. (Guildford, UK). Microtox diluent and osmotic adjusting solution (OAS) were purchased from Strategic Diagnostics Inc. (Newark, DE USA). Stock solutions were prepared using DI water to about 3 g/L as SiO_2, CeO_2 or Al_2O_3. Dilute NaOH and HCl solutions were used to adjust pH to neutral range (about 7.0), as the bacteria

reagent is sensitive to pH. In the experiment, the stock solution was first mixed with OAS (10:1, v/v) for maintaining the osmotic pressure of the sample. Then the solution was diluted to different concentrations with Microtox diluent. The light levels were tested at 0, 5, 15 and 30 min. All tests were performed in duplicate.

In the Microtox test, the parameter gamma (Γ_t), the radio of the light loss to the remaining light level at time *t* is commonly used for data processing. The value of light loss is achieved by the following equations [85]:

$$\Gamma_t = \frac{Corrected\ Light\ Loss}{Remaining\ Light\ Level} = \frac{R_t \cdot I_0 - I_t}{I_t} = \frac{R_t \cdot I_0}{I_t} - 1 \qquad (3-1)$$

$$R_t = \frac{C_t}{C_0} \qquad (3-2)$$

where: R_t is the light output ratio of negative control at time *t* (C_t) to the value at time *0* (C_0). It is used to correct and normalize the light variation in the test. I_0 and I_t are the light levels of the samples at time *0* and time *t*. Percent inhibition and activity can be derived by the following equations:

$$Inhibition\ (\%) = \frac{Light\ Loss}{Light\ Loss + Ramaining\ light} = \frac{\Gamma_t \cdot I_t}{\Gamma_t \cdot I_t + I_t} \times 100 = \frac{\Gamma_t}{\Gamma_t + 1} \times 100 \qquad (3-3)$$

$$Activity\ (\%) = (1 - Inhibition\%) \times 100 = \left(1 - \frac{\Gamma_t}{\Gamma_t + 1}\right) \times 100 = \frac{1}{\Gamma_t + 1} \times 100 \qquad (3-4)$$

The stability of CMP ENPs in Microtox medium was evaluated. Stock solutions were first prepared using the same method described previously in this section. The solutions were then mixed with Microtox diluent (1:1, v/v). Well mixed dispersions were taken and analyzed for PSD, ζ-potential and the concentration of corresponding element. After 30 min, the supernatants of the samples were also collected for the same measurement.

The toxicity of soluble compounds in the slurry was also tested in order to understand the source of toxicity. Suspended particles were first removed by ultrafiltration (30 kDa), and then the supernatants were used for Microtox test.

3.4 Results and discussion

3.4.1 CMP slurry physical and chemical characterization

CMP slurry concentration, particle size and pH values were summarized in Table 3-1. Firstly, the pH values determined were generally within the range of reported values. Secondly, the concentration of nanoparticles in the as-received slurries ranged from 9.6 to 50 g/L, which is in agreement with the data reported by the manufacturer 1 to 5% (wt%). Thirdly, the particle size distribution of slurries diluted 10 times with DI water was analyzed by DLS. In the four slurries, c-SiO_2 had the smallest diameter while f-SiO_2 had the largest particle size. The hydrodynamic diameter of these ENPs through DLS was larger compared the size determined for the primary particles through electron microscopy (Table 3-1). For example, DLS size of f-SiO_2 was about 4 times higher than that determined by SEM. Hydrodynamic diameter is only applicable to particles in dispersion or molecules in solution; it is defined as the size of a hypothetical sphere that diffuses in the same fashion as the particle being measured. In practice, particles in solution are not necessarily spherical, surface hydration or particle aggregation could also happen. Therefore, the measured DLS size was higher than the primary size of these ENPs. Finally, surface charge is a critical factor controlling the stability of NP dispersions. The ζ-potential values of c-SiO_2, f-SiO_2, CeO_2 and Al_2O_3 were -17.1 ± 0.1, -51.9 ± 2.6, 37.5 ± 1.2 and 59.7 ± 1.4 mV, respectively. NPs with ζ potentials higher than +30 mV or lower than -30 mV are typically considered very stable, therefore, the results indicate the NPs were well dispersed in the slurry, with the only exception of c-SiO_2 NPs. This result is not surprising as SiO_2 particles typically have an isoelectric point (IEP) of 2-3.5 [86]. Since the pH of the c-SiO_2 slurry (3.3) is close to the concentrations of the IEP, it is conceivable that SiO_2 NP has lower surface charge.

The concentrations of slurry additives were summarized in Table 3-2. The results indicate our data is generally in agreement with that reported by the manufacturer.

Table 3-1 Summary of slurry pH, particle size and the concentration of corresponding NPs.

slurry name	pH		particle size (d. nm)		nano-oxide concentration (g/L)	
	reported	tested	reported[a]	tested	reported	tested
c-SiO_2	2.5-4.5	3.3	37 ± 7	37.4 ± 0.5	30.0	27.5 ± 0.4
f-SiO_2	10.0	10.6	38 ± 14	168.1 ± 3.5	50.0	47.6 ± 0.4
CeO_2	3.0-4.0	4.0	43 ± 16	89.4 ± 1.4	10.0	7.9 ± 0.3
Al_2O_3	4.5-5.0	4.2	85 ± 21	124.6 ± 2.3	30.0	29.6 ± 0.5

[a] Primary particle size determined through scanning electron microscopy (SEM) [60].

Table 3-2 Summary of the concentration of slurry additives.

slurry name	reported additives	results from experiment (mg/L)
c-SiO_2	acetic acid < 1%	801.9 ± 1.3[a]
f-SiO_2	potassium hydroxide < 1%	1130.0 ± 10.0[b]
Al_2O_3	nitric acid < 1%	134.7 ± 0.8[c]

[a] The concentration was derived from DOC data.
[b] KOH cocentration was derived from K concentraion.
[c] Concentration was derived from nitrate concentration, there is no nitrite in the slurry.

3.4.2 CMP slurry Microtox acute toxicity test

Microtox acute toxicity test results are summarized in Fig. 3-1. The results indicate that CMP slurries were not or only mildly inhibitory to *A. fischeri* at relatively high concentration: for f-SiO_2 and CeO_2 slurries, no metabolic inhibition was observed in the experiment at the tested concentrations up to 700 mg/L (f-SiO_2) and 1000 mg/L (CeO_2); on the other hand, the cell activity decreased by 37.6% and 28.4%, respectively, after 30 min of exposure to high concentration of c-SiO_2 and Al_2O_3 (about 1300 mg/L). Binaeian et al. [87] compared the effects of 7 ENPs on *A. fischeri*. In the study, SiO_2 NPs had the lowest toxicity: after 5 min exposure, the 50% inhibition concentration (IC_{50}) was about 700 mg/L; IC_{50} at 30 min was about 350 mg/L. For Al_2O_3, literature results confirm no toxicity was observed in Microtox assays supplemented with concentrations of Al_2O_3 up to 100 mg/L [88, 89]. To our best knowledge, so far there is no available information about CeO_2 toxicity to *A. fischeri*.

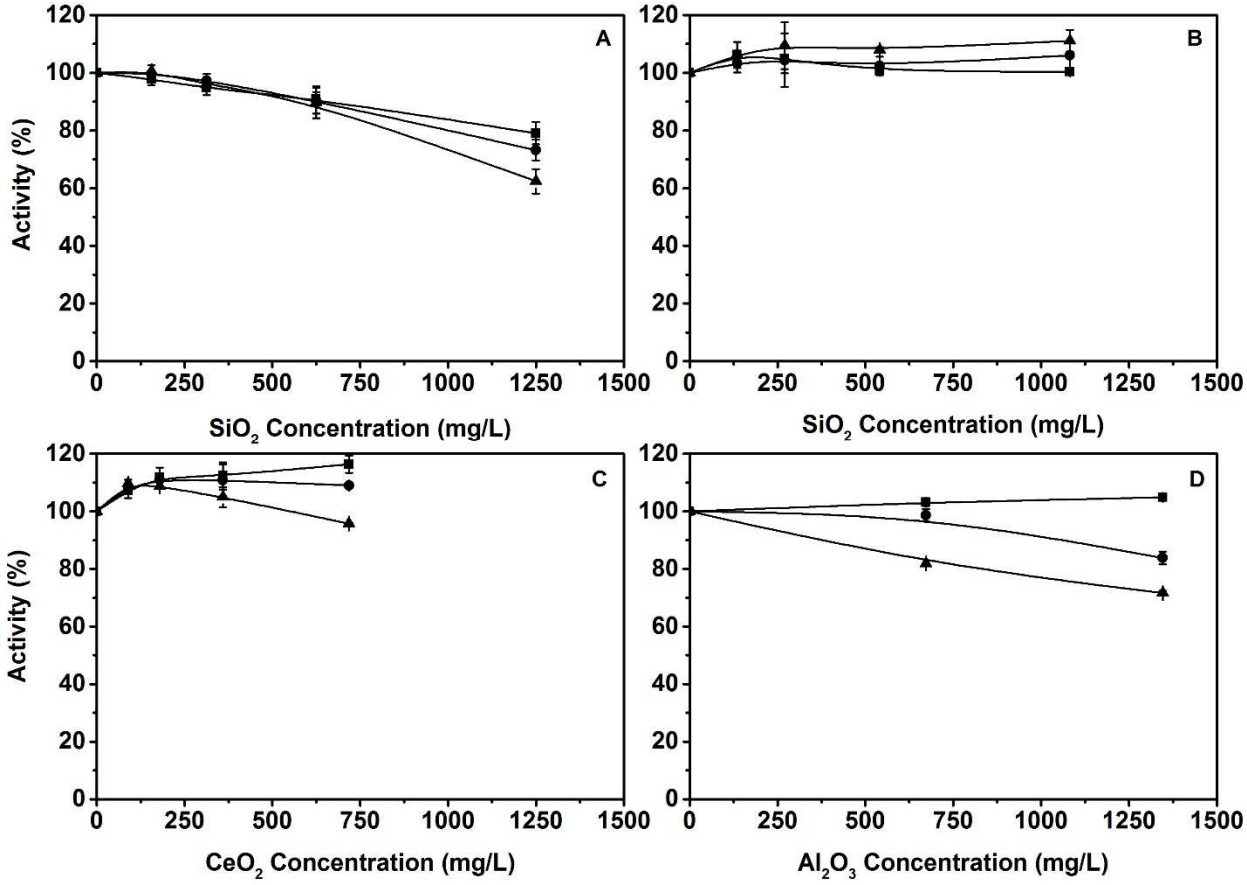

Fig. 3-1. Normalized activity of *A. fischeri* as a function of CMP slurries at 5 min (■), 15 min (●) and 30 min (▲): (A) c-SiO_2, (B) f-SiO_2, (C) CeO_2, (D) Al_2O_3.

Fig.3-2 shows cell activity values in response to exposure to undiluted CMP slurry supernatant. No obvious effect was observed form f-SiO_2, CeO_2 and Al_2O_3 slurries, while the supernatant from c-SiO_2 resulted in 98.6% inhibition of cellular activity. This result indicates that the mild toxicity of c-SiO_2 slurry could be due mainly to unidentified soluble substances in the slurry.

Particle size and ζ-potential values of CMP ENPs in Microtox medium were summarized in Fig. 3-3. The results show these ENPs were unstable in the medium as the absolute values of ζ-potential were lower than 30 mV and the particle sizes were larger than those in original slurry (*Section 3.4.1*). These could mainly cause by the high ionic strength and neutral pH in the medium. Microtox tests were conducted under pH about 7.0, which was close to the IEP of CeO_2 (6.7-8.6) and Al_2O_3 (7-8); also, in the assay, the Microtox diluent was 2% NaCl (20 g/L) and this high ionic

strength could compress the electrical double layer. These factors can make Van der Waals attraction outweigh the electrostatic repulsion and cause aggregation. This is particularly evident in the case of CeO_2 which had ζ-potentials lower than 20 mV and particle sizes more than 20 times larger than those in the original slurry.

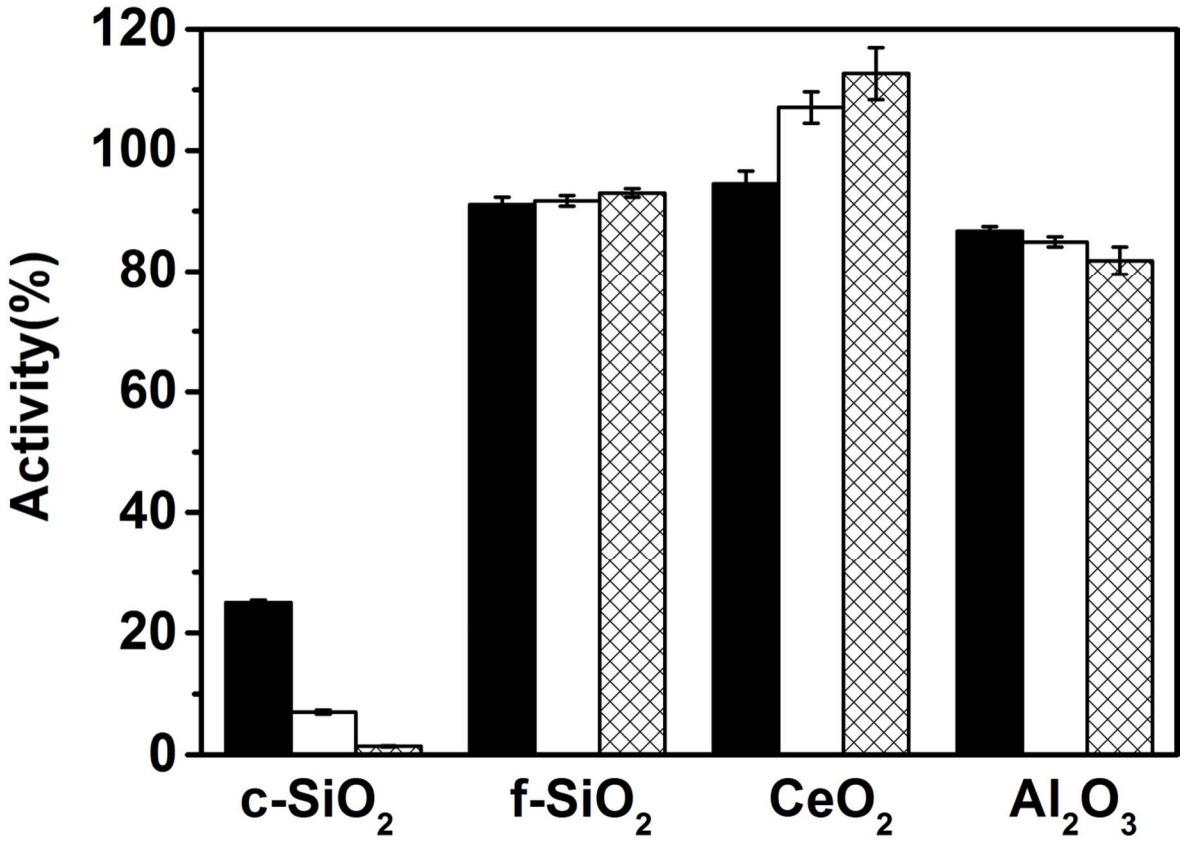

Fig. 3-2. Activity of A. fischeri treated with undiluted slurry supernatants after ultrafiltration at 5 min (filled bar), 15 min (empty bar) and 30 min (cross-hatched bar).

In the experiments, particle settling of the ENPs was observed in the bioassay medium, especially for CeO_2, where two different layers were observed in the dispersion, a very clear supernatant on top and a turbid suspension occupying the rest of the vial. This is in agreement with the results show in Fig. 3-3. The recoveries of c-SiO_2, f-SiO_2, CeO_2 and Al_2O_3 in the supernatant after 30 min were 48.3%, 41.3%, 6.5% and 15.4%, respectively. The stability of NP suspensions controls their mobility in aquatic systems: stable colloidal suspensions of NPs are readily for efficient interactions with aquatic organisms [2]. Therefore, particle aggregation and

sedimentation in the testing medium could be an factor responsible for the limited toxicity of the CeO_2 and Al_2O_3 slurries in the Microtox assay.

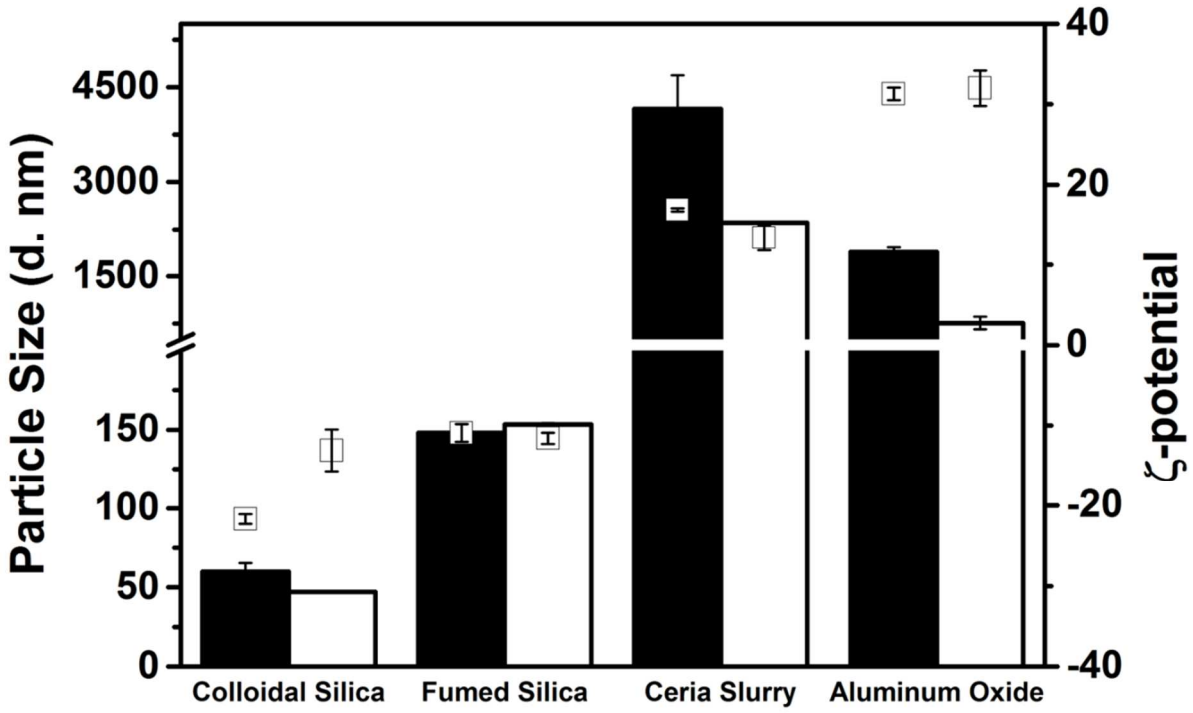

Fig. 3-3. Particle size and zeta-potential (□) of CMP NPs in the Microtox test medium (2% NaCl, pH at about 7.0): well-mixed samples (filled bar), supernatant (empty bar).

3.5 Conclusions

In this work we have studied the physical, chemical and toxicological characterization of four model slurries. The results suggest the ENPs were well dispersed and very stable in the pristine slurries. In addition, the ENPs used in CMP are not likely to cause acute ecotoxicity as they were not inhibitory to *A. fischeri* at concentrations up to about 600 mg/L, which is much higher than the relevant ENP concentrations in the environment (< 1mg/L). The ENPs in the model slurries used in this study are representative of those used in commercial slurries, but lack the complexity of the slurries used in practice. Thus, this is only the first step to understand the behavior and toxicity of these ENPs in real wastewaters and effluents discharged from semiconductor manufacturing.

CHAPTER 4 TRANSPORT AND ABATEMENT OF FLUORESCENT SILICA NANOPARTICLE (SiO_2 NP) IN GRANULAR FILTRATION: EFFECT OF POROUS MEDIA AND IONIC STRENGTH

4.1 Abstract

The extensive production and application of engineered silica nanoparticles (SiO_2 NPs) will inevitably lead to their environmental release. Granular media filtration is a widely used process in water and wastewater treatment plants which has the potential for NP abatement. In this work, laboratory scale column experiments were performed to study the transport and retention of SiO_2 NPs on three widely used filtering materials, *i.e.,* sand, anthracite and granular activated carbon (GAC). Synthetic fluorescent core-shell SiO_2 NPs (83 nm) were used to facilitate NP traceability. Sand showed very low capacity for SiO_2 filtration as this material has a surface with limited surface area and a high concentration of negative charge. Also, we found that the stability and transport of SiO_2 NP was strongly dependent on the ionic strength of the solution. Increasing ionic strength led to NP agglomeration and facilitated SiO_2 NP retention, while low ionic strength resulted in release of captured NPs from the sand bed. Compared to sand, anthracite and GAC showed higher efficiency for SiO_2 NP capture. The superior capacity of GAC was primarily due to its porous structure and high surface area. A process model was developed to simulate NP capture in the packed bed columns and determine fundamental filtration parameters. This model provided an excellent fit to the experimental data. Taken together the results obtained indicate that GAC is an interesting material for SiO_2 NPs filtration.

This chapter has been submitted for publication.
C. Zeng, F. Shadman, R. Sierra-Alvarez, Transport and abatement of fluorescent silica nanoparticle (SiO_2 NP) in granular filtration: effect of porous media and ionic strength, J. Nanopart. Res.

4.2 Introduction

Nanomaterials are defined as materials with at least one dimension between 1-100 nm. Due to the extreme size, nanomaterials have unique electronic, optical, chemical and mechanical characteristics compared to their bulk counterparts. Because of these novel properties, massive nanomaterials are intentionally produced for desired applications, which are known as engineered nanomaterials (ENMs). Nano-sized silica (SiO_2) is one of the most important ENMs [6] with a global production estimated to be more than 2.4 million tons per year [5]. SiO_2 nanoparticles (NPs) are widely used in chemical mechanical planarization (CMP) processes for the manufacture of integrated circuits, cosmetics, printer toners, construction materials and biomedical applications in biomedical imaging and drug delivery. With this extensive production and application, some portion of SiO_2 NPs will inevitably enter the environment. So far a lot of work has been done to study the toxic effects of SiO_2 NPs on microorganisms, animals and human cells through *in vitro* and *in vivo* assays [84], and some of these studies indicate that SiO_2 NPs may pose a threat to environmental and human health [75, 79, 80]. In addition, it has been reported that some NPs could behave like shuttles (or vectors) and facilitate contaminant transport [69]. For example, SiO_2 colloids and NPs were found to be responsible for the enhanced migration of uranium, thorium and cesium in different studies [90, 91]. Therefore, there are concerns about the release of these NPs into the environment.

Industrial and municipal discharges are two major sources of NPs release. Although the release of NPs can be reduced by some regulations (e.g., turbidity, total suspended solids), there are no regulations specifically for the discharge of NPs. It has been reported that some of the industrial processes have the potential to generate large quantities of effluent containing a high concentration of NPs. For example, the concentration of SiO_2 NPs (used as abrasive) in CMP effluents is estimated to range between 1300-8500 mg/L [64]. Wastewater treatment plants play an important role in controlling the release of these NPs to aquatic or terrestrial environments. The effectiveness of standard wastewater treatment processes has been evaluated in a few studies. Jarvie et al. [92] found SiO_2 NPs did not flocculate in wastewater with typical residence times for primary treatment. Biological wastewater treatment using the activated sludge process has also been shown to provide low removal efficiencies for SiO_2 NPs [93]. Granular media filtration is another standard process that is used in water and wastewater treatment for removing suspended

solids and colloidal particles (particle size 1-1000 nm). The effectiveness of this technique to remove colloidal particles indicates its potential for NP treatment. Also, since the method is widely applied in current water and wastewater treatment treating systems, it could be a cost-effective process for NP abatement. However, only very few studies are available on the transport of SiO_2 NPs in porous media [12, 94-96]. In these studies, the effects of particle concentration, size and electrolyte has been evaluated using glass beads and sand as filter media. Sand and anthracite are two common media used in tertiary wastewater treatment; granular activated carbon (GAC) is commonly used in drinking water treatment. To our best knowledge there is only one study considering NP filtration by GAC [10]; and anthracite has never been used for NP removal. Therefore, it is of great interest to understand the retention and transport of SiO_2 NPs in these porous media.

The main objective of this study was to investigate the transport and retention of SiO_2 NPs in columns packed with sand, anthracite, or GAC. In this work, synthesized fluorescent core-shell SiO_2 NPs (83 nm) were used in laboratory-scale column breakthrough experiments. The effect of ionic strength on NP retention was also evaluated. Finally, a process model was developed to determine the fundamental parameters (attachment/detachment rate coefficient and the capacity of the porous media) for NP abatement. This model can be used to find suitable materials for NP removal and guide the design of treatment processes.

4.3 Materials and methods

4.3.1 Chemicals

Tetraethyl orthosilicate (TEOS, 98%), (3-Aminopropyl) triethoxysilane (APTES, 99%), acetone (≥ 99.9%), Triton X-100 (TX-100) and rhodamine B isothiocyanate (RITC) were obtained from Sigma-Aldrich (St. Louis, MO, USA). Ammonium hydroxide (NH_4OH, 28-30%) was purchased from Spectrum Chemical (New Brunswick, NJ, USA). 1-hexanol (99%) and cyclohexane (> 99%) were purchased from Alfa Aesar (Ward Hill, MA, USA).

4.3.2 Synthesis and characterization of fluorescent SiO_2 (f-SiO_2) NPs

The ideal f-SiO_2 NPs for transport study should have good traceability and share the same behavior with pure SiO_2 NPs. In this study, core-shell f-SiO_2 NPs were synthesized using a micro-emulsion (or sol-gel) method according to a previously published protocol [93]. The fluorescent core of the NPs was made by the conjugate between fluorescent dye RITC and APTES. The fluorophore was then capped with a shell of pure SiO_2. Synthesized NPs were characterized by measuring their particle size distribution, zeta-potential (ζ potential), silicon (Si) concentration, and fluorescence intensity.

The primary particle size of f-SiO_2 was determined by transmission electron microscopy (TEM). The sample was prepared in isopropanol and the NPs were dispersed using an ultrasonic bath (2510, Branson Ultrasonics, Danbury, CT, USA) for 5 min before the analysis. TEM images were obtained on a Hitachi H-8100 TEM instrument (Hitachi, Tokyo, Japan) at 200 kV. The hydrodynamic particle size of f-SiO_2 was measured by dynamic light scattering (DLS) using a Zetasizer Nano ZS (Malvern Instruments, Sirouthborough, MA, USA) with a laser wavelength of 633 nm and a scattering angle of 173°. The refractive index applied for SiO_2 NP was 1.47.

The ζ potential of f-SiO_2 dispersions was also measured using the Zetasizer instrument. The data were determined by the Smoluchowski equation that correlates particle electrophoretic mobility to ζ potential value. The isoelectric point (IEP) of f-SiO_2 was acquired by testing the ζ potential under a range of pH (from 3.0 to 8.0) using an autotitrator (MPT-2, Malvern Instruments) connected to the Zetasizer Nano ZS.

The concentration of Si was determined by inductively coupled plasma−optical emission spectroscopy (ICP-OES, Optima 2100 DV, Perkin-Elmer, Waltham, MA, USA) at a wave length of 251.611 nm. Prior to ICP analysis, SiO_2 dispersions were first digested using a microwave assisted digestion system (MARS 5, CEM Corporation, Matthews, NC, USA). In the process, the SiO_2 sample (1 mL) were supplemented with 1% HF (10 mL) and digested at 120°C for 45 min (25-min ramp time) with a power level of 1600 W. After digestion, the samples were diluted with 2% HNO_3 to the proper concentration for Si analysis.

The fluorescence of f-SiO_2 was measured using a fluorescence spectrometer (LS55, Perkin Elmer, Waltham, MA, USA), at an excitation wavelength at 559 nm (slit width 4 nm) and emission wavelength at 579 nm (slit width 10 nm).

4.3.3 Porous media

Sand (quartz) was purchased from Acros Organics (Geel, Belgium); anthracite was obtained from Fresh Water Systems (Greenville, SC, USA); GAC (F400) was from Calgon Carbon (Pittsburgh, PA, USA). These materials were sieved using U.S. standard meshed sieves. The particle size of the sieved sand was between 180 and 250 μm. For anthracite and GAC, the particle size after sieving was between 425 and 600 μm. These granular media were washed prior to use: sand was first soaked in diluted hydrochloric acid (1 M HCl) for 24 h and then washed with deionized (DI) water; anthracite and GAC were washed with DI water. These materials were dried at 105°C for 8 h.

The net surface charge and IEP values of these porous media were determined by acidimetric-alkalimetric titration[13]. In the experimental process, 10 mM NaCl solution (20 mL) and 0.2 g porous medium were supplied to centrifuge tubes (50 mL). Aliquots of HCl (0.1 M) or NaOH (0.1 M) ranging from 0.05 to 1.5 mL were added to 14 vials. One vial with no addition of acid/base was used as reference. These 15 samples were mixed in a shaker at 120 rpm at room temperature for 24 h. Then the equilibrium pH was measured and used for surface charge calculation based on site balance. The surface charge was plotted as a function of the pH to determine the IEPs of the granular media.

For anthracite and GAC, scanning electron microscopy (SEM) micrographs were obtained on a Hitachi S-4800 Type II instrument (Hitachi, Tokyo, Japan) at 2 kV. BET surface area measurements were performed by N_2 adsorption using a Tristar II 3020 analyzer (Micrometritics, Norcross, GA, USA).

4.3.4 Column breakthrough experiments

Fig. 4-1 shows a schematic representation of the column experimental set up. A glass column (Omnifit Labware, Diba Industries, Danbury, CT, USA) was used in all the experiments. The inner diameter of this column is 1.5 cm, the bed height is 12 cm, and the bed volume is 21.2 mL. In this

study sand (35 g), anthracite (18 g) or GAC (11 g) was wet-packed into the column. During packing, the porous medium was slowly introduced into the column and the water level was kept above the solids to prevent formation of air bubbles. In addition, the sides of the column were continuously tapped to achieve uniform packing. The pore volume (PV) of the column packed with sand was 7.8 mL with a column porosity of 36.8%; for anthracite and GAC, the PV was 8.5 mL with a porosity of 40.1%. The NP stock solution was prepared by dispersing 10 mg/L f-SiO_2 into 10 mM NaCl (pH 7.0, adjusted with 1 mM $NaHCO_3$). The suspension was then sonicated for 5 min at 70% amplitude with an ultrasonic processor (130W, Sonics, Newtown, CT, USA).

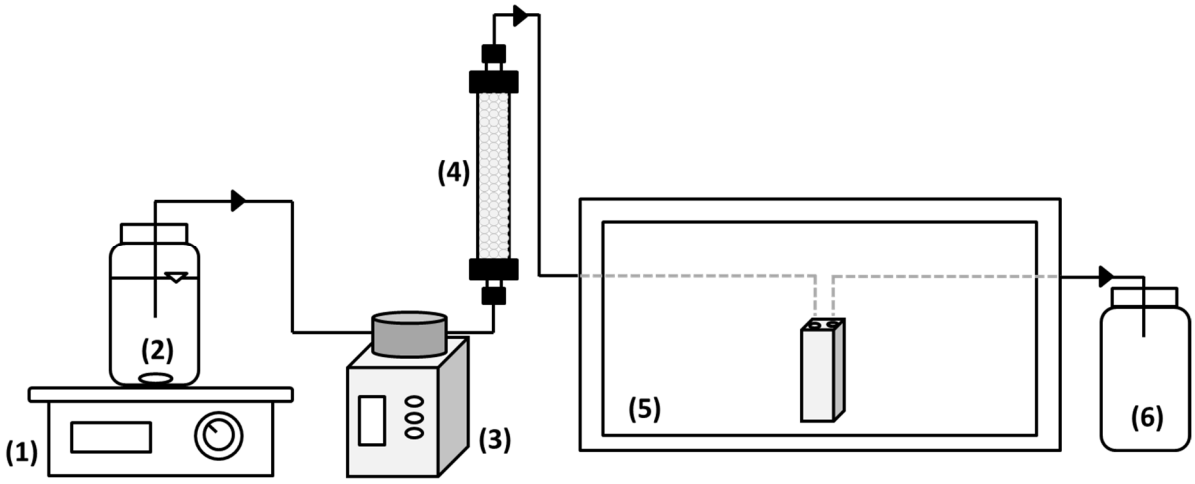

Fig. 4-1. Experimental setup of the column tests. In the experiment, the dispersion of SiO_2 NPs (2) was continuously stirred by a magnetic stirrer (1), the influent was introduced into a column packed with porous medium (4) using a peristaltic pump (3), the concentration of fluorescent SiO_2 NPs in the effluent was measured online using a fluorescence spectrometer equipped with a flow-through cell (5), the effluent was collected (6).

A peristaltic pump (MINIPULS 3, Gilson, Inc., Middleton, WI, USA) was connected to the inlet at the bottom of the column to regulate the upward flow at a constant flow rate of 2.6 mL/min. Before each experiment, 15 PV of background solution (without NPs) were fed through the saturated column. The breakthrough experiment was then initiated following a three-phase procedure. In the first stage (stage 1), the f-SiO_2 suspension was fed to the column for 5 PV. Afterwards, in the second stage (stage 2) and third stage (stage 3), background solution and DI water were supplied successively for five PV in each phase. The concentration of f-SiO_2 NPs in

the influent and effluent was monitored on line using a fluorescent spectrometer equipped with a flow through quartz cuvette with 10 mm path length (Starna Cells, Atascadero, CA, USA) using the method described in *Section 4.3.2*. The fluorescence data were recorded online once per second. The SiO_2 concentration in the effluent (C) is expressed as a percentage of the SiO_2 concentration in the influent (C_0). All the breakthrough experiments were performed in duplicate.

In the experiments, anthracite and GAC showed comparatively high affinity for f-SiO_2 retention. Their capacity for f-SiO_2 removal was evaluated by continuously introducing a dispersion containing 10 mg/L of f-SiO_2 NPs for 200 PV or until the effluent reached 100% breakthrough.

4.3.5 Ionic strength effects on SiO_2 NP retention

A similar procedure as discussed in *Section 4.3.4* (three-phase column test) was performed to evaluate the effects of ionic strength on the stability of f-SiO_2 NP dispersions and their transport in porous medium. In this experiment, sand was used as the porous medium; f-SiO_2 NPs were dispersed in 1 mM or 100 mM NaCl (pH 7.0). Particle size, ζ potential and the retention behavior of f-SiO_2 were determined and compared with those acquired at an ionic strength of 10 mM.

4.3.6 Modeling work

A model was developed to simulate NP capture and removal in the packed bed abatement processes. The process model has two major applications. The first is to determine the fundamental parameters that define the kinetics of the capture (attachment) and release (detachment) as well as the transport of particles in these systems. The second application is the ability to extend the results from laboratory scale systems to large systems. This is valuable for design as well as optimization of operating conditions in large-scale applications.

The mass conservation equation for NP retention in porous media is shown as follows:

$$\frac{\partial C}{\partial t} = D_e \nabla^2 C - v \cdot \nabla C - A \frac{\partial C_s}{\partial t} \quad (4-1)$$

where: t [min] is time; D_e [m^2/min] is the dispersion coefficient; C [mol/m^3] is the concentration of NP in the fluid phase; C_s [mol NP/m^2 of porous media] is the concentration of NP captured in porous media; v [m/min] is the interstitial fluid velocity and A [m^2/m^3] is the area per unit volume of sorbent.

If we assume the fluid in the column is uniform, one dimensional flow along the direction of column length, then Eq. 4-1 can be simplified as:

$$\frac{\partial C}{\partial t} = D_e \frac{\partial^2 C}{\partial z^2} - v\frac{\partial C}{\partial z} - A\frac{\partial C_s}{\partial t} \quad (4-2)$$

where the first two terms on the right side describe the dispersive and convective flux. The last term represents the interactions between NPs and porous media surface, which includes both the rate of retention and remobilization. The attachment and detachment reactions are represented by the following equation:

$$\frac{\partial C_s}{\partial t} = k_a C(S_0 - C_s) - k_d C_s \quad (4-3)$$

where: S_0 [mol NP/m^2 porous medium] is the capacity of the solid adsorbent; k_a [m^3/(mol·min)] is the second order attachment rate coefficient and k_d [1/min] is the first order detachment rate coefficient. In this study the COMSOL numerical package (COMSOL, Inc., Burlington, MA, USA) was used to solve the above equations.

4.4 Results and discussion

4.4.1 Characterization of fluorescent SiO_2 NPs

Fig. 4-2 shows a TEM image of f-SiO_2 NPs, indicating that the synthetic particles are spherical and very homogeneous with an average diameter of 83 ± 6 nm. The average particle size determined by DLS was 146.1 ± 0.6 nm, a value that is 1.5 times higher than that determined using TEM. The DLS technique measures the hydrodynamic diameter of a hypothetical sphere that diffuses at the same speed as the particle under examination. The hydrodynamic diameter is

indicative of the apparent size of the hydrated/solvated particle; therefore, this size is normally larger than that from TEM image.

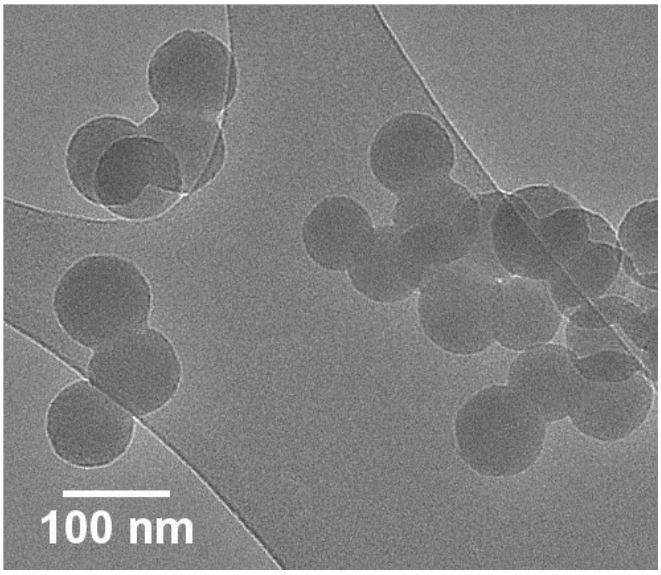

Fig. 4-2. TEM image of the synthetic fluorescent SiO_2 NPs used in this study.

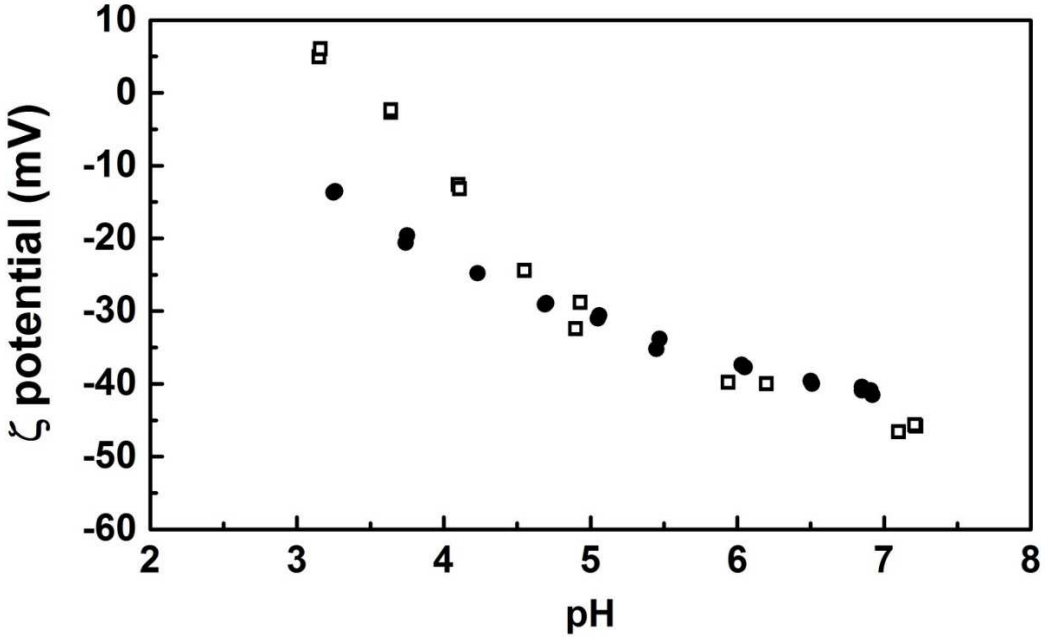

Fig. 4-3. ζ potential of the synthesized fluorescent SiO_2 NP (●) and commercial SiO_2 NP (□) as a function of pH.

Fig. 4-3 compares the ζ potential values of the synthesized f-SiO_2 NPs and commercial SiO_2 NPs (10-20 nm) over a range of pH values. The results show that the ζ potential of the synthesized NPs was very similar to that of the commercial SiO_2 NPs in the neutral pH range and somewhat higher under acidic pH (pH < 4). The IEP of the f-SiO_2 NPs was about 3.4, which is within the typical range reported for SiO_2 particles (2.0-3.5) [86]. Therefore, the results indicate the surface of our NPs was well capped with pure silica and that the behavior of f-SiO_2 NPs should be very similar as pure SiO_2 NPs in the aqueous system.

A representative calibration curve of f-SiO_2 fluorescence intensity as a function of NP concentration is shown in Fig. S1 (*Appendix A*). The synthesized NPs showed very high fluorescence, enabling a detection limit of about 0.1 mg/L f-SiO_2 NPs in the fluorescence spectrometer used in this study.

4.4.2 Characterization of porous media

The surface area, IEP and surface charge of the various model porous media utilized are summarized in Table 4-1. The surface charge values of anthracite and GAC over a broad pH range (2-12) are shown in Fig. S2 (*Appendix A*). The results show that GAC had a much higher surface area than sand and anthracite. Also, at pH 7, the surface of the sand and anthracite particles was negatively charged, while GAC was characterized by a low concentration of positive charge on its surface. The surface area of the GAC utilized (Calgon F400) has been reported to range between 800 to 100 m^2/g [97]; Salih et al. [98] has determined the ζ potential of this GAC and found an IEP of about 7.8. These data are in good agreement with our results.

Table 4-1 Surface area, isoelectric point and surface charge of the porous media used in this study.

Material	**Sand**	**Anthracite**	**GAC**
Surface area (m^2/g)	-	43	911
Surface charge (C/m^2)[a]	-21.70	-0.043	0.004
Isoelectric point	2.8	4.0	7.7

[a] Surface charge measured at pH 7

SEM images of anthracite and GAC were shown in Fig. S3 (*Appendix A*). From the image, it is clear that GAC has a porous structure with very high surface roughness.

4.4.3 The effect of ionic strength on the stability and transport of f-SiO_2 NPs in saturated sand

The stability of NP dispersions is largely controlled by the ionic strength of the solution [99-101]. As described by classical Derjaguin-Landau-Verwey-Overbeek (DLVO) theory, colloidal particles are surrounded by an electrical double layer (EDL) and the interaction between particles is determined by the sum of attractive van der Waals forces and electrostatic repulsion forces. Increasing ionic strength results in compression of the electrical double layer and, consequently, decreases energy barrier preventing particle agglomeration. Table 4-2 provides a summary of particle size and ζ potential of f-SiO_2 under different ionic strength levels. The results show that the absolute values of the measured ζ potential decreased in response to increasing ionic strength. Colloidal dispersions with ζ potentials higher than +30 mV or lower than -30 mV are typically considered stable. Therefore, the data indicate that f-SiO_2 NPs were stable at low ionic strength (1 and 10 mM). At high ionic strength (100 mM), the particles became unstable and particle aggregation occurred as the hydrodynamic particles size became much higher under this condition.

Table 4-2 Hydrodynamic particle size and ζ-potential of f-SiO_2 NPs dispersed in aqueous solutions with 1, 10 and 100 mM NaCl (pH 7.0).

Ionic Strength (mM)	**Particle Size** (nm)	**ζ-potential** (mV)
1	151.3 ± 2.3	-37.2 ± 1.6
10	179.8 ± 3.0	-33.5 ± 1.0
100	279.8 ± 22.4	-10.7 ± 2.2

Sand particles showed very poor efficiency for f-SiO_2 filtration at low ionic strength levels (Fig. 4-4A). The NPs reached 100% breakthrough very fast (within two PV) after they were introduced into the column. Although some f-SiO_2 NPs were retained by the sand bed, all of them were detached when the input solution was switched from f-SiO_2 dispersion to background solution (stage 2) or DI water (stage 3). This result was likely caused by the strong electrostatic repulsion between the sand collector and f-SiO_2 NPs as the surface of both materials possessed a

high concentration of negative charges on their surface under this experimental condition (pH 7.0) (Tables 4-1 and 4-2). In addition, the sand particles used had a smooth surface with very limited porous structure and low surface area, which could be another major factor explaining the rapid breakthrough observed for f-SiO_2 NPs in these experiments.

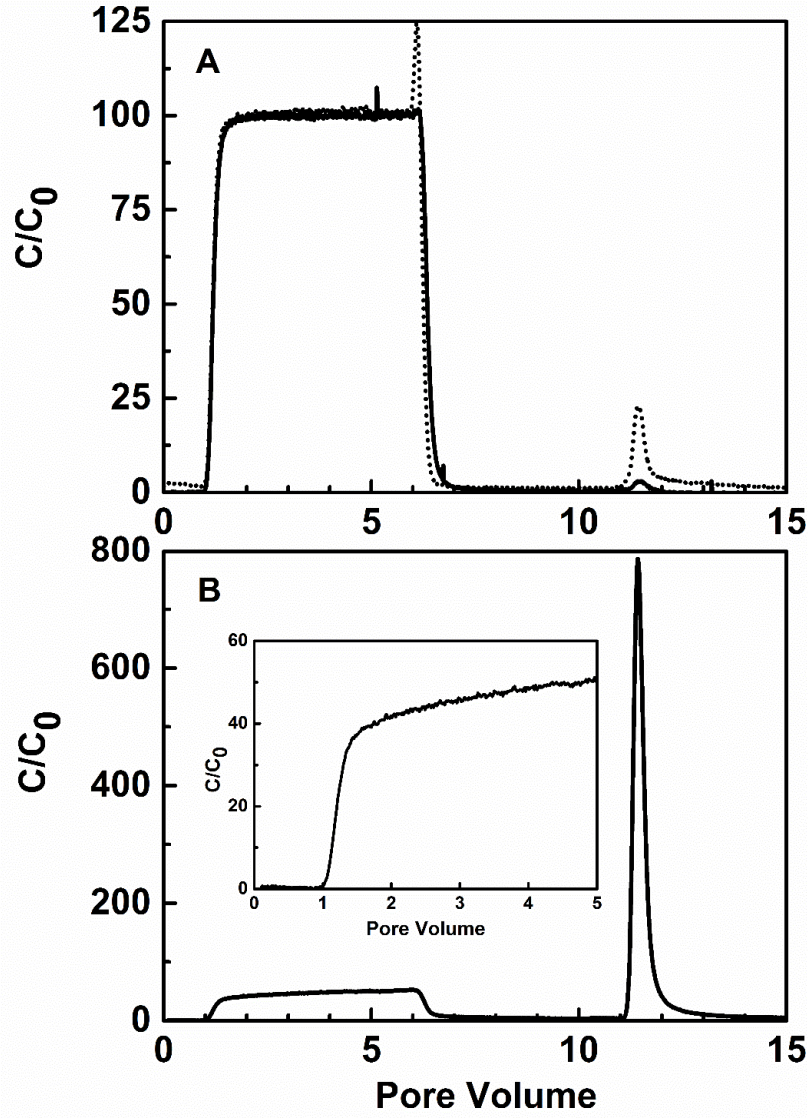

Fig. 4-4. Effect of the ionic strength on the retention of fluorescent SiO_2 NP in a flow-through column packed with sand: 1 mM (—) and 10 mM (···) ionic strength (panel A); and 100 mM ionic strength (panel B). The influent composition changed depending on the stage: f-SiO_2 suspension (stage 1); background solution (stage 2), and DI water (stage 3), each stage for 5 PV.

The transport behavior of f-SiO_2 NPs dispersed in 100 mM NaCl solution (Fig. 4-4B) was very different compared with that observed under low ionic strength. In the experiment, the f-SiO_2 concentration in the effluent only reached about 50% of the injected concentration with 0.007 mg SiO_2/g sand retained in the column after 5 PV. However, similar with the experiments conducted at low ionic strength, the NPs retained in the column were detached and released back into the pore water when the influent was switched to DI water (stage 3). This phenomenon has also been observed in different studies. Wang et al.[96] found retained SiO_2 NPs were released upon lowered solution ionic strength in the column experiments using Accusands as porous media. In another study, when DI water or 0.5 mM Na_2SO_4 solution was injected, retained SiO_2 NPs (prepared in 100 mM NaCl) were immediately and completely released from calcium carbonate sands [94].

4.4.4 Transport and retention of f-SiO_2 NPs on anthracite and GAC

Saturated anthracite and GAC media showed much higher affinity for f-SiO_2 retention as shown in Fig. 4-5. After 5 PV, the C/C_0 values for anthracite and GAC were 80% and 32%, respectively. For both media there was no NP detachment after the introduction of background solution (10 mM NaCl) (stage 2). However, mass balances showed that all the SiO_2 NPs were released from the anthracite medium after the influent was switched to DI water (stage 3).

Fig. 4-6 shows the breakthrough curves for anthracite and GAC in long term column tests. In the experiment with anthracite, f-SiO_2 NPs reached 100% breakthrough at about 50 PV (Fig. 4-6A) and 0.28 mg/g anthracite (10.2% of total f-SiO_2 supplied) was adsorbed. On the other hand, full breakthrough was not observed in the GAC column even after 200 PV (C/C_0: 83.5%). 1.55 mg SiO_2/g GAC was captured after 200 PV (36.8% of the total f-SiO_2 supplied). Both the anthracite and GAC used only possess very low concentrations of charges on the surface (Table 4-1) under the conditions of these experiments, therefore, it is unlikely that electrostatic interactions played a major factor in controlling NP retention. Physical interactions due to the porous structure of these materials are likely to be the cause for NP capture. Compared to anthracite, GAC has much higher surface area and intricate pore structures. This physical property facilitates NP straining and prevents detachment.

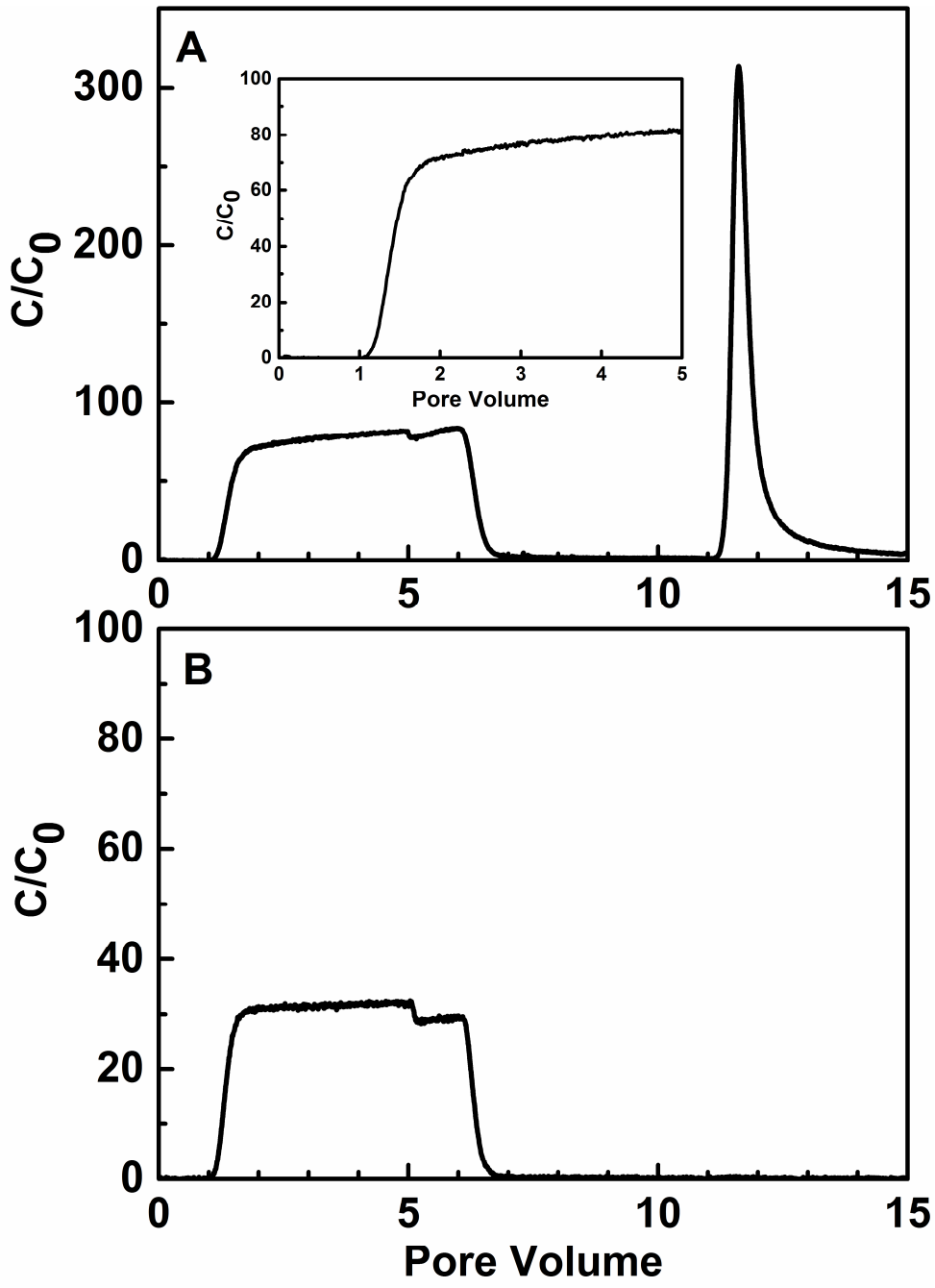

Fig. 4-5. Retention of fluorescent SiO_2 NPs in flow-through columns packed with anthracite (A) and GAC (B). The influent composition changed depending on the stage: f-SiO_2 suspension (stage 1); background solution (stage 2), and DI water (stage 3), each stage for 5 PV.

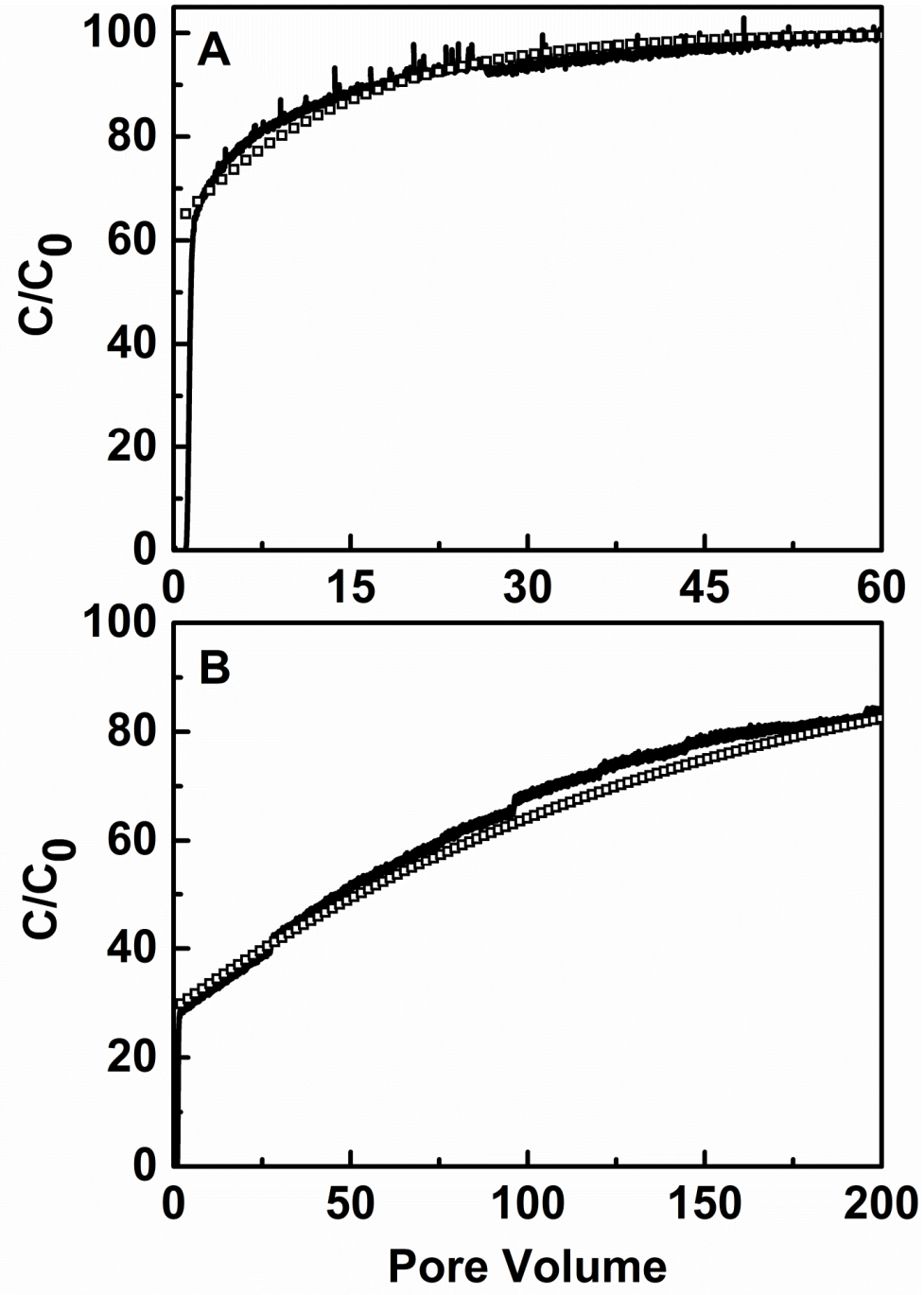

Fig. 4-6. SiO_2 NP breakthrough curves in flow-through columns packed with anthracite (A) and GAC (B): experimental data (–) and modeling fit (□).

4.4.5 Model simulations

The process model developed and described in *Section 4.3.6* was used to analyze the experimental data and determine the fundamental parameters of the abatement process for NP capture in anthracite and GAC columns. As shown in Fig.4-6, the model provides an excellent fit to the experimental data. In the experiment, the initial rapid rise, shown in the experimental data was due to the fact that in the laboratory columns a portion of the fluid bypassed the filtration process and went through the packed bed without coming in contact with the sorbent surface. This bypass, which is inevitable in small scale lab columns was included in this process model.

The parameters found by fitting the model to the experimental data are given in Table 4-3. The results show the k_a (second-order attachment rate coefficient) of GAC was about 1.2 times higher than that of anthracite, indicating GAC had slightly higher affinity for SiO_2 NP deposition. However, GAC also had a k_d (first-order detachment rate coefficient) 1.4 times higher than anthracite. It should be noted that the filtration effectiveness of a sorbent is primarily governed by its net rate of attachment and capacity. In comparing anthracite with GAC, both the net rate and the capacity for GAC were much higher than those for anthracite partially due to a higher k_a but primarily due to the dominant effect of S_0 (sorbent capacity); S_0 was 24 times larger for GAC.

The excellent fit between the model simulations and experimental breakthrough data indicates that this model can be used to describe the fate and transport of SiO_2 NPs in porous media and facilitate process scale up.

Table 4-3 Parameters found from modeling work for SiO_2 NP retention in anthracite and GAC.

Parameters	Anthracite	GAC
k_a [m^3/(mol·min)]	0.14	0.17
k_d [1/min]	0.30	0.42
S_0 [mol NP/m^2 porous medium]	0.0051	0.120

4.6 Conclusions

The results suggest that retention of f-SiO_2 is strongly dependent on the ionic strength of the solution and the nature of the granular media. High ionic strength led to destabilization of SiO_2 NPs and facilitated the capture; on the other hand, retained SiO_2 NPs were released under lowered ionic strength. Breakthrough experiments revealed that GAC provided comparatively high capacity for SiO_2 NP filtration due to the high surface area and intricate porous structure with large number of available sites for NP retention. Taken together the results obtained indicate that GAC is an interesting material for the abatement of SiO_2 NPs in granular medium filtration.

CHAPTER 5 ECOTOXICITY ASSESSMENT OF IONIC As(III), As(V), In(III) AND Ga(III) SPECIES POTENTIALLY RELEASED FROM NOVEL III-V SEMICONDUCTOR MATERIALS

5.1 Abstract

III-V materials like indium arsenide (InAs) and gallium arsenide (GaAs) are increasingly used in electronic and photovoltaic devices. The extensive application of these materials may lead to release of III-V ionic species during semiconductor manufacturing or disposal of decommissioned devices into the environment. Although arsenic is recognized as one of the most notorious contaminants, there is a lack of information about the toxic effects of indium and gallium ions. In this study, acute toxicity of As(III), As(V), In(III) and Ga(III) species was evaluated using two microbial assays, testing for methanogenic activity and O_2 uptake, as well as two bioassays targeting aquatic organisms, including *Aliivibrio fischeri* (bioluminescence inhibition) and crustacean *Daphnia magna* (mortality). We found the toxicity of these ions was strongly dependent on the bioassay target. In(III) and Ga(III) were not or only mildly toxic in the experiments. *D. magna* was the most sensitive organism with 50% lethal concentrations of 0.5 and 3.4 mM for In(III) and Ga(III), respectively. On the other hand, As(III) and As(V) showed clear inhibitory effects on different microbial activities, particularly in the methanogenic toxicity bioassay. The 50% inhibitory concentrations of both arsenic species towards methanogens were about 0.02 mM, which is lower than the regulated maximum allowable daily effluent discharge concentration (2.09 mg/L or 0.03 mM) for facilities manufacturing electronic components in the US. Overall, the results indicate the ecotoxicity of In(III) and Ga(III) is much lower than that of As species. This finding is important in filling the knowledge gap regarding the ecotoxicology of In and Ga.

This chapter has been submitted for publication.
C. Zeng, A. Gonzalez-Alvarez, E. Orenstein, J. A. Field, F. Shadman, R. Sierra-Alvarez, Ecotoxicity assessment of ionic As(III), As(V), In(III) and Ga(III) species potentially released from novel III-V semiconductor materials, Ecotoxicol. Environ. Saf.

5.2 Introduction

III-V materials such as indium arsenide (InAs), gallium arsenide (GaAs) and indium phosphide (InP) are novel materials with high electron mobility, low power requirement and favorable optoelectronic properties. Because of these attractive properties, III-V materials are increasingly used in semiconductor manufacturing as light emitting diodes (LEDs), laser diodes, liquid crystal displays (LCDs), biosensors and microcircuits [35, 36]. III-V materials are also finding extensive application in thin-film photovoltaic devices, thin film photovoltaic solar modules and other photovoltaic devices [102]. It has been reported that the demand for Ga and In has increased significantly during the past 30 years [39, 40]. The world primary production of Ga in 2014, estimated at 440 metric tons, was four times higher than in 2010 [41]. This rapid growth has been mainly attributed to the higher content of GaAs in different electronic devices, especially smartphones, and increasing use of GaAs-based LEDs [103]. Global indium consumption in 2014 was about 1,500 metric tons. Increased indium consumption was reportedly driven by increased demand for LCD televisions in developing countries and for smartphones and tablets in developed countries [41].

The extensive application of III-V materials may contribute to the release of hazardous material through corrosion of decommissioned electronic and photovoltaic devices. Manufacturing activities could also potentially contribute to the environmental release of III-V materials. For example, chemical mechanical planarization (CMP) of thin films containing III-V materials, such as GaAs and gallium indium arsenide (GaInAs), generates large amounts of waste effluents containing particulate and ionic III-V species. High levels of arsenic and other hazardous materials in the waste stream require treatment prior to discharge to surface water in order to meet environmental regulations. In the United States, the arsenic discharge limits for effluents produced by facilities manufacturing electronic components are 2.09 mg/L as one-day maximum and 0.83 mg/L as 30-day average concentration [66]. However, there are no current regulatory limits for the discharge of indium (In) and gallium (Ga) in wastewater.

Arsenic is one of the most notorious toxicants and it has been widely studied. There is a close relation between As toxicity and speciation, and usually, inorganic As species are more toxic than many organic As forms to living organisms [43-45]. The toxicity of trivalent arsenic (As(III) or arsenite) is related to its high affinity for sulfhydryl groups of biomolecules [46]. The formation

of these bonds leads to inhibition of crucial enzymatic functions within the cells [44]. On the other hand, the microbial toxicity of arsenate (As(V)) is often the result of its potential for phosphate replacement. Consequently, it inhibits enzymes that use phosphate and uncouples ATP formation, which ultimately results in depletion of cell energy [47]. Compared to As, there is a lack of available information regarding the ecotoxicity of In(III) and Ga(III). So far most studies concerned with the toxicity of In and Ga have focused on occupational exposure and consequent adverse effects to human health [48-51]. Only a very limited number of studies have evaluated their ecotoxicity [52-54].

The objective of this study was to investigate the ecotoxicity of ionic As(III), As(V), In(III) and Ga(III). To this end, two toxicity bioassays were performed, in which inhibition of bioluminescence activity in the marine bacterium, *Aliivibrio fischeri,* and lethal effects on *Daphnia magna*, a multicellular aquatic microcrustacean, were tested. The Microtox test and acute toxicity bioassays with daphnids are used by municipalities and industries worldwide as standard methods to test the toxicity of chemicals and effluent streams, and both methods are accepted by organizations such as the U.S. Environmental Protection Agency (U.S. EPA), the Organization for Economic Co-operation and Development (OECD), and the International Organization for Standardization (ISO) [104-108]. In addition, two microbial assays, testing the impact of the various ionic species towards the methanogenic activity of an anaerobic mixed culture and on O_2 uptake by aerobic bacteria in wastewater treatment sludge, were applied as well. Methanogens and aerobic heterotrophic bacteria are microorganisms commonly found in natural environments that play important roles in matter and energy cycles. These microorganisms are also widely used in wastewater treatment systems. Therefore, these microorganisms are often used as indicators in ecotoxicity studies.

5.3 Materials and methods

5.3.1 Chemicals

Gallium(III) chloride ($GaCl_3$, > 99.99%), sodium meta-arsenite ($NaAsO_2$, ≥ 90%), sodium arsenate dibasic heptahydrate ($Na_2HAsO_4 \cdot 7H_2O$, ≥ 98%), and citric acid ($C_6H_8O_7$), were purchased from

Fisher Scientific (Pittsburgh, PA, USA). Indium(III) chloride tetrahydrate ($InCl_3 \cdot 4H_2O$, > 99.99%) was obtained from Strem Chemicals (Newburyport, MA, USA).

Indium and gallium have very low aqueous solubility in the neutral pH range [55]. In order to avoid precipitation, citrate was used as complexing agent in In(III) and Ga (III) stock solution preparation at a molar ratio of 3.75 (In/Ga:citrate). Citrate is a common metabolite of living cells in nature [109], it is also used as important chelating agent in metal processing industries including semiconductor manufacturing [56]. Therefore, the use of citrate in this study is relevant to In(III) and Ga(III) exposure scenarios.

5.3.2 Microtox acute toxicity bioassay

Microtox is an *in vitro*, metabolic inhibition test system that uses a strain of a naturally bioluminescent marine bacterium named *A. fischeri* that produces light as byproduct of cellular respiration. The toxicity of test chemicals can be recognized by the loss of luminescence level that results from cellular activity inhibition.

In the study, all samples were tested using a Microtox M500 analyzer following the Microtox Acute Toxicity Test protocol. Microtox reagent (*A. fischeri*), reconstitution solution, osmotic adjusting solution, and diluent were obtained from Fisher Scientific. Stock solutions (6 mM As(III) and As(V), and 20 mM Ga(III) and In(III)) were prepared prior to the experiments. Ga(III) and In(III) were both complexed with citrate as explained in *Section 5.3.1*. The pH of each stock solutions was adjusted to about 7.0 through addition of either diluted HCl or NaOH. In order to maintain the osmotic pressure of the samples, the stock solution was first mixed with osmotic adjusting solution (10:1, v/v). Then the solution was diluted to the designed concentrations using Microtox diluent. Luminescent levels were tested at 0, 15 and 30 min. All tests were performed in duplicates; blank controls were run in parallel. Percent microbial activity was calculated as described in *Section 3.3.5*.

5.3.3 Methanogenic toxicity bioassay

The methanogenic sludge was obtained from an anaerobic bioreactor treating brewery wastewater (Mahou, Spain) with 7.92% of volatile suspended solids (VSS) per unit wet weight. Batch experiments were conducted in duplicate using glass serum flasks (160 mL) supplemented with

inoculum (1.5 g VSS/L), and acetate-containing basal medium (25 mL) (described in *Appendix B*). The flasks were then sealed with butyl rubber stoppers and aluminum crimp seals. The headspace was flushed with a mixture of N_2 and CO_2 (80:20, v/v) to create anaerobic conditions. Pre-incubation was performed overnight to ensure the methanogens were adapted to experimental conditions. The following day, As(III) or As(V) (0–0.2mM) was added to the As assays. For the In and Ga assays, In(III) (0-1.08 mM) and Ga(III) (0–1.25 mM), both complexed with citrate as explained in *Section 5.3.1*, were added. The flasks were incubated in a shaker (115 rpm) at 30 ± 2 °C. Methane (CH_4) production was determined periodically until 80% or more of the substrate in toxicant-free controls was depleted. The normalized microbial activity (NMA) was calculated as shown below:

$$NMA(\%) = \frac{Maximum\ Specific\ Activity\ of\ Experimental\ Group}{Maximum\ Specific\ Activity\ of\ Control} \times 100 \quad (5-1)$$

where the maximum specific activity was calculated from the slope of cumulative CH_4 production.

5.3.4 Aerobic toxicity bioassay

Aerobic return activated sludge (RAS) from a local municipal wastewater treatment plant (Tucson, AZ, USA). The VSS content of the sludge was 0.78% (wet wt). The assays were conducted in glass serum flasks (160 mL) supplemented with basal medium (25 mL, *Appendix B*) and RAS inoculum (0.5 g VSS/L). The flasks were spiked with As (0–0.6 mM), In(III) (0–1.08 mM) or Ga(III) (0–1.8 mM), sealed and flushed with a mixture of $He/CO_2/O_2$ (60:20:20, v/v). In(III) and Ga(III) were complexed with citrate as explained in *Section 5.3.1*. O_2 content was measured periodically until the O_2 consumption rate resembled that of the endogenous control without acetate. NMA was calculated using Eq. 5-1, only in this case the maximum specific activity was calculated based on the slope of the O_2 consumption versus time graph.

5.3.5 Daphnia toxicity bioassay

The acute toxicity of Ga(III) and In(III) to *D. magna* was tested according to EPA Ecological Effects Test Guidelines [110]. In the experiment, *D. magna* was exposed to 0–5.0 mM Ga(III) or In(III) and the number of dead organisms was determined after 48 h of exposure. All samples were

run in quadruplicate. Arsenic toxicity data for *D. magna* are widely available in literature [111-114], therefore As(III) and As(V) were not tested using this assay.

5.3.6 Analytical methods

Aqueous As, In and Ga were measured using an inductively coupled plasma–optical emission spectrometry (ICP–OES) system (Optima 2100 DV from Perkin-Elmer, Shelton, CT, USA). The wavelengths used for As, In and Ga analyses were 193.696, 230.606 and 417.206 nm, respectively.

The headspace samples in the batch bioassays were measured using a Hewlett Packard 5890 Series II gas chromatograph (Agilent Technologies, Palo Alto, Ca, USA) with He as the carrier gas. CH4 was determined using a flame ionization detector with a Restek Stabilwax-DA column (30×0.35 mm, ID 0.25 μm). O2 was analyzed using a thermal conductivity detector with a Carboxen®-1010 Plot column.

5.4 Results and discussion

5.4.1 Microtox acute toxicity bioassay

Fig. 5-1 shows the dose response curves of *A. fischeri* exposed to As(III) and As(V) for 5, 15 and 30 min. As can be seen, the presence of arsenic resulted in *A. fischeri* inhibition. The luminescence decreased with the higher As concentration and longer exposure time. As(III) was only mildly inhibitory at comparatively low concentration (< 0.2 mM), while As(V) caused a rapid decrease of luminescence. After 15 min, 2.7 mM As(III) and As(V) led to 71.6 and 90.0% loss in light emission, respectively. For As(III), the 50% inhibition concentration (IC_{50}) values at 5, 15 and 30 min were 2.23, 1.07 and 0.90 mM, respectively. For As(V), the IC_{50} values were 0.16, 0.04 and 0.05 mM, respectively. In this assay, As(V) had higher toxicity than As(III), which is in agreement with previously published literature [106, 115]. It has been reported that light production in *A. fischeri* through aerobic respiratory pathways requires ATP [116]. Therefore, the higher toxicity from As(V) may have been due to the blockage of ATP formation by As(V) replacing phosphate in biochemical reactions.

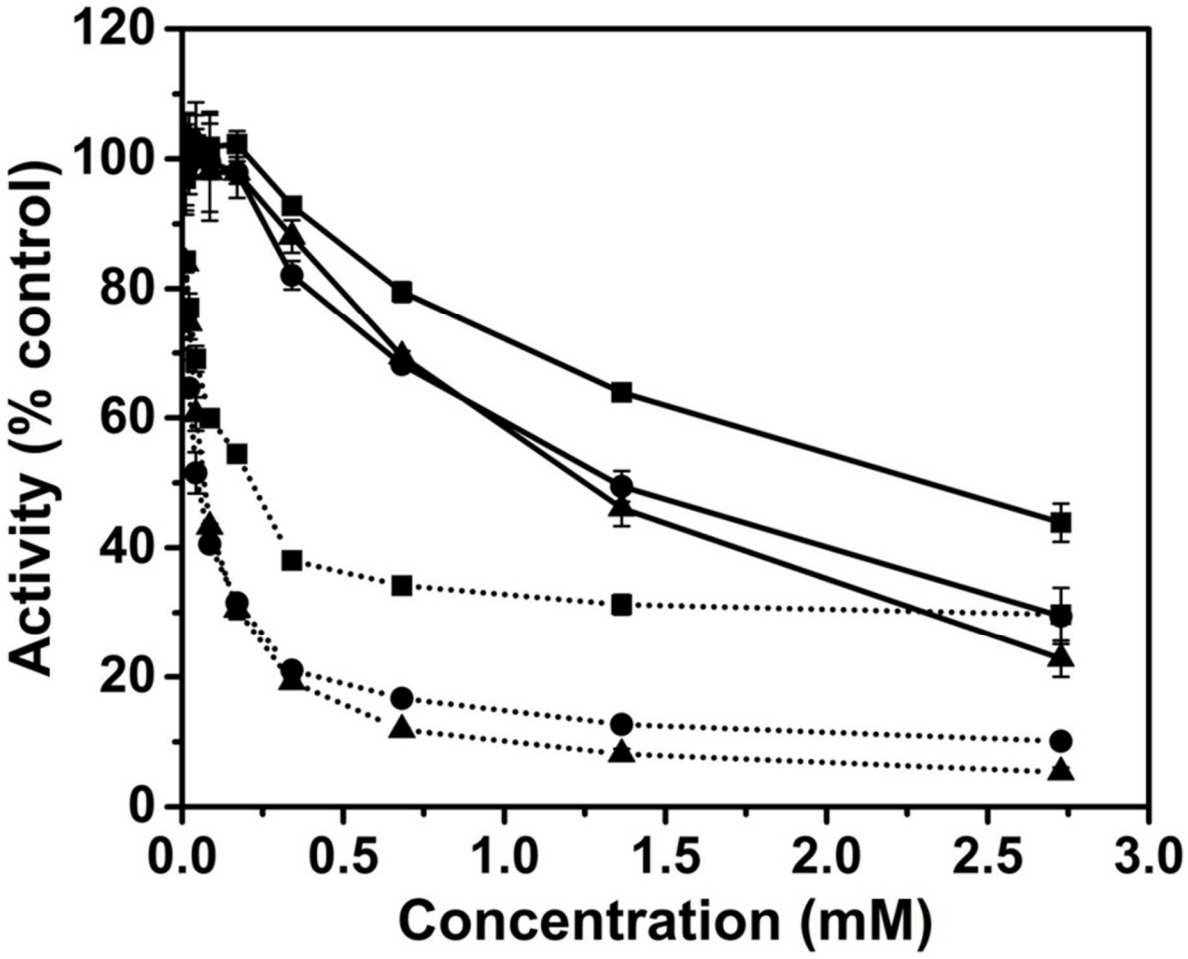

Fig. 5-1. Dose-response curves for Microtox acute toxicity assay: relative light emission of *A. fischeri* at 5 min (■), 15 min (●) and 30 min (▲) as a function of As(III) (solid line) and As(V) (dashed line) concentration.

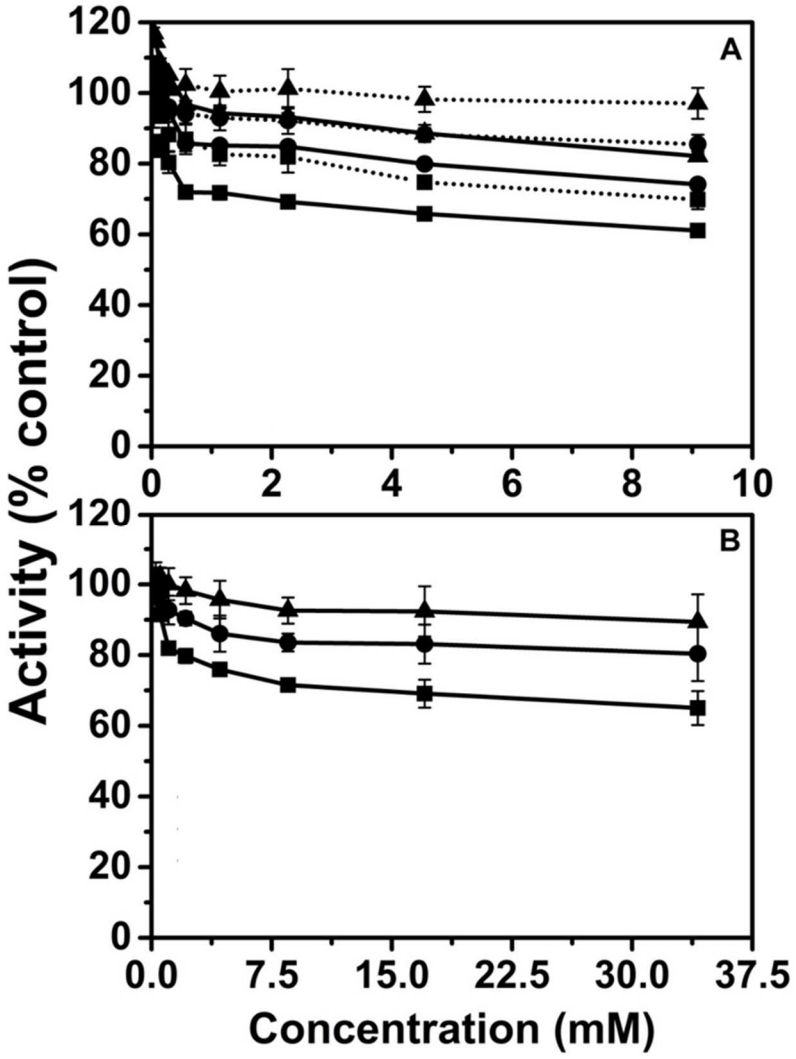

Fig. 5-2. Dose-response curves for Microtox acute toxicity assay: relative light emission of *A. fischeri* at 5 min (■), 15 min (●) and 30 min (▲) as a function of (A) In(III) (solid line) and Ga(III) (dashed line), and (B) corresponding citrate concentration used for In and Ga stock solution preparation.

The relative luminescence activity of *A. fischeri* as a function of In(III), Ga(III) or citrate concentration is displayed in Fig.5-2. Citrate-complexed In(III) and Ga(III) did not cause any greater inhibition of *A. fischeri* luminescence compared to samples exposed to citrate alone at the same concentration present in the corresponding In and Ga samples. Exposure to relative high concentrations citrate resulted in mild inhibition (10.6% inhibition at highest concentration tested, 34 mM after 30 min exposure). No inhibition was observed with Ga(III) at concentrations up to

9.1 mM, and only very limited inhibition for In(III) at high concentrations (4.5 and 9.1 mM) since the luminescence was about 5% lower than that from citrate alone at each exposure time (5, 15, 30 min). Luminescence inhibition in the Microtox experiments with In, Ga and citrate was strongest at 5 min, but thereafter with longer exposure time the inhibition decreased. This trend is in contrast with the increased inhibitory effect observed for As(III) and As(V) with exposure time, as previously described. Marisal et al. [117] has reported some organic compounds could affect the general sensitivity in bioluminescence toxicity assays. Citrate, which was present in these bioassays, could be used as carbon source and substrate in *A. fischeri* metabolism [105, 116]. Intracellular citrate has been reported to induce bioluminescence [118]. Therefore, the elevated light emission may have resulted from the introduction of citrate in this assay.

Studies assessing the susceptibility of *A. fischeri* to Ga(III) and In(III) are widely lacking. We are only aware of one previous study testing the inhibitory impact of In(III) (supplied as $In(NO_3)_3$) to this bacterial species [53]. The reported IC_{50} values at 5 and 15 min were 0.06 and 0.04 mM, a value that is in stark contrast with the low inhibitory effects determined in the present study (9.1 mM only caused 5% inhibition).

5.4.2 Methanogenic toxicity bioassay

Fig. S4 (Appendix B) illustrates the time courses of methane production by an anaerobic sludge consortium exposed to increasing concentrations of the III-V species. The methanogenic toxicity can be determined by comparing the maximum slope of the methane production versus time plots obtained in the bioassays with the toxicants with that of the toxicant-free control. For example, the methane production rate (slope) from the samples exposed to As(III) and As(V) was lower than that from As-free control, indicating that both As species were inhibitory to methanogenic activity. Fig. 5-3 shows the normalized methanogenic activity with respect to the As(III), As(V), In(III) and Ga(III) concentration in the bioassays. The results indicate that both As(III) and As(V) were not toxic at the lowest concentration tested (0.005 mM), however, toxicity was observed at higher concentrations. Both As species caused similar inhibition responses and more than 95% inhibition of methanogenic activity was observed at 0.2 mM. The IC_{50} value calculated for both As(III) and As(V) in this bioassay was 0.02 mM. The inhibition results obtained for As(III) are in close agreement with those reported in a previous study using a similar experimental protocol [119]. On

the other hand, the acetoclastic methanogens in the inoculum utilized in this study were more sensitive to As(V) than previously reported by Sierra-Alvarez and coworkers for a methanogenic mixed culture (IC_{50} > 0.5 mM) [45]. In that study anaerobic sludge treating recycled paper wastewater was used and the period of exposure was shorter (8-24 h). Since As(V) could undergo microbial reduction to As(III) under anaerobic conditions [120, 121], the concentration of the individual As species was tested in methanogenic bioassay. In this study we found that only 10% of As(V) was converted to As(III) after 100 h of exposure. Therefore, the enhanced toxicity was probably not due to a change in As speciation.

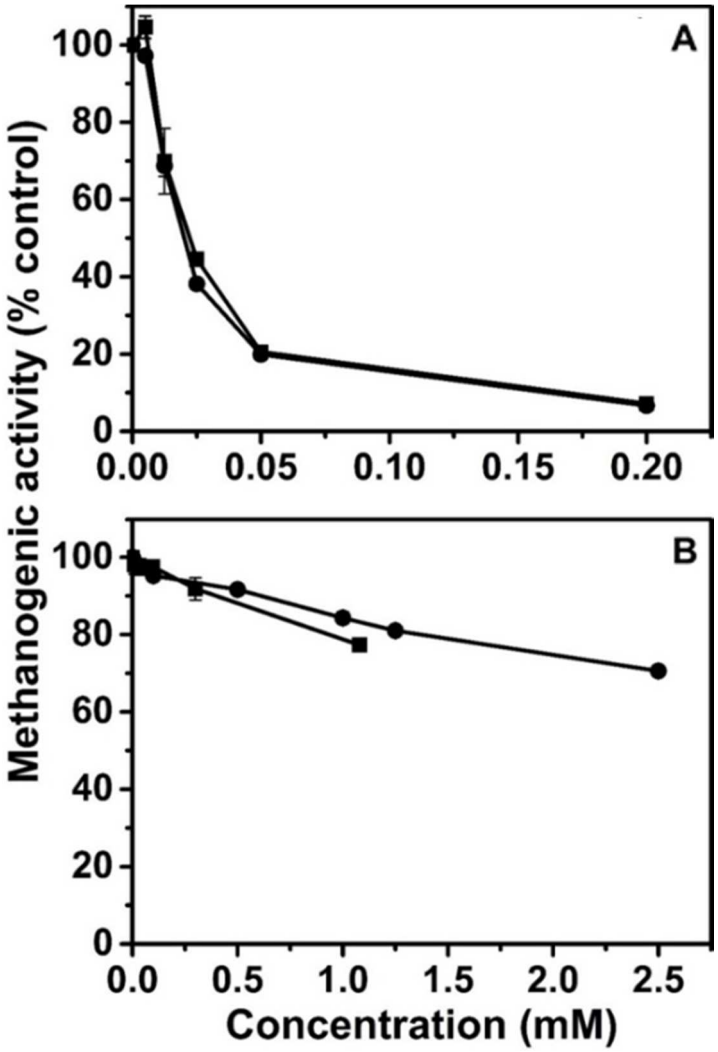

Fig. 5-3. Methanogenic activity of mixed anaerobic culture as a function of the concentration of (A) As(III) (■) and As(V) (●), and (B) In(III) (■) and Ga(III) (●).

In the assays with In(III) and Ga(III), the methanogenic activity only decreased by 22.7% and 29.4%, respectively, at the highest concentration tested. The 20% inhibitory concentration (IC_{20}) values for In(III) and Ga(III) were 0.90 and 1.26 mM, respectively, indicating that In(III) was slightly more inhibitory than Ga(III). Citrate is not inhibitory to methanogens at the concentrations present in these assays.

5.4.3 Aerobic toxicity bioassay

The time courses of oxygen consumption by aerobic activated sludge exposed to increasing concentrations As(III), As(V), In(III) and Ga(III) are summarized in Fig. S5 (*Appendix B*). Dose-response curves for the various metal and metalloid species are shown in Fig. 5-4. In the experiments, aerobic sludge showed very high resistance to all the ionic III-V species as there was no clear reduction of oxygen consumption rate compared to controls. Only when exposed to high concentrations of Ga(III) did a slight inhibition occur (26.7% at 1.8 mM). The IC_{20} value determined for Ga(III) was 0.45 mM. The robustness of the mixed aerobic heterotrophic bacterial community from RAS is likely due to the high diversity of microorganisms in activated sludge enabling at least some cells to be tolerant. The fact that microorganisms tend to form flocs may also attribute to their high resistance to toxicants by avoiding direct exposure to III-V ionic species.

Stasinakis et al. [122] studied inhibition of activated sludge respiration by inorganic As species. Inhibition was found to depend on As speciation and the sludge age. The reported IC_{50} for As(V) was 2.64 mM at sludge age of 10 days. This very high concentration, which is unlikely to occur in wastewater streams, is much larger than the highest concentration used in the present study (0.6 mM). On the other hand, the IC_{50} value calculated for As(III) in the same report was 0.14 mM, indicating a higher sensitivity of the mixed culture used by Stasinakis and coworkers compared to the present study where As(III) only had a negligible effect on aerobic heterotrophic bacterial activity at 0.6 mM. The age of the sludge utilized in the current study (13-18 days) [123] was considerably longer compared to that of the sludge utilized in the former study which could partly account for the difference tolerance observed.

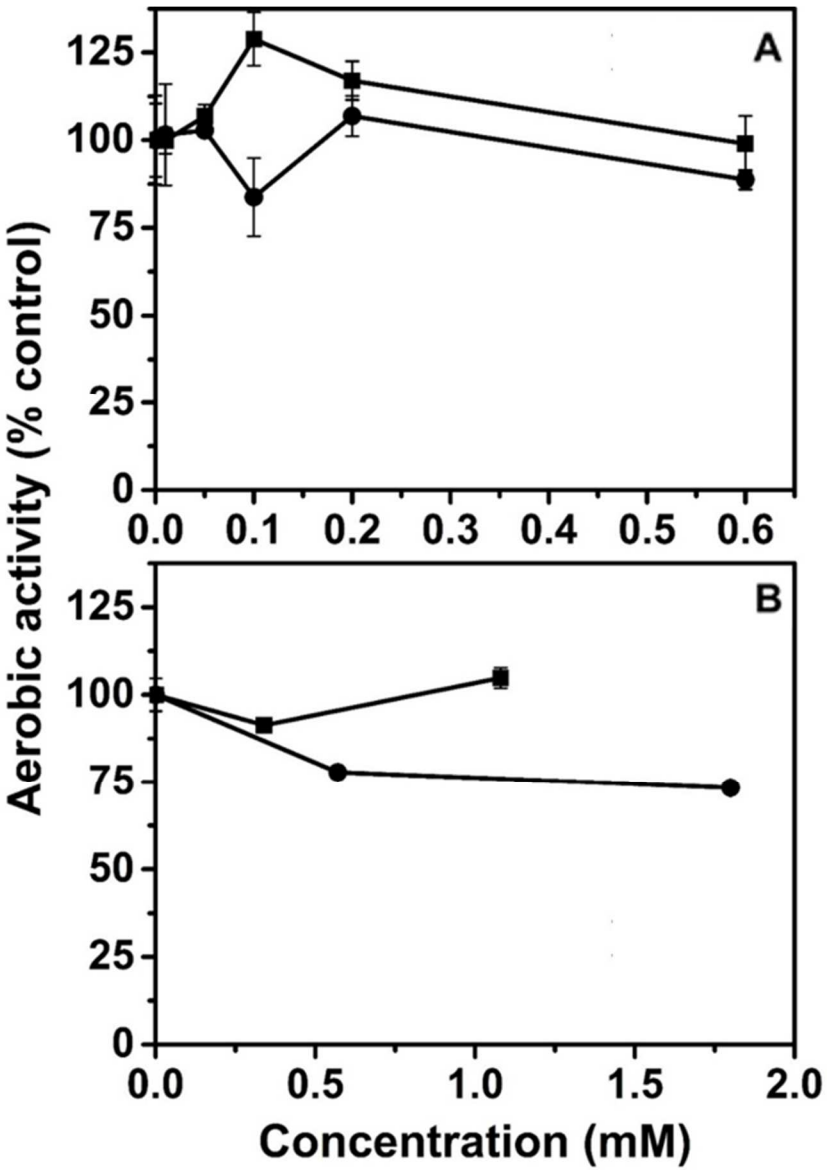

Fig. 5-4. Inhibition of oxygen consumption activity by return activated sludge as a function of (A) As(III) (●) and As(V) (■), and (B) In(III) (■) and Ga(III) (●).

5.4.4 Daphnia toxicity bioassay

Fig. 5-5 shows the dose–response curves determined in acute toxicity bioassays with *D. magna* exposed to In(III) and Ga(III) for 48 h. The results show that In(III) caused higher mortality than Ga(III). Mortality increased rapidly with increased In(III) concentration (90% lethal effect was observed at 1.25 mM) and then, tended to reach 100% gradually. For Ga(III), the dose–response curve was almost linear in the tested concentration range. Mortality was 40% at 1.25 mM and it

reached 95% at 5 mM after 48 h of exposure. The 50% lethal concentration (LC_{50}) values for In(III) and Ga(III) were 0.5 and 3.4 mM, respectively. These results indicate that In(III) and Ga(III) are much less toxic than As species as reported LC_{50} values for As(III) and As(V) are about 0.05 and 0.12 mM, respectively (Table 5-1).

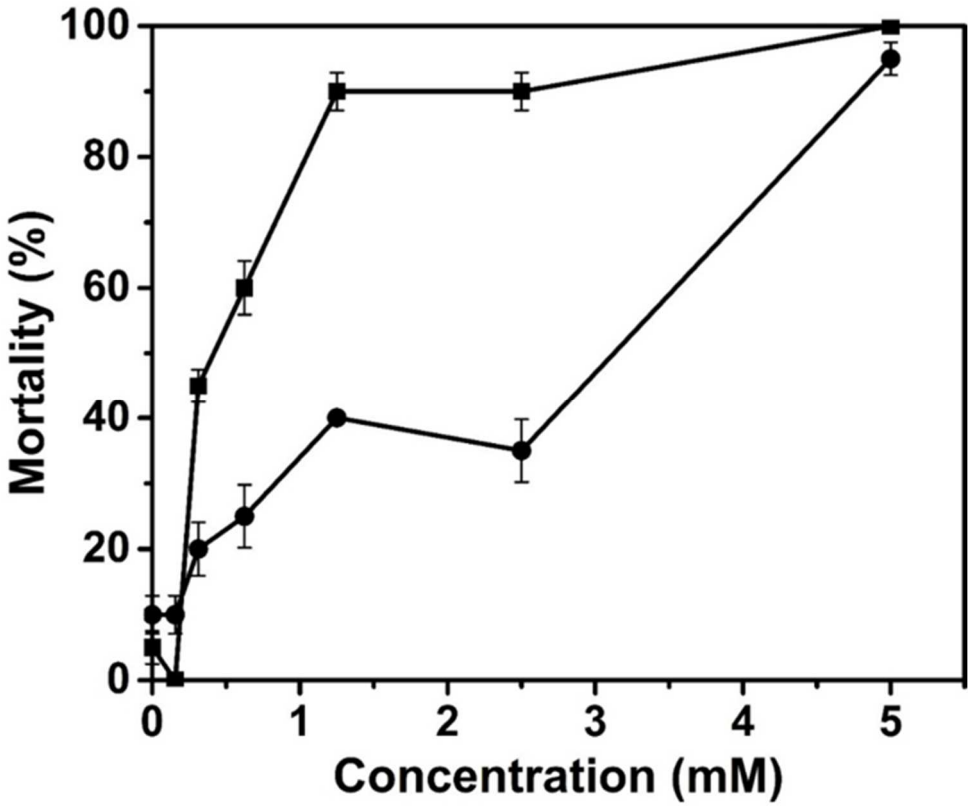

Fig. 5-5. Percent cell mortality of *D. magna* in response to different concentrations of In(III) (■) and Ga(III) (●) after 48-h exposure.

The toxicity of Ga(III) and In(III) to *D. magna* and other daphnids is very poorly understood. We are only aware of a previous study that investigated the lethal impact of In(III) (supplied as $In(NO_3)_3$) on *D. magna* and reported an 24 h-LC_{50} value of 0.23 mM (26.4 mg/L) [53]. The enhanced In(III) toxicity in these assays was likely due to the use of nitrate. It is also important to note that, in the absence of a suitable chelating agent such as citrate, the aqueous solubility of In(III) at neutral pH and ambient temperature is in the low μg/L level (solubility product of $In(OH)_3 = 1.3 \times 10^{-34}$) [40], which is several orders of magnitude lower than the 24 h-LC_{50} value reported in the latter study.

5.4.5 Comparison of As(III), As(V), In(III) and Ga(III) toxicity in different bioassays

The IC_{20} and IC_{50} values determined in the microbial toxicity bioassays as well as the LC_{50} values obtained in the *D. magna* toxicity bioassays conducted in this study are summarized in Table 5-1. The results show that the toxicity of As, In and Ga is dependent on the target organism. Arsenic species showed clear inhibitory effects on different organisms. Acetoclastic methanogens were most sensitive to As inhibition and the IC_{50} value determined for both As(III) and As(V) was very low, 0.02 mM (1.5 mg/L). This concentration is lower than the maximum allowable one-day effluent discharge concentration (2.09 mg/L or 0.03 mM of total As) for facilities manufacturing electronic components, as discussed previously. Compared to As species, In(III) and Ga(III) ions were much less toxic. Among all the organisms tested in this study, *D. magna* was the most sensitive to In(III) and Ga(III), with 48-h LC_{50} values of 0.50 and 3.4 mM, respectively.

The ecotoxicity results reported here for Ga(III) and In(III) are generally in agreement with scant literature previously published for other aquatic species. Recent studies evaluating the toxicity of Ga(III) in marine and brackish fish have shown that these metallic species are only inhibitory at moderate to high concentrations (96-h LC_{50} values ranging from 0.28-0.78 mM) [124, 125]. Toxic effects of Ga(III) and In(III) complexed with citrate were also recently evaluated in a study led by our laboratory using the embryonic zebrafish (*Danio rerio*) model [52]. The authors found that survival and developmental behavior of zebrafish embryos was not significantly affected by the highest tested concentration of 0.9 mM. The embryonic zebrafish was also evaluated for developmental abnormalities associated with exposure to Ga(III) and In(III) and not effect was detected at concentrations up to 0.9 mM. Overall, our results represent the first comprehensive characterization of acute ecotoxicity effects of Ga(III) and In(III) ions towards daphnids and environmentally-relevant microbial populations. The results and insights from this study will contribute to fill a significant knowledge gap regarding the potential ecotoxicity implications of III-V ion contamination. The introduction of III-V materials in the manufacturing of electronic and photovoltaic devices is likely to increase environmental release of these metallic species.

Table 5-1 Summary of inhibitory concentrations for As(III), As(V), In(III) and Ga(III) in different toxicity bioassays.

Compound	Microtox (30min)		Methanogens		Aerobic		Daphnia (48 h)	
(mM)	IC_{20}	IC_{50}	IC_{20}	IC_{50}	IC_{20}	IC_{50}	LC_{20}	LC_{50}
As(III)	0.36	0.90	0.01	0.02	>0.6[b]	>0.6[b]	-	0.05[c]
As(V)	0.02	0.05	0.01	0.02	>0.6[b]	>0.6[b]	-	0.12[c]
In(III)	>9.1[b]	>9.1[b]	0.90	>1.08[b]	>1.08[b]	>1.08[b]	0.22	0.50
Ga(III)	>9.1[b]	>9.1[b]	1.26	>2.5[b]	0.45	>1.78[b]	0.35	3.40

[a] Data reported at 30 min.
[b] The highest concentration tested in this study.
[c] Data reported by He et al. and Wang et al. [112, 114].

5.5 Conclusions

This present study demonstrates that the toxicity of As(III), As(V), In(III) and Ga(III) ions is dependent on the target organisms. Among these ionic III-V materials, both As(III) and As(V) induced acute ecotoxicity after 5 min to 48 h of exposure time in different bioassays. In contrast, In(III) and Ga(III) showed no or mild acute inhibitory effects even at comparatively high concentrations, suggesting that short exposure to these ions might not pose a threat to aquatic organisms in the natural environment unless they are present at relatively high concentrations.

CHAPTER 6 CYTOTOXICITY ASSESSMENT OF ENGINEERED NANOPARTICLES USED IN SEMICONDUCTOR INDUSTRY AND THEIR EFFECT ON ARSENIC TOXICITY TO HUMAN BRONCHIAL EPITHELIAL CELLS THROUGH IMPEDANCE-BASED REAL TIME CELL ANALYSIS

6.1 Abstract

Nanoparticles (ENPs) are increasingly used in different applications due to their interesting technical properties. SiO_2, Al_2O_3 and CeO_2 are important ENPs utilized in a variety of applications, including chemical and mechanical planarization (CMP) processes in semiconductor manufacturing. CMP processes generate high volumes of waste containing abrasive ENPs, therefore, there are concerns about the potential environmental and health risks from these novel materials. In addition, the application of III-V materials (e.g. GaAs, InAs, GaInAs) in semiconductor manufacturing releases toxic arsenic ions in the CMP wastewater. Physico-chemical interactions between CMP ENPs and arsenic ions could affect their fate and toxicity. In this work, the potential cytotoxicity of CMP ENPs to 16HBE14o- human bronchial epithelial cells was evaluated using a novel impedance-based real time cell analyzer (RTCA). In addition, the impact of CeO_2 NPs on cell inhibition by arsenite (As(III)) was also investigated. Both colloidal silica (c-SiO_2) and fumed silica (f-SiO_2) caused cell death and detachment at high concentrations ($\geq$ 250 mg/L). On the other hand, CeO_2 and Al_2O_3 NPs were not inhibitory at concentrations up to 1250 mg/L. As(III) was found to cause severe inhibition (81.3%) of cell viability and proliferation at concentrations as low as 0.5 mg/L As(III). Addition of CeO_2 NPs (250 mg/L) caused a marked decrease in the cytotoxicity of As(III) to only 13.0%, most likely due to the decrease of soluble As(III) caused by sorption onto the NPs. The results demonstrate that the interaction between toxic ions and NPs can affect the fate and toxicity of these materials.

This chapter will be submitted to peer-reviewed journal for publication.

6.2 Introduction

Engineered nanoparticles (ENPs) are intentionally produced nanoscale materials with favorable shape, size and surface properties for desired applications. Due to their novel characteristics ENPs have been widely used in biological (biological labels, drug delivery), environmental (contaminant remediation) and industrial (heat transfer, food industry, personal care products) applications [3, 4]. Nano-sized silica (SiO_2), alumina (Al_2O_3) and ceria (CeO_2) are three important ENPs with the annual global production estimated to be 35,000 to >200,000, 7,500 to <10,000 and 82,500 to >2,400,000 metric tons, respectively [5, 6]. An important use of these ENPs is in chemical and mechanical planarization (CMP) slurries. CMP is a key process applied to polish wafers when fabricating integrated circuits in semiconductor manufacturing [57-60]. As the name implies, the removal of excess materials and surface planarization is accomplished by synergistic combination of chemical and mechanical actions. SiO_2, Al_2O_3 and CeO_2 NPs (20 to 200 nm, 1-5 wt%) are used as abrasive particles in CMP slurries [61]. It has been reported that ENPs used for semiconductor manufacturing accounted for 60% of the $1 billion market for nanomaterials in 2005 [62].

Semiconductor manufacturing requires large amounts of water and ultra-pure water and, consequently, it generates high volumes of waste effluents. A typical wafer production step may cost 0.2 to 0.8 L of CMP slurry, 1 to 2 L rinse water as well as more than 5 L of pad cleaner and rinse water during its production [60]. The total quantity of wastewater generated in CMP process is estimated in the order of 10 L or more per wafer [60]. The waste stream from CMP contains original slurry components together with dissolved and particulate materials removed from the wafer during this process [61]. As reported, the concentration of solids in CMP waste stream varies between 0.05% to 0.5% (wt) [126]. SiO_2 NP is the most widely used abrasive in CMP, its concentration in the wastewater is about 500 to 2,000 mg/L [127]. Regulations controlling water qualities (e.g. turbidity and total suspended solids) could reduce the release of CMP, but NP discharge from semiconductor industry is not directly regulated. So far ecological and human toxicity related to SiO_2, Al_2O_3 and CeO_2 NPs has been evaluated through different *in vitro* and *in vivo* approaches, these studies show their toxicity is related to the particular properties (e.g. particle size) and the assays being utilized (e.g. cell lines, assay end point) [76, 89, 128-132]. Therefore, there are concerns about the potential risks from these NPs to the natural environment and human health.

III-V materials such as indium arsenide (InAs) and gallium arsenide (GaAs) are a group of materials with high electron mobility and low power requirement [32-34], making them favorable semiconductor materials in applications such light emitting diodes (LEDs), liquid crystal displays (LCDs), and photovoltaics biosensors and microcircuits [34-37, 133]. As mentioned previously, the wastewater generated from CMP process contains dissolved materials from the wafer being polished. The concentration of dissolved arsenic in GaAs polishing slurry was reported to be in the range of Soluble arsenic species 1,800-2,400 mg/L [134]. Release of arsenic into CMP wastewater is a concern since it is one of the most notorious contaminants and a well known carcinogen. In addition, since wastewater generated from CMP contains both ENPs and soluble species from the wafer, the interaction between these materials could affect their fate and toxicity. It has been reported that colloidal and fumed SiO_2 NPs have very low capacity for arsenic adsorption [135], while CeO_2 and Al_2O_3 are excellent sorbents for As species [67, 136, 137]. Also, recent studies suggest that some NPs could act as "Trojan horse", which facilitates the transport of adsorbed materials into cells, the following release of toxicant could then result in cytotoxicity [69, 138]. Therefore, there is a need to understand the effect of CMP NPs (CeO_2 and Al_2O_3) on arsenic toxicity.

Conventional techniques designed for analysis of cytotoxicity (e.g. MTT assay) depend on absorbance, fluorescence or luminescence measurements. These methods have a defect as the test results can be greatly obscured when measuring materials (e.g. mesoporous SiO_2 NPs) tend to interfere with optical measurements [139, 140]. Also, single end-point assays provide only limited information about the interaction between testing materials and the target cells. In order to avoid these issues, a real time cell analysis (RTCA) system is used in this work. RTCA is a novel label-free, dynamic and high throughput technique based on impedance measurements. When cells attach to the plate, they create impedance that can be detected by the microelectrodes integrated at the bottom of the 96-well testing plates (E-Plates). In this system, cell biological statuses as cell number, morphology, adhesion all affect impedance measurement. For example, larger cell number, bigger cell size, stronger attachment will all increase the impedance. Because of this, RTCA is able to measure both cell viability and proliferation. In addition, since impedance measurement is not invasive, the cells remain in their normal physiological state during RTCA assays. Otero-González et al. [141]. applied this method to measure the toxicity of 11 inorganic

nanomaterials and the results were compared to those obtained from MTT. The study demonstrated that the RTCA technique is reliable for nanoparticle toxicity screening.

The objectives of this study are to evaluate the potential cytotoxicity of ENPs used in semiconductor industry as well as their effect on As(III) toxicity. To this end, RTCA was applied to assess the cytotoxicity of four ENPs in model slurries including colloidal silica (c-SiO_2), fumed silica (f-SiO_2) cerium oxide (CeO_2) and aluminum oxide (Al_2O_3). The same method was also used to test the toxicity of As(III) in the presence and absence of CeO_2 NP. Human bronchial epithelial cells (16HBE14o-) were used as target cells in this work. Human epithelial cells are usually the primary targets of environmental toxicants for damage [142]. Human lung bronchial epithelial cells are often used as model cell lines to study pulmonary adsorption, transport and permeability to airway exposure [143-145]. These cells are also important as they form a barrier and protect the internal milieu of different organs.

6.3 Materials and Methods

6.3.1 Materials

CeO_2 NP powder (20 nm) was from MTI Corporation (Richmond, CA, USA), NP characterization is reported elsewhere [146]. Four industry relevant model CMP slurries, including c-SiO_2, f-SiO_2, CeO_2 and Al_2O_3 were acquired from a major slurry manufacturer [60]. c-SiO_2 and f-SiO_2 slurries were prepared in acetic acid (< 1 wt%) and potassium hydroxide (< 1 wt%); there is no additives reported for CeO_2 slurry; Al_2O_3 slurry was provided with dilute nitric acid (< 1 wt%). According to the supplier, these slurries have the simplest formulation to generate stable suspensions of ENPs. They do not share the complexity of commercial CMP slurries, which normally contain additives such as oxidizers, chelating agents and biocides [57, 58, 63]. The composition, morphology and physico-chemical properties of these inorganic oxide NPs have been studied previously in detail [60].

Minimum essential medium with Earle's salts (MEM) were purchased from Invitrogen (Carlsbad, CA, USA). Fetal bovine serum (FBS) and sodium meta-arsenite ($NaAsO_2$, ≥ 90%) were from Sigma-Aldrich (St Louis, MO, USA). Before experiments, NP dispersions and As(III)

solution with designed concentrations were prepared in MEM (with 5% FBS), the pH of the stocks was adjusted to about 7.0 using diluted NaOH or HCl.

6.3.2 Cell culture

16HBE14o-, an adherent and immortalized human bronchial epithelial cell line was obtained from California Pacific Medical Center Research Institute (San Francisco, CA, USA). The growth condition for the cells has been described previously [147]. In brief, cells were grown in tissue culture flasks coated with a collagen/fibronectin/bovine serum albumin (CFB) matrix in a controlled growth medium (CGM) that contains MEM supplemented with 10% (v/v) FBS, 2mM glutamax, penicillin and streptomycin at 37°C in a 5% CO_2 atmosphere. Subsequently, the cells were transferred to assay plates with a low serum medium containing 5% FBS.

6.3.3 RTCA assay

First 16HBE14o- cells were plated onto 96-well E-plates (Roche Applied Science, Indianapolis, IN, USA) coated with CFB with a cell density of ~100,000 cells/well. Then the cells were incubated for about 16 h at 37°C and 5% CO_2, where impedance was continuously monitored using the RTCA device (xCELLigence, ACEA Biosciences, San Diego, CA, USA). Finally, 50 µL of NP dispersion was supplemented into the wells with 150 µL cell culture (so the final concentration of NPs was one quarter as compared to the stock). Cell responses to NPs were measured and recorded every 15 min for 24 h. In the experiments, assays were performed in quadruplicate, NP-free controls were run in parallel.

In this assay, the measured impedance is expressed as Cell Index (CI). The CI is defined as $(R_n\text{-}R_b)/15$, where R_n is the impedance of the well when it contains cells, while R_b is the background impedance with only the medium. Normalized CI (NCI) was then calculated for data analysis and results comparison, using the following equation:

$$NCI_t = \frac{CI_t}{CI_0} \qquad (6-1)$$

where CI_t is the CI at any time t and CI_0 is the CI at the time of NPs dosing (where NCI is equal to 1). The percentage response and inhibition were calculated using the following equations:

$$Response(\%) = \frac{NCI(sample) - 1}{NCI(control) - 1} \times 100 \quad (6-2)$$

$$Inhibition(\%) = \frac{NCI(control) - NCI(sample)}{NCI(control) - 1} \times 100 \quad (6-3)$$

where the percentage response was calculated as the ratio between the slope of the samples treated with NPs and the slope of NP-free control. In this study, when calculated percent inhibition values were higher than 100% (NCI of the samples < 1), they were reported as 100%; when NCIs of the samples were higher than the control, percent inhibition values were reported as 0%.

6.3.4 As(III) toxicity in the presence/absence of CeO_2 NPs

In this experiment, As(III) solution was first mixed with CeO_2 NPs for 48 h to attain adsorption equilibrium, then the mixture was used for RTCA assay. Briefly, As(III) solutions at different concentrations (2, 10 and 20 mg/L as As) were prepared in 10 mL MEM (pH about 7.0) in 50 mL centrifuge tubes and commercial CeO_2 NPs (1g/L) were added into each tube. Then the dispersions were mixed for 48 h using an orbital shaker at 150 rpm at room temperature (25 °C). NP-free As(III) solutions were run in parallel during this process. After this pre-adsorption step, the cytotoxicity of As(III) in the presence and absence of CeO_2 NPs was evaluated using the same assay described in the previous section (*Section 6.3.3*).

In addition, at the end of the adsorption step, the suspensions/solutions were collected for analysis of dissolved As(III). The samples were first centrifuged at 13,300 g for 10 min, and then the supernatants were filtered through 25-nm membrane filters in order to remove all the particles. The concentration of As in the filtrates was determined by inductively coupled plasma - optical emission spectroscopy (ICP-OES, 5100, Agilent Technologies, Santa Clara, CA, USA) at a wavelength of 188.98 nm.

6.4 Results and discussion

6.4.1 Cytotoxicity of CMP NPs to 16HBE14o- cells

The cytotoxicity of ENPs used in CMP slurries to 16HBE14o- human lung bronchial epithelial cells was evaluated using RTCA. In the experiments, as shown in Fig. S6-S9 (*Appendix C*), the

cells were first incubated overnight until they reached required number; cell response to the model slurries were monitored and recoded every 15 min for 24 h. Fig. 6-1 shows the toxic effects of c-SiO_2 NPs and f-SiO_2 NPs on 16HBE14o- cells. After the introduction of the ENPs, the cells first showed a response due to the mixing. As mentioned, in RTCA system, CI value is proportional to cell number and morphology [148]. A decreased cell index (negative slope) indicates cytotoxicity leading to cell death and toxicity induced detachment [149, 150]; while a positive slope (yet lower than the slope of control) indicates inhibitory effects on cell viability and proliferation. In this case, high concentrations of c-SiO_2 NPs (250 and 500 mg/L) showed clear toxicity in the experiment as the slopes of the curves became negative immediately after NP dosing (Fig. 6-1A). On the other hand, low concentration of c-SiO_2 NPs (5, 25 and 50 mg/L) did not show any effect on human lung cells as the sample behaved almost the same as compared to the control. Similar with c-SiO_2, f-SiO_2 NPs led to cell detachment at 250 and 500 mg/L about 6 and 10 h after NP introduction; while no effects were observed at lower concentrations. In the experiments, soluble species in these two SiO_2 slurries did not show any inhibitory effects (Fig. S10, *Appendix C*). These results confirmed that the toxicity from c-SiO_2 and f-SiO_2 slurries was induced by the NPs dispersed in the fluids. However, these NPs are inhibitory only at concentrations much higher than their corresponding environmentally relevant levels [5, 6].

The cytotoxicity of SiO_2 NPs to 16HBE14o- cells has been reported in a previous RTCA study [141]. Commercial SiO_2 NPs (10-20 nm) resulted in cell detachment at concentrations equal or higher than 200 mg/L. At 300 mg/L, cell death occurred after 3 h of NP dosing. These results are generally in agreement with what we have observed in this work. *In vitro* studies have shown that SiO_2 NPs induced toxicity to human cells is related to reactive oxygen species (ROS), which could cause oxidative stress and inflammatory response [22, 80, 151]. These studies demonstrated the role of particles size in ROS production, showing NPs with smaller particles sizes are more likely involved in oxidative stress due to their high specific surface area. The primary particle size of the c-SiO_2 and f-SiO_2 NPs used in this study was about 36 nm [60]. In the experiments, f-SiO_2 NPs showed higher toxicity than c-SiO_2, after 24 h of exposure, 30 mg/L f-SiO_2 led to 88% inhibition. This may be related to its higher catalytic and surface redox reactivity than c-SiO_2 as reported from previous studies [60, 152].

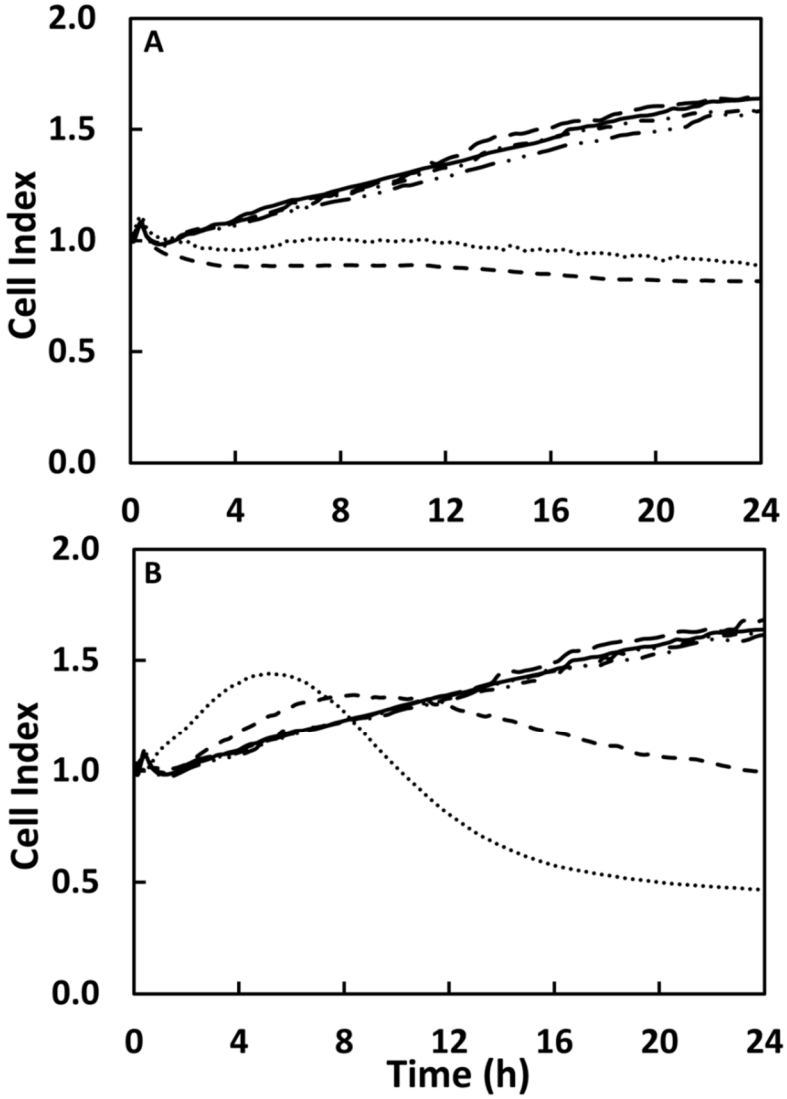

Fig. 6-1. Dynamic cytotoxicity response of human bronchial epithelial cells (16HBE14o-) exposed to different concentrations of NPs using RTCA system. (A): c-SiO_2 NP concentrations (mg/L): 0 (──), 5 (─ • • ─), 25 (─ ─), 50 (─ • ─), 250 (- - -) and 500 (••••). (B): f-SiO_2 NP (mg/L): 0 (──), 5 (─ • • ─), 25 (─ ─), 50 (─ • ─), 250 (- - -) and 500 (••••).

In the experiments, there was no evidence showing cytotoxicity from CeO_2 and Al_2O_3 slurries at concentrations up to 1250 mg/L (Fig. 6-2). Exposure to the highest concentrations of CeO_2 and Al_2O_3 NPs after 24 h only led to about 20% inhibition of cell viability and proliferation. Wei et al. [153] has performed *in vitro* experiments to study the cytotoxicity of Al_2O_3 NPs (10 and 50 nm) on human lung epithelium cells (A549). They found that Al_2O_3 NPs were inhibitory at the

highest concentration level (10 g/L) tested in their study, while 1 g/L of Al_2O_3 NPs (both 10 nm and 50 nm) did not show any effects on cell viability and proliferation. This result is in agreement with what we've observed in this study [154]. Toxicity results reported in the literature for CeO_2 NPs are often contradictory. Nanoscale CeO_2 particles were found to induce apoptosis in human blood monocytes [155]. Due to the chemical transformation between Ce^{3+} and Ce^{4+}, previous research suggests that CeO_2 NPs could scavenge electrons and decrease natural ROS generation [156]. For example, Rubio et al. [157] confirmed the antioxidant properties of CeO_2 NPs using human epithelial lung cell line BEAS-2B.

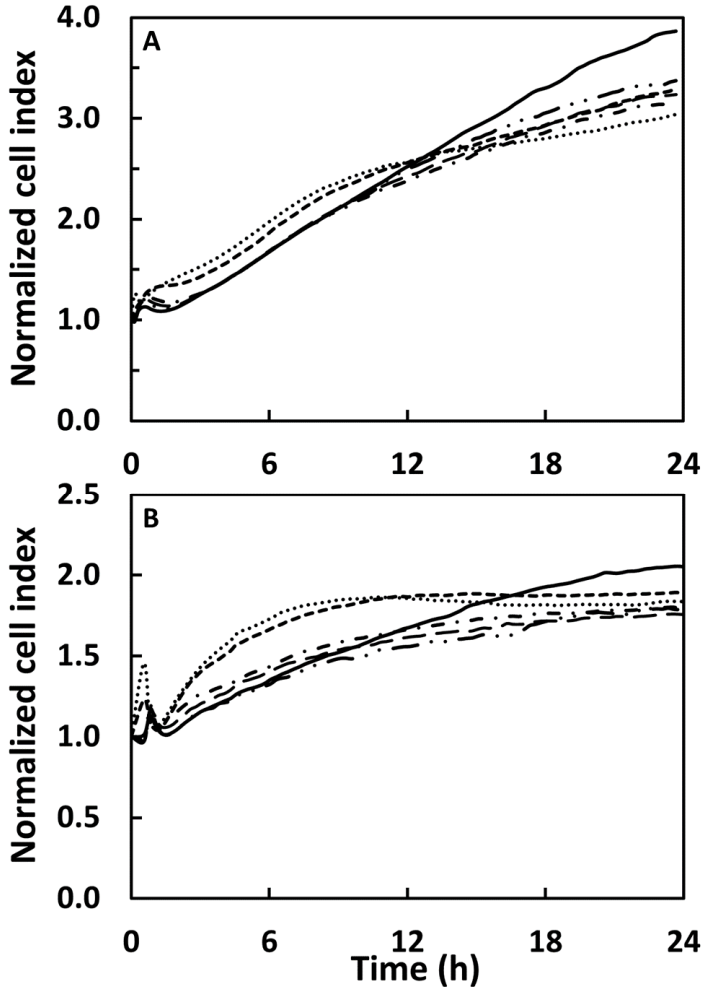

Fig. 6-2. Dynamic cytotoxicity response of human bronchial epithelial cells (16HBE14o-) exposed to different concentrations of NPs using RTCA system. (A): CeO_2 NP concentrations (mg/L): 0 (——), 12.5 (— • • —), 62.5 (— —), 125 (— • —), 625 (- - -) and 1250 (••••). (B): Al_2O_3 NP (mg/L): 0 (——), 12.5 (— • • —), 62.5 (— —), 125 (— • —), 625 (- - -) and 1250 (••••).

The stability of the NPs in the bioassay medium (MEM) was evaluated by determining the particle size distribution (PSD) and ζ-potential. The hydrodynamic diameter of c-SiO_2 NPs measured through dynamic light scattering (DLS) was -46.5 ± 0.3 nm; the ζ-potential was determined to be -27.4 ± 0.3 mV. This result indicates c-SiO_2 NP suspensions were fairly stable in the experiments. On the other hand, particle agglomeration was observed for all the other NPs. The ζ-potential of f-SiO_2 was -8.8 ± 2.3 nm; the average particle size of the NPs was 458.0 ± 12.2 nm, which was more than 10 times higher than the reported primary size (about 36 nm). ζ-potentials for CeO_2 NPs and Al_2O_3 NPs were 0.3 ± 0.9 mV and -7.7 ± 1.4 mV, respectively. These data indicate the NPs were unstable in the suspension. NP aggregation and sedimentation was observed for CeO_2 NPs and Al_2O_3 NPs with hydrodynamic diameters of 4482 ± 127 nm and 6852 ± 806 nm, respectively. These values were more than 100-fold higher compared to their reported primary size of the NPs (about 40 nm). This aggregation and sedimentation might decrease their surface reactivity and bioavailability and subsequently lower their toxicity.

6.4.2 As(III) toxicity to 16HBE14o- cells in the presence and absence of CeO_2 NPs

As mentioned previously, CMP wastewater is a mixture contains both abrasive NPs and soluble materials (such as As(III)) removed from the wafer surface. CeO_2 NP is a very good sorbent for As(III), therefore, it is important to understand whether this interaction could affect the toxicity of As(III). In this work, the cytotoxicity of As(III) to 16HBE14o- human lung bronchial epithelial cells was evaluated in the presence and absence of CeO_2 NPs (20 nm) as described in *Section 6.3.4*. Fig. 6-3 shows the cell response to As(III) solutions with/without CeO_2 NPs (250 mg/L) as a function of exposure time. In the experiment, CeO_2 NPs were not toxic to the cells, as the NCI values from the sample exposed to CeO_2 NP alone were very close to those from As(III) and NP free control. Particle size distribution of the NPs in MEM is summarized in Fig. S11. The average hydrodynamic diameter of the NPs was 1463.0 ± 108.9 nm. As(III) alone showed clear toxicity at relatively low concentrations. Cell death and detachment was observed for the samples exposed to 2.5 mg/L and 5.0 mg/L at about 5 h after NP dosing. Fig. 6-4 summarizes percentage inhibition as a function of As(III) concentration at different exposure time. It is clear the cytotoxicity induced by As(III) increases with exposure time. At 12 h, the 50% inhibition concentration (IC_{50}) of As(III) was 3.5 mg/L; at 24 and 48 h, the IC_{50} is about 0.3 mg/L. The toxic

effects of inorganic As(III) on human lung bronchial epithelial cells have been widely reported [145, 158] . For example, Cara et al. [159] found that As(III) altered wound-induced ATP-dependent Ca^{2+} signaling pathways in human bronchial epithelial cell line (16HBE14o-) under environmentally relevant levels (< 4 μM; ~0.3 mg/L).

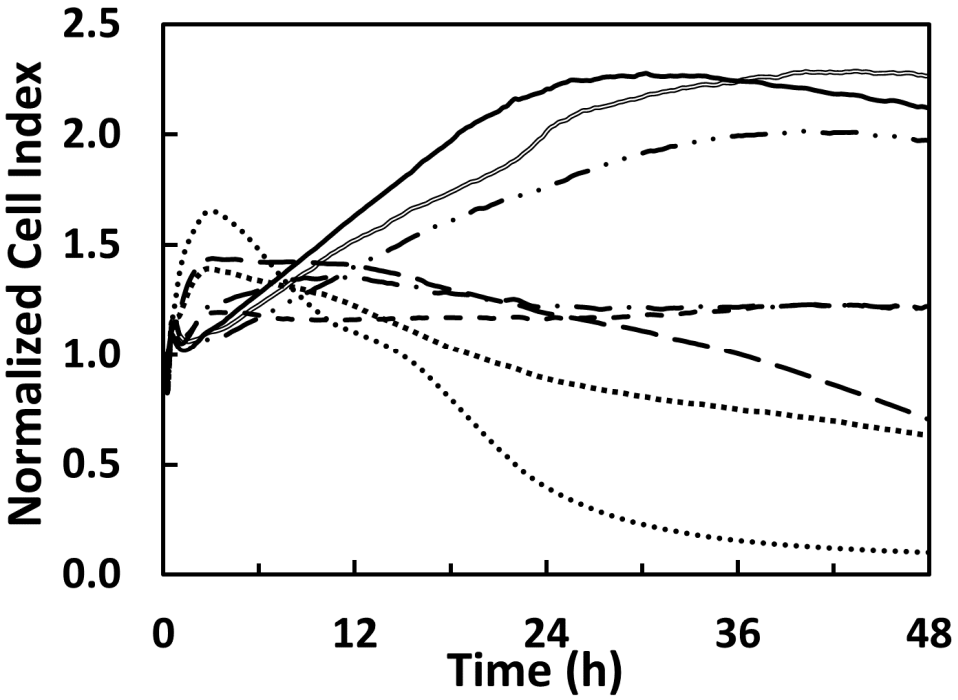

Fig. 6-3. Dynamic cytotoxicity response of human bronchial epithelial cells (16HBE14o-) exposed to different concentrations of As(III) in the presence and absence of 250 mg/L CeO_2 NPs. Before the experiment, As(III) solution and CeO_2 NPs were first mixed for 2 days in the bioassay medium (MEM) in order to attain adsorption equilibrium. Legends: As(III) and NP free control (——), control with only 250 mg/L of CeO_2 NPs (═══), 5 mg/L As(III) (••••), 5 mg/L of As(III) with CeO_2 NPs (▪▪▪▪), 2.5 mg/L of As(III) (— —), 2.5 mg/L of As(III) with CeO_2 NPs (- - -), 0.5 mg/L of As(III) (— • • —) and 0.5 mg/L of As(III) with CeO_2 NPs.

In the experiment, CeO_2 NPs decreased the toxicity exerted by As(III), as the NCI values from the sample with the presence of CeO_2 NPs were much higher than those treated with only As(III). This was most obvious for the samples exposed 0.5 mg/L As(III). At this concentration, As(III) showed clear toxicity that resulted in cell detachment; however, with the presence of CeO_2, only limited inhibitory effect on cell proliferation was observed. Furthermore, as showing in Fig.

6-5, the longer exposure time led to more significant effect of As(III) detoxification. At 48 h, 0.5 mg/L As(III) resulted in 81.3% inhibition on cell viability and proliferation, while the number decreased to only 13.0% with the presence of CeO_2.

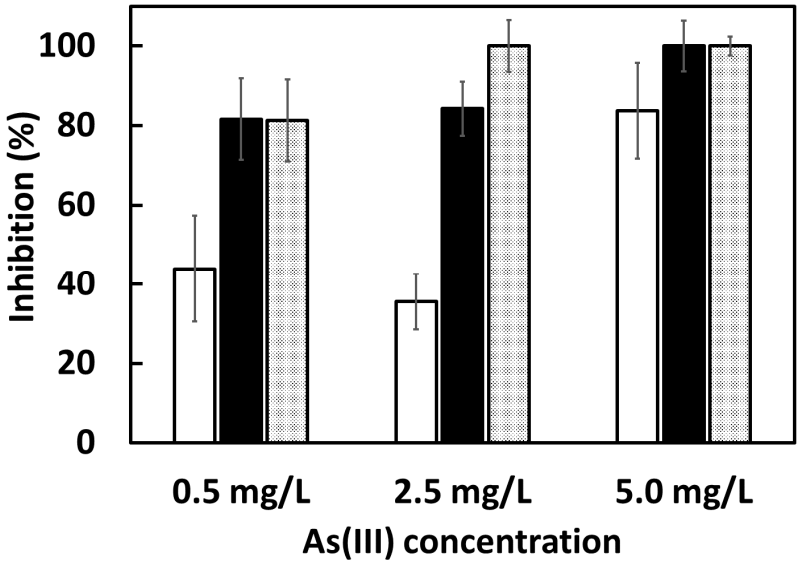

Fig. 6-4. Inhibition (%) of As(III) solutions on human bronchial epithelial cells (16HBE14o-) at different exposure time: 12 h (empty bar), 24 h (filled bar) and 48 h (dotted bar).

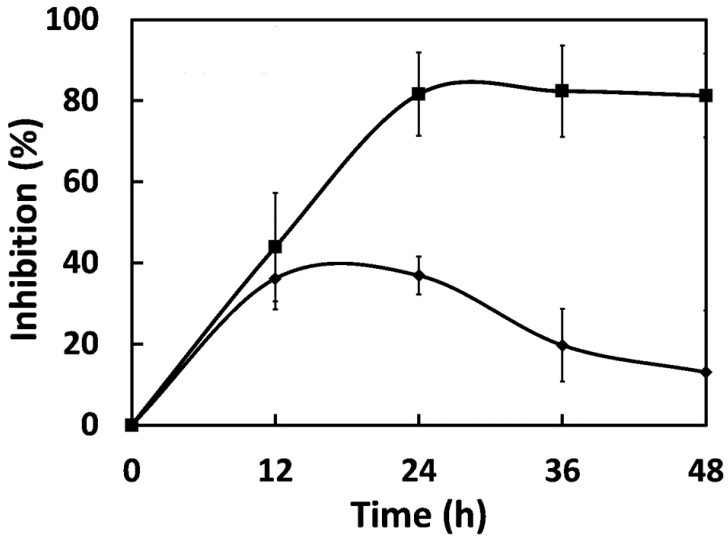

Fig. 6-5. Arsenic inhibitory effects on human bronchial epithelial cells (16HBE14o-) cells in the presence and absence of CeO_2 NPs (250 mg/L) as a function of time: 0.5 mg/L As(III) (■) and 0.5 mg/L As(III) with CeO_2 NPs (♦).

The observed detoxification effect was likely related to As(III) adsorption onto the CeO_2 NPs. Table 6-1 shows the concentrations of dissolved As(III) determined in liquid samples incubated for 2 days with/without CeO_2 NPs (250 mg/L). The results confirm that CeO_2 NPs have a high capacity for As(III) adsorption, and that addition of CeO_2 NPs resulted in a marked decrease of the concentration of dissolved As. For example, soluble As was reduced from 0.5 to 0.03 mg/L after 2 days. This result is in agreement with recent studies showing that nano-sized CeO_2 is a good As(III) sorbent [67, 137]. Several recent studies indicate that some inorganic oxide NPs could act as a "Trojan horse", facilitating the transport of materials adsorbed onto NPs into cells and that subsequent release of the toxicant inside the cell could result in cytotoxicity. For example, Hu et al. (2012) [69] verified the accumulation of As(V) on Al_2O_3 NPs and reported that 48 h mortality of *Cerodaphnia dubia* at 2.4 mg/L of As(V) increased from 22.5% without NPs to 95% with 25 mg/L of Al_2O_3 NPs. Likewise, the same group found that CeO_2 NPs increased the toxicity of Pb(II) to *C. dubia* [160]. On the other hand, several studies have shown that various nanomaterials (e.g. single-walled carbon, carbon nanotubes and TiO_2 NPs) can hinder the transport and some pollutants (cadmium and organic compounds such as phenanthrene, pyrene and pentachlorophenol) into cells/organisms and reduce their toxicity [161-165]. Hartmann et al. (2009) [162] demonstrated that the ecotoxicity of cadmium to algae was reduced in the presence of TiO_2 NP due to decreased Cd bioavailability resulting from Cd^{2+} sorption/complexation to TiO_2 surface. This finding is in agreement with the results acquired in this work.

Table 6-1 Concentrations of dissolved arsenic species for the samples pre-mixed with/without CeO_2 NPs.

Initial As(III) and NP concentration*	Final dissolved As concentration (mg/L)
5.0 mg/L of As(III)	4.93
5.0 mg/L of As(III) with 250 mg/L of CeO_2 NP	1.36
2.5 mg/L of As(III)	2.47
2.5 mg/L of As(III) with 250 mg/L of CeO_2 NP	0.29
0.5 mg/L of As(III)	0.50
0.5 mg/L of As(III) with 250 mg/L of CeO_2 NP	0.03

*As(III) solutions were contacted with CeO_2 NPs for days at room temperature (25°C) to attain sorption equilibrium.

6.5. Conclusions

In summary, it is evident that RTCA system is a powerful tool in studying the effects of potential toxicants on adherent cells as this high throughput, label-free, impedance-based methodology allows monitoring of cell viability and proliferation in real time. The results indicate the NPs used in CMP are generally safe for human health, as they only result in toxicity at levels much higher than the relevant concentrations in the environment. The adsorption of As(III) on CeO_2 NPs significantly lowered the soluble As species in the solution, reducing their bioavailability and subsequently led to a detoxification effect. This result demonstrates that the interaction between toxic ions and NPs could affect their fate and toxicity.

In CMP wastewater, As(V) could be the predominant As species with the presence of oxidants (used as additives in CMP slurry). Therefore, it is meaningful to test the toxicity of As(V) in the presence and absence of CeO_2 NPs. In addition, Al_2O_3 NP is another important abrasive using in CMP that has high affinity for As adsorption. Therefore, it is important to understand the interactions between Al_2O_3 NPs and ionic As(III)/As(V) and the effect on their fate and toxicity.

CONCLUSIONS

This work investigated the potential environmental and health risks from ENPs and III-V materials used in semiconductor industry. The toxicity of four models slurries containing c-SiO_2, f-SiO_2, CeO_2 and Al_2O_3 ENPs were tested using different bioassays. We found these slurries did not induce acute toxicity *A. fischeri* and 16HBE14o- human lung bronchial epithelial cells at concentrations much higher than their environmentally relevant levels, indicating these ENPs are generally safe for the natural environment and human health after their release.

NP transport in porous media is important in controlling their fate in the environment. Laboratory scale column experiments indicate the retention of SiO_2 NPs is strongly dependent on the ionic strength of the solution and the nature of the granular media. High ionic strength led to SiO_2 NP destabilization and facilitated their capture in sand, while lowed ionic strength resulted in NP release of once retained SiO_2 NPs in sand and anthracite. The experimental data and model simulation reveals GAC is an interesting material for SiO_2 NP filtration as GAC has large number of available sites for NP retention due to the high surface area and intricate porous structure.

Among the ionic III-V materials, In(III) and Ga(III) showed no or mild acute inhibitory effects at very high concentration (about 100 mg/L) in different ecotoxicity assays using *A. fischeri*, methanogens, mixed aerobic heterotrophic culture and *D. magna*, suggesting short exposure to these ions might not pose a threat to aquatic organisms in the natural environment unless they are present at relatively high concentrations. On the other, the results show that arsenic could induce toxic effects to microorganisms (*A. fischeri* and methanogens) and human cells (16HBE14o-) under current discharge limit set for semiconductor industry.

Finally, this work demonstrated that the adsorption of As(III) on CeO_2 NPs significantly lowered the soluble As, reducing its bioavailability and, subsequently, leading to As(III) detoxification. Since CMP wastewater contains both ENPs and soluble species removed from wafer surface, there is a need to understand the interactions between these materials and how they could affect their fate, transport, bioavailability and toxicity.

In summary, this dissertation provides methodology and experimental results that can help better understanding the potential environmental and health risks from ENPs and III-V materials used in semiconductor industry. The results indicate that the ENPs used in semiconductor industry

(SiO_2, CeO_2 and Al_2O_3) are not expected to cause acute toxicity at environmentally relevant concentrations (< 1 mg/L). Among the III-V ionic species, arsenic could induce ecotoxicity and damage human health. In addition, this work verifies that the interactions between ENPs and ionic III-V species in CMP wastewater could alter the behavior and toxicity of these materials. In practice, CMP slurries also contain additives such as buffers, complexing agents, oxidizers and corrosion inhibitors as well as particulate materials removed from wafer surface, therefore, this study is only the first step to understand the potential risks from real effluents discharged from semiconductor manufacturing.

APPENDICES

APPENDIX A. Supplementary data for CHAPTER 4

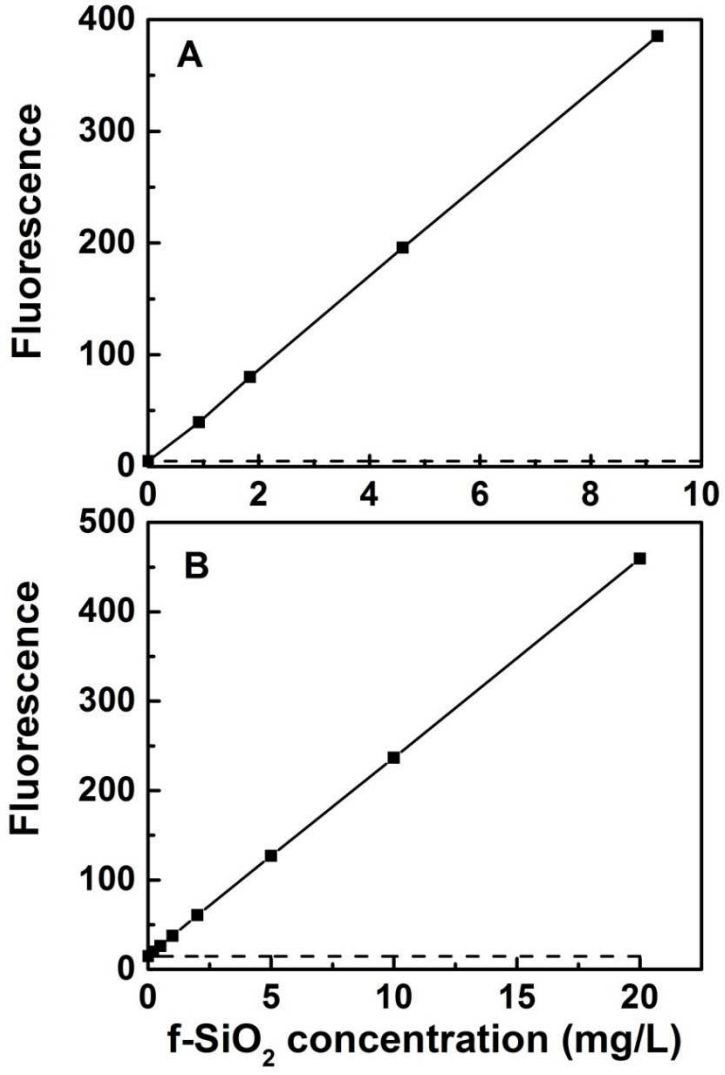

Fig. S1. Calibration curve of f-SiO_2 NPs fluorescence (■) as a function of SiO_2 concentration: (A) fluorescence measured in a fluorometer cell with a path length of 4 mm, (B) calibration made in the flow through cell (10 mm path length) used in the column tests. The dashed line indicates the fluorescence of the background solution (DI water).

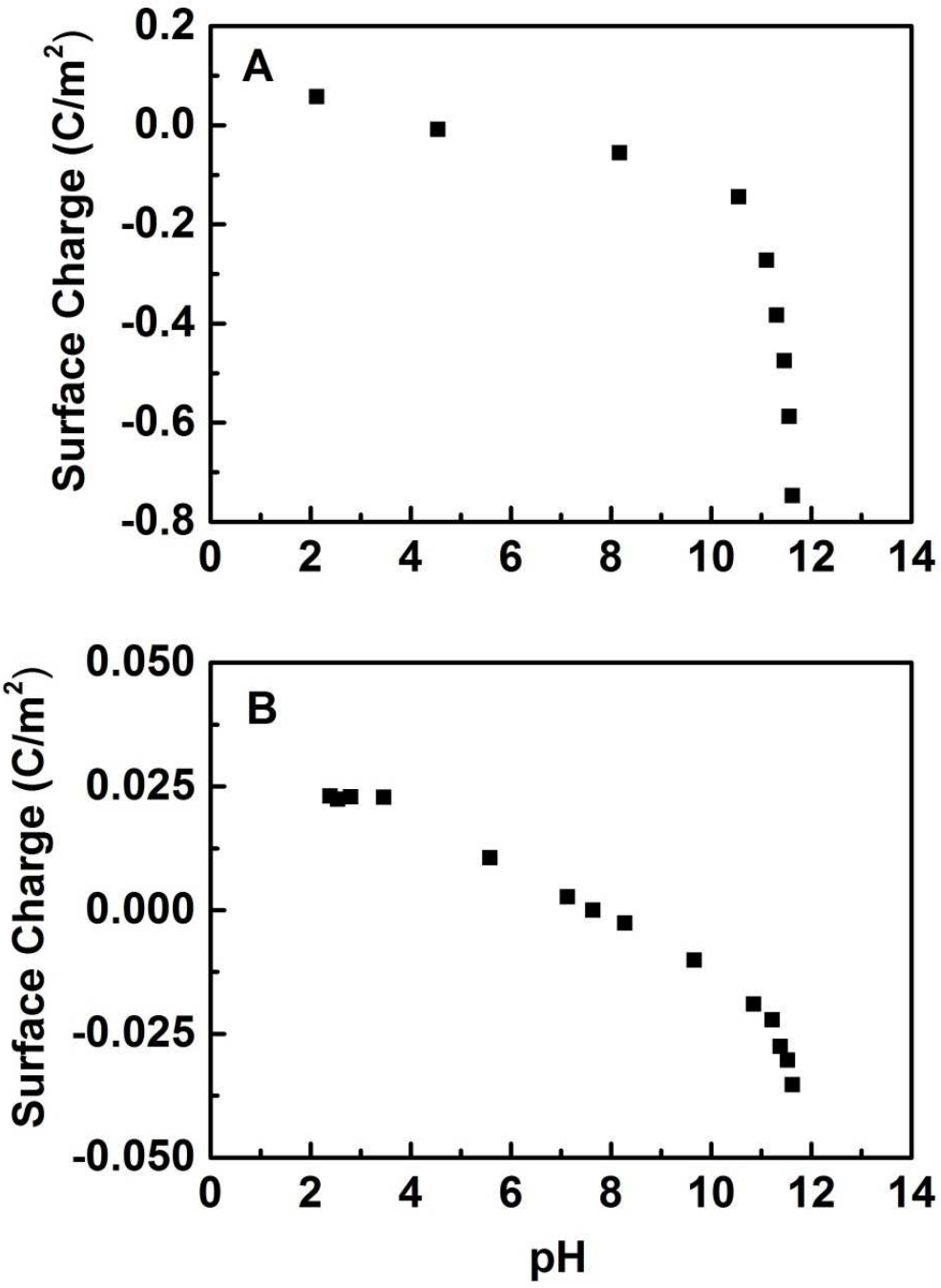

Fig. S2. Surface charge of anthracite (A) and granular activated carbon (B) at different pH values.

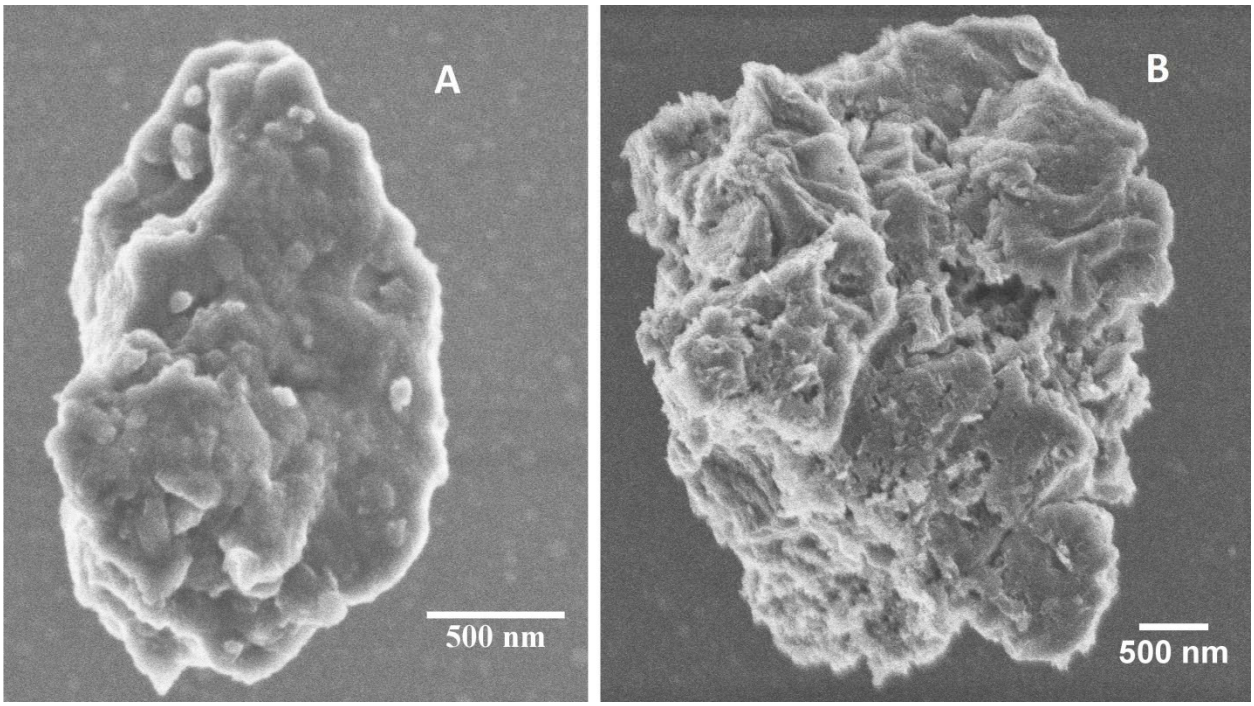

Fig. S3. Scanning electron microscopy (SEM) images of the anthracite (A) and granular activated carbon (B) utilized in this study.

APPENDIX B. Supplementary data for CHAPTER 5

Methanogenic toxicity bioassay

Basal medium was prepared in demineralized (DI) water and contained (in mg/L): CH_3COONa (2561), NH_4Cl (280), $NaHCO_3$ (3000), K_2HPO_4 (250), $CaCl_2•2H_2O$ (10), $MgCl_2•6H_2O$ (100), $MgSO_4•7H_2O$ (100), yeast extract (100) and 1 mL of trace elements (Table S1). The pH of the medium was adjusted to 7.0-7.2.

Aerobic toxicity bioassay

Basal medium was prepared in DI water contained (in mg/L): CH_3COONa (1921.9), NH_4Cl (280), $NaHCO_3$ (4000), K_2HPO_4 (250), $CaCl_2•2H_2O$ (10), $MgCl_2•6H_2O$ (100), $MgSO_4•7H_2O$ (100), yeast extract (100) and 1 mL of trace elements solution (Table S1). The pH of the medium was adjusted to 7.0-7.2.

Table S1 Composition of the trace elements solution.

Compound	Concentration (mg/L)
H_3BO_3	50
$FeCl_2•4H_2O$	2000
$ZnCl_2$	50
$MnCl_2•4H_2O$	50
$(NH_4)_6Mo_7O_{24}•4H_2O$	50
$AlCl_3•6H_2O$	90
$CoCl_2•6H_2O$	2000
$NiCl_2•6H_2O$	50
$CuCl_2•2H_2O$	30
$NaSeO_3•5H_2O$	100
EDTA	1000
Resazurin	200
36% HCl	1 mL

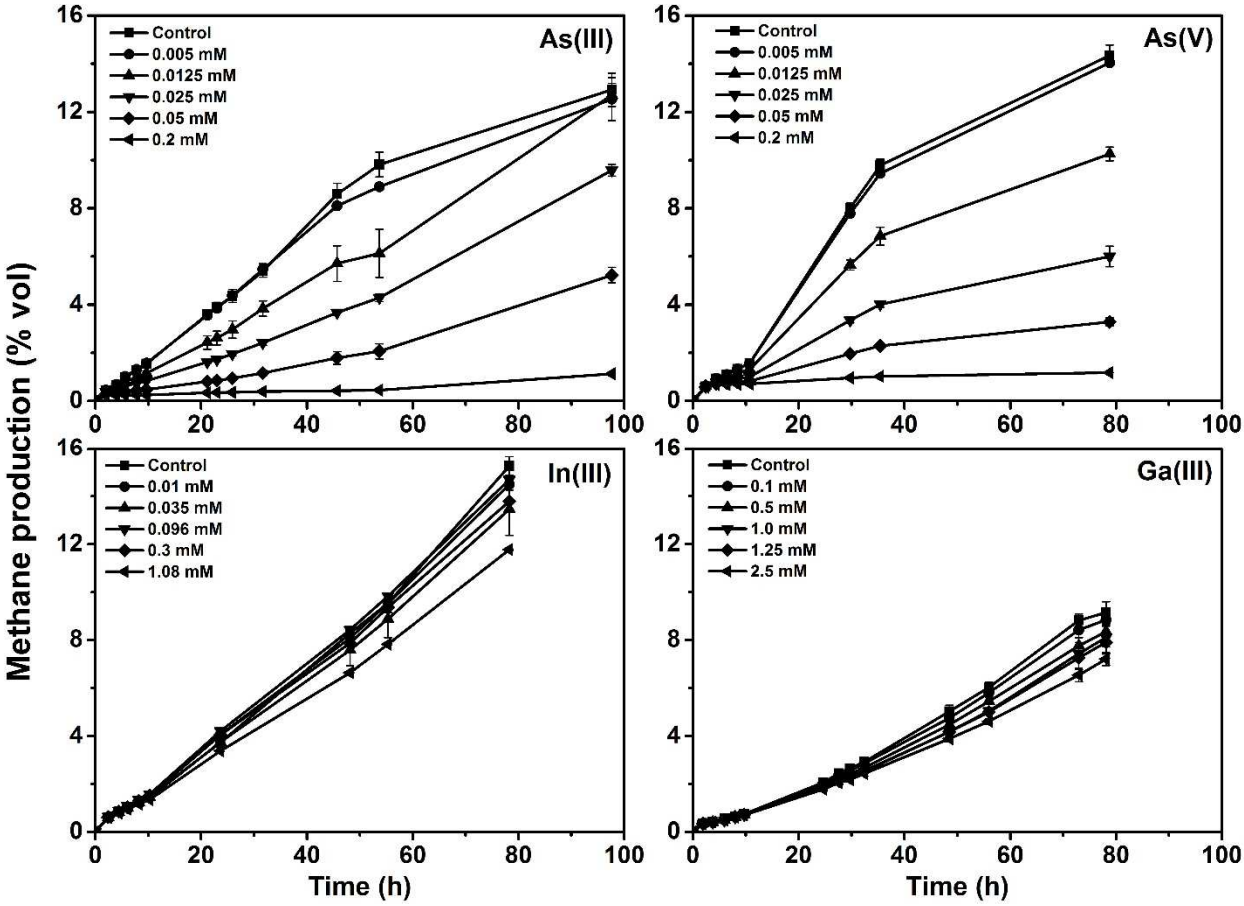

Fig. S4. Methane production from anaerobic granular sludge exposed to different concentrations of As(III), As(V), In(III) and Ga(III) as a function of time.

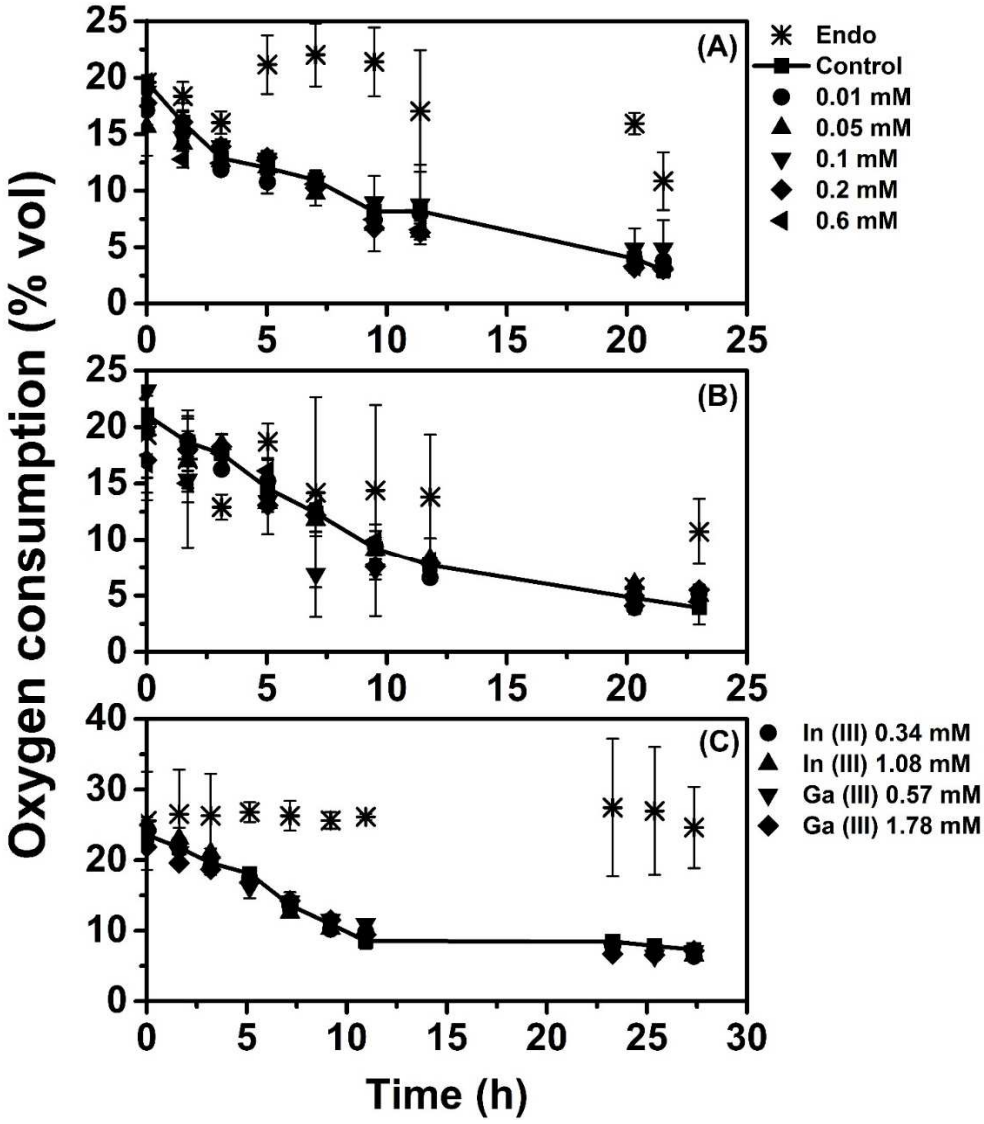

Fig. S5. Oxygen consumption from activated sludge as a function of time in the presence of **(A)** As(III), **(B)** As(V) and **(C)** In(III)/Ga(III). The control was not spiked with metal ions. The endogenic control had no electron donor as substrate.

APPENDIX C. Supplementary data for CHAPTER 6

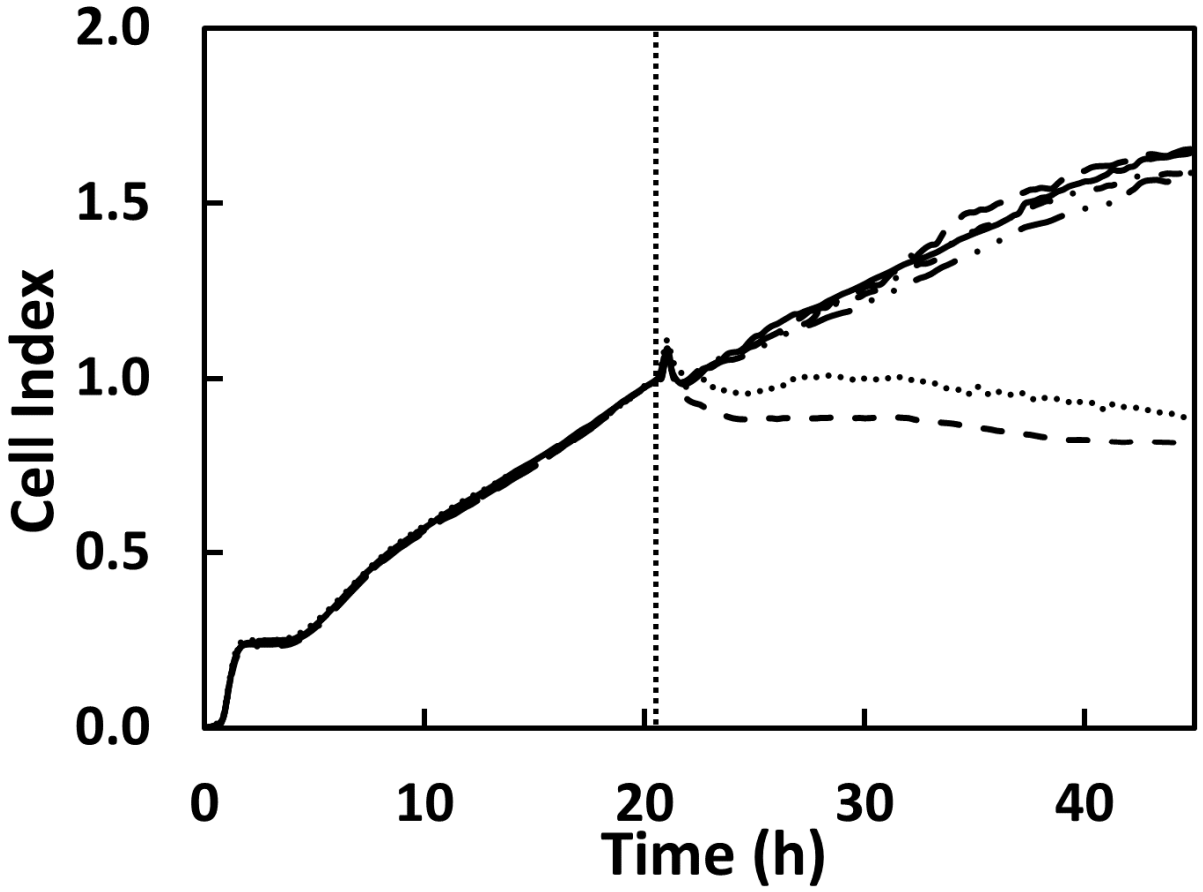

Fig. S6. Dynamic monitoring cytotoxicity response of human bronchial epithelial cells (16HBE14o-) exposed to colloidal silica nanoparticles (c-SiO_2 NPs) at different concentrations (mg/L): 0 (——), 5 (— • • —), 25 (— —), 50 (— • —), 250 (- - -) and 500 (••••).

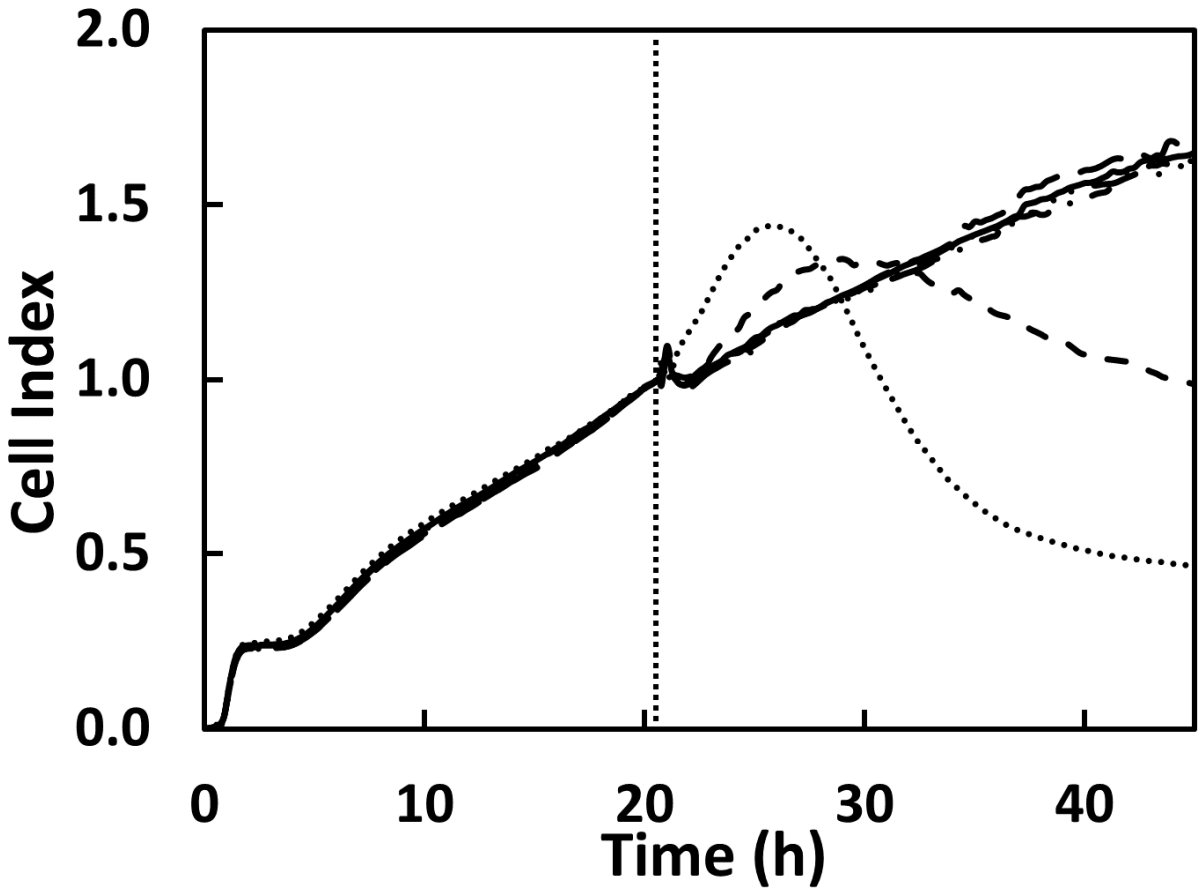

Fig. S7. Dynamic monitoring cytotoxicity response of human bronchial epithelial cells (16HBE14o-) exposed to fumed silica nanoparticles (f-SiO_2 NPs) at different concentrations (mg/L): 0 (──), 5 (─ • • ─), 25 (─ ─), 50 (─ • ─), 250 (- - -) and 500 (••••).

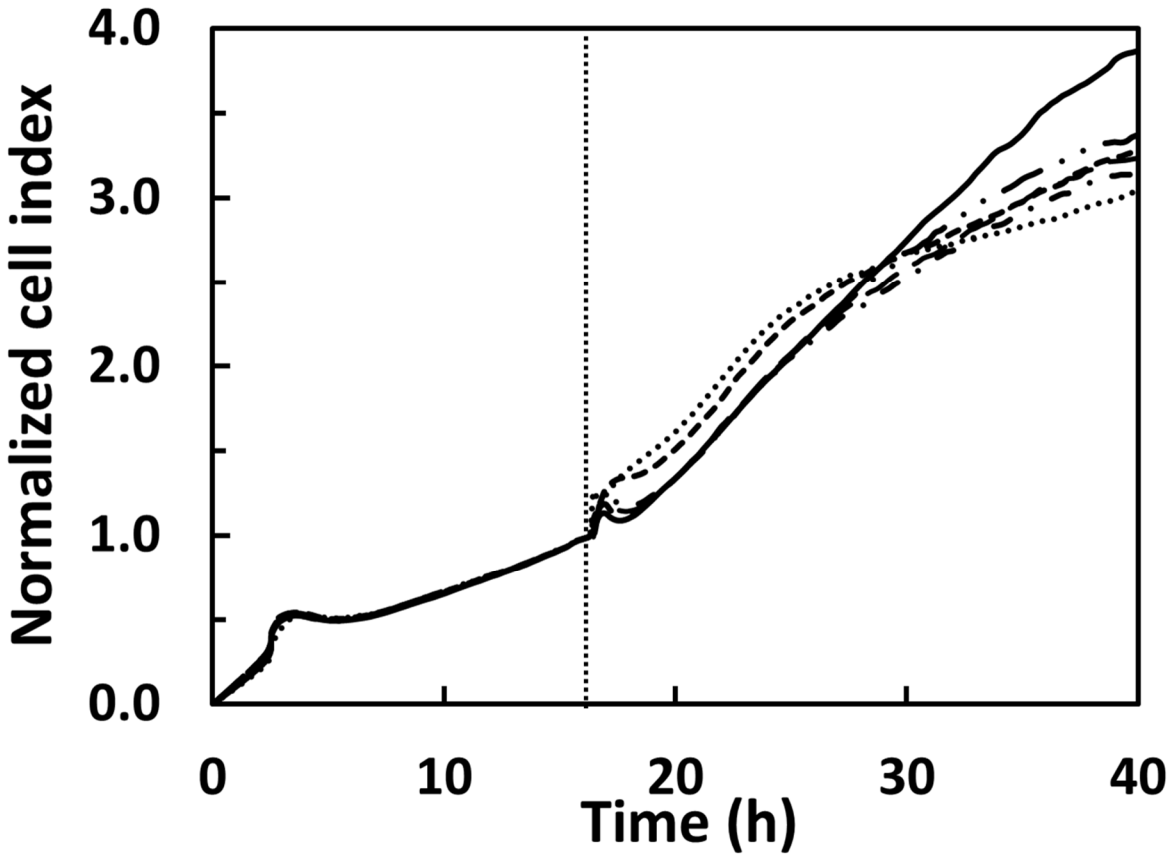

Fig. S8. Dynamic monitoring cytotoxicity response of human bronchial epithelial cells (16HBE14o-) exposed to cerium oxide nanoparticles (CeO_2 NPs) at different concentrations (mg/L): 0 (──), 12.5 (─ • • ─), 62.5 (─ ─), 125 (─ • ─), 625 (- - -) and 1250 (••••).

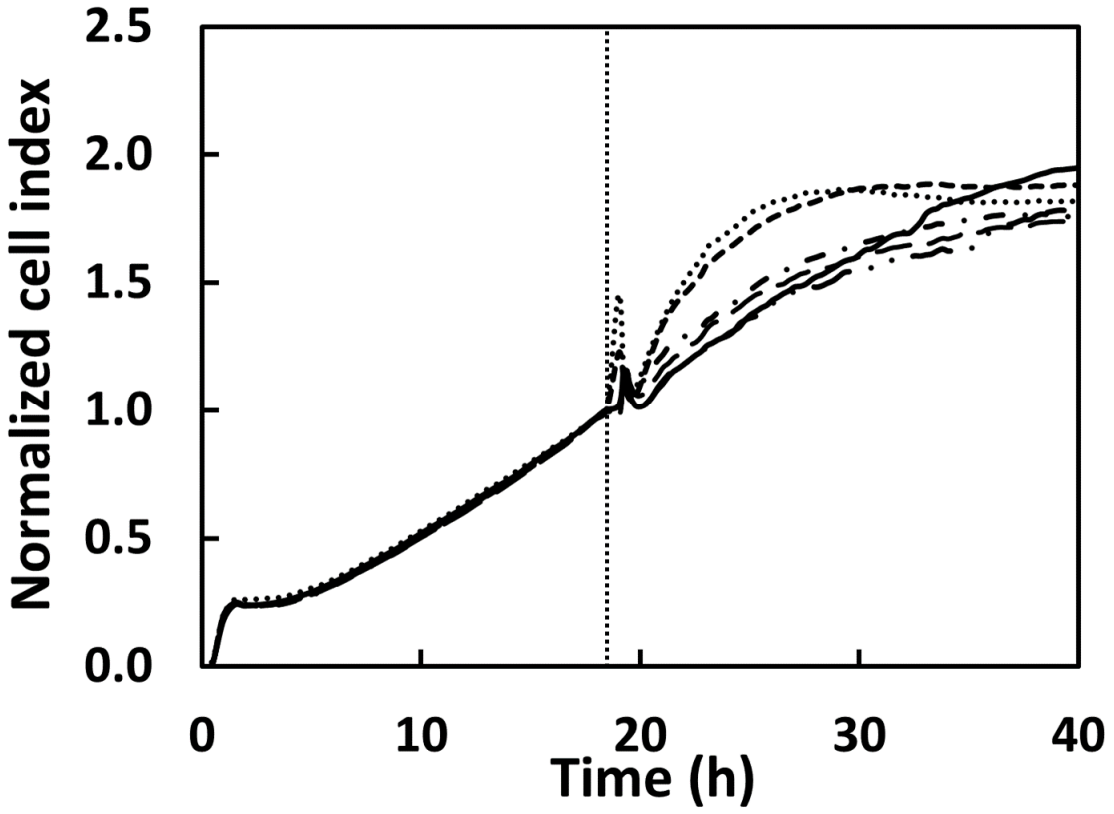

Fig. S9. Dynamic monitoring cytotoxicity response of human bronchial epithelial cells (16HBE14o-) exposed to aluminum oxide nanoparticles (Al_2O_3 NPs) at different concentrations (mg/L): 0 (──), 12.5 (─ • • ─), 62.5 (─ ─), 125 (─ • ─), 625 (- - -) and 1250 (••••).

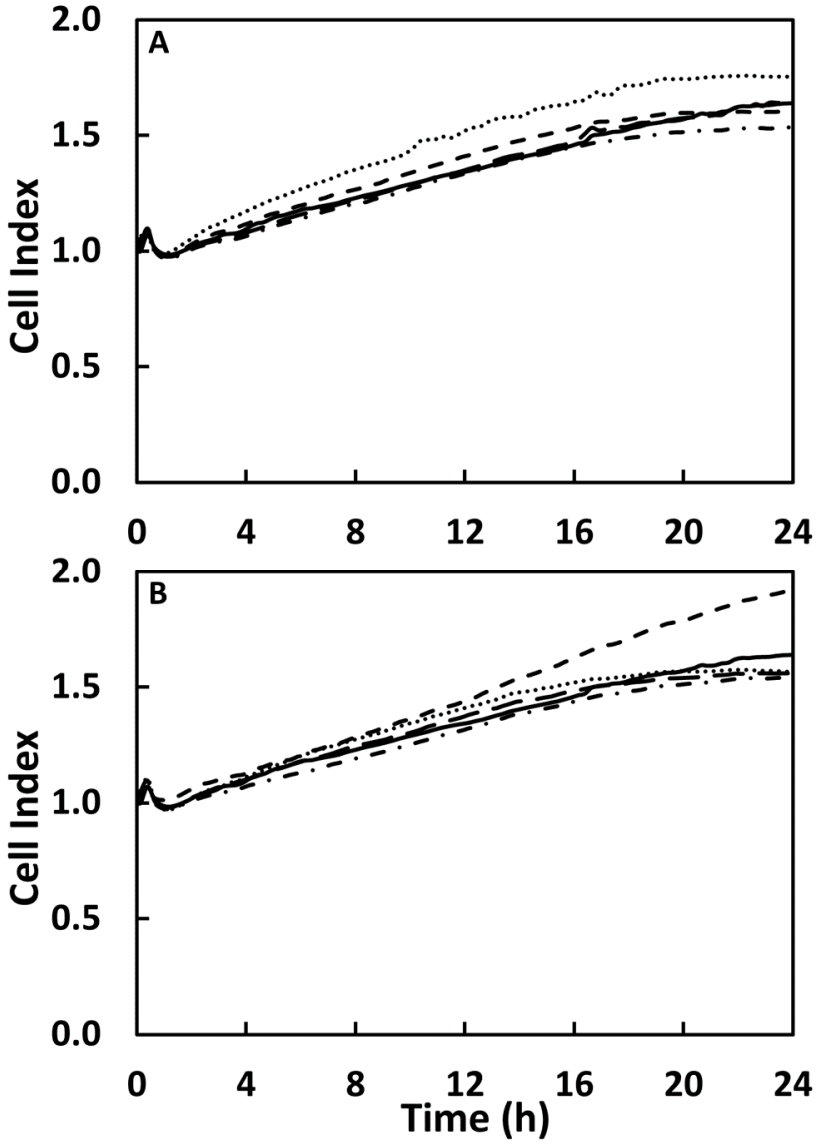

Fig. S10. Dynamic cytotoxicity response of human bronchial epithelial cells (16HBE14o-) exposed to soluble species in c-SiO_2 and f-SiO_2 slurries. (A): slurry supernatant corresponding to c-SiO_2 NP concentrations (mg/L): 0 (——), 25 (— —), 50 (— • —), 250 (- - -) and 500 (••••). (B): slurry supernatant corresponding to f-SiO_2 NP (mg/L): 0 (——), 25 (— —), 50 (— • —), 250 (- - -) and 500 (••••). The samples were prepared by the following steps: first the slurries were centrifuged at 13,300 g for 10 min, the supernatant was then filtered through 25 nm membrane filters, the filtrates were collected and used for cytotoxicity tests using RTCA system.

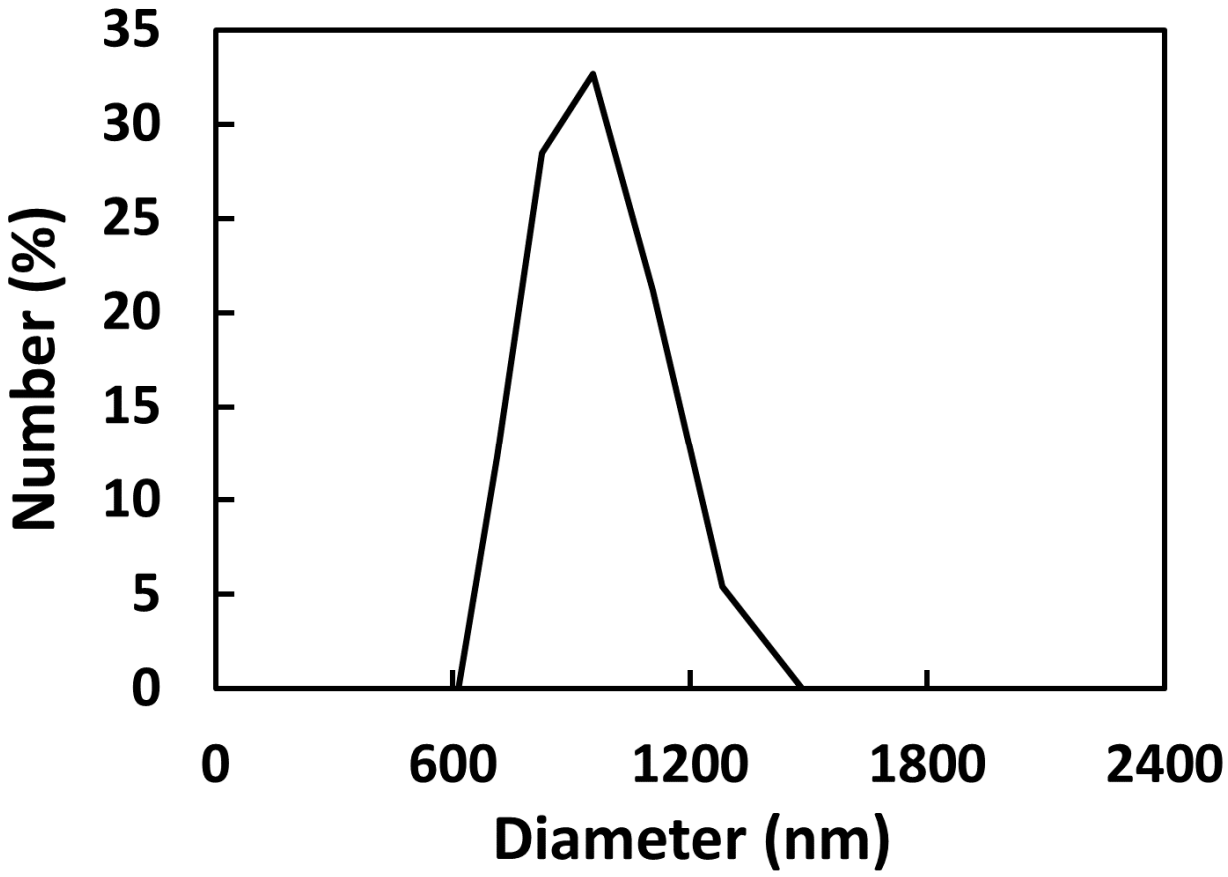

Fig. S11. Particle size distribution for CeO_2 NPs in MEM. Particle size is measured by DLS.

References

[1] S.J. Klaine, P.J.J. Alvarez, G.E. Batley, T.F. Fernandes, R.D. Handy, D.Y. Lyon, S. Mahendra, M.J. McLaughlin, J.R. Lead, Nanomaterials in the environment: Behavior, fate, bioavailability, and effects, Environ Toxicol Chem 27 (2008) 1825-1851.

[2] E. Navarro, A. Baun, R. Behra, N.B. Hartmann, J. Filser, A.J. Miao, A. Quigg, P.H. Santschi, L. Sigg, Environmental behavior and ecotoxicity of engineered nanoparticles to algae, plants, and fungi, Ecotoxicology 17 (2008) 372-386.

[3] A. Gajewicz, B. Rasulev, T.C. Dinadayalane, P. Urbaszek, T. Puzyn, D. Leszczynska, J. Leszczynski, Advancing risk assessment of engineered nanomaterials: Application of computational approaches, Adv Drug Deliver Rev 64 (2012) 1663-1693.

[4] A. Lopez-Serrano, R.M. Olivas, J.S. Landaluze, C. Camara, Nanoparticles: a global vision. Characterization, separation, and quantification methods. Potential environmental and health impact, Anal Methods-Uk 6 (2014) 38-56.

[5] P.A. Holden, F. Klaessig, R.F. Turco, J.H. Priester, C.M. Rico, H. Avila-Arias, M. Mortimer, K. Pacpaco, J.L. Gardea-Torresdey, Evaluation of Exposure Concentrations Used in Assessing Manufactured Nanomaterial Environmental Hazards: Are They Relevant?, Environ Sci Technol 48 (2014) 10541-10551.

[6] A.A. Keller, A. Lazareva, Predicted Releases of Engineered Nanomaterials: From Global to Regional to Local, Environ Sci Tech Let 1 (2014) 65-70.

[7] F. Gomez-Rivera, J.A. Field, D. Brown, R. Sierra-Alvarez, Fate of cerium dioxide (CeO_2) nanoparticles in municipal wastewater during activated sludge treatment, Bioresource Technol 108 (2012) 300-304.

[8] P. Westerhoff, G.X. Song, K. Hristovski, M.A. Kiser, Occurrence and removal of titanium at full scale wastewater treatment plants: implications for TiO_2 nanomaterials, J Environ Monitor 13 (2011) 1195-1203.

[9] D.A. Ladner, M. Steele, A. Weir, K. Hristovski, P. Westerhoff, Functionalized nanoparticle interactions with polymeric membranes, J Hazard Mater 211 (2012) 288-295.

[10] M. Inyang, B. Gao, L. Wu, Y. Yao, M. Zhang, L. Liu, Filtration of engineered nanoparticles in carbon-based fixed bed columns, Chem Eng J 220 (2013) 221-227.

[11] I.G. Godinez, C.J.G. Darnault, Aggregation and transport of nano-TiO_2 in saturated porous media: Effects of pH, surfactants and flow velocity, Water Res 45 (2011) 839-851.

[12] H.F. Lecoanet, J.Y. Bottero, M.R. Wiesner, Laboratory assessment of the mobility of nanomaterials in porous media, Environ Sci Technol 38 (2004) 5164-5169.

[13] J. Rottman, L.C. Platt, R. Sierra-Alvarez, F. Shadman, Removal of TiO_2 nanoparticles by porous media: Effect of filtration media and water chemistry, Chem Eng J 217 (2013) 212-220.

[14] K.L. Garner, A.A. Keller, Emerging patterns for engineered nanomaterials in the environment: a review of fate and toxicity studies, J Nanopart Res 16 (2014).

[15] M. Wang, B. Gao, D.S. Tang, Review of key factors controlling engineered nanoparticle transport in porous media, J Hazard Mater 318 (2016) 233-246.

[16] B.T.A. Muyssen, K.A.C. De Schamphelaere, C.R. Janssen, Mechanisms of chronic waterborne Zn toxicity in Daphnia magna, Aquat Toxicol 77 (2006) 393-401.

[17] T. Xia, M. Kovochich, M. Liong, L. Madler, B. Gilbert, H.B. Shi, J.I. Yeh, J.I. Zink, A.E. Nel, Comparison of the mechanism of toxicity of zinc oxide and cerium oxide nanoparticles based on dissolution and oxidative stress properties, ACS Nano 2 (2008) 2121-2134.

[18] T.J. Baker, C.R. Tyler, T.S. Galloway, Impacts of metal and metal oxide nanoparticles on marine organisms, Environ Pollut 186 (2014) 257-271.

[19] S.J. Soenen, P. Rivera-Gil, J.M. Montenegro, W.J. Parak, S.C. De Smedt, K. Braeckmans, Cellular toxicity of inorganic nanoparticles: Common aspects and guidelines for improved nanotoxicity evaluation, Nano Today 6 (2011) 446-465.

[20] A. Elsaesser, C.V. Howard, Toxicology of nanoparticles, Adv Drug Deliver Rev 64 (2012) 129-137.

[21] A. Nel, T. Xia, L. Madler, N. Li, Toxic potential of materials at the nanolevel, Science 311 (2006) 622-627.

[22] I. Passagne, M. Morille, M. Rousset, I. Pujalte, B. L'Azou, Implication of oxidative stress in size-dependent toxicity of silica nanoparticles in kidney cells, Toxicology 299 (2012) 112-124.

[23] A.A. Shvedova, A. Pietroiusti, B. Fadeel, V.E. Kagan, Mechanisms of carbon nanotube-induced toxicity: Focus on oxidative stress, Toxicol Appl Pharm 261 (2012) 121-133.

[24] N. Gou, A. Onnis-Hayden, A.Z. Gu, Mechanistic Toxicity Assessment of Nanomaterials by Whole-Cell-Array Stress Genes Expression Analysis, Environ Sci Technol 44 (2010) 5964-5970.

[25] A.O. Choi, S.J. Cho, J. Desbarats, J. Lovric, D. Maysinger, Quantum dot-induced cell death involves Fas upregulation and lipid peroxidation in human neuroblastoma cells, Journal of Nanobiotechnology 5 (2007) 1-Article No.: 1.

[26] A. Manke, L.Y. Wang, Y. Rojanasakul, Mechanisms of Nanoparticle-Induced Oxidative Stress and Toxicity, Biomed Res Int (2013).

[27] G. Oberdorster, V. Stone, K. Donaldson, Toxicology of nanoparticles: A historical perspective, Nanotoxicology 1 (2007) 2-25.

[28] B. Nowack, T.D. Bucheli, Occurrence, behavior and effects of nanoparticles in the environment, Environ Pollut 150 (2007) 5-22.

[29] A. Seaton, L. Tran, R. Aitken, K. Donaldson, Nanoparticles, human health hazard and regulation, J R Soc Interface 7 (2010) S119-S129.

[30] C. Buzea, I.I. Pacheco, K. Robbie, Nanomaterials and nanoparticles: Sources and toxicity, Biointerphases 2 (2007) Mr17-Mr71.

[31] M. Crosera, M. Bovenzi, G. Maina, G. Adami, C. Zanette, C. Florio, F.F. Larese, Nanoparticle dermal absorption and toxicity: a review of the literature, Int Arch Occ Env Hea 82 (2009) 1043-1055.

[32] I. Vurgaftman, J.R. Meyer, L.R. Ram-Mohan, Band parameters for III-V compound semiconductors and their alloys, J Appl Phys 89 (2001) 5815-5875.

[33] K.A. Dick, P. Caroff, J. Bolinsson, M.E. Messing, J. Johansson, K. Deppert, L.R. Wallenberg, L. Samuelson, Control of III-V nanowire crystal structure by growth parameter tuning, Semicond Sci Tech 25 (2010).

[34] M. Yamaguchi, K. Nishimura, T. Sasaki, H. Suzuki, K. Arafune, N. Kojima, Y. Ohsita, Y. Okada, A. Yamamoto, T. Takamoto, K. Araki, Novel materials for high-efficiency III-V multi-junction solar cells, Sol Energy 82 (2008) 173-180.

[35] H.J. Joyce, Q. Gao, H.H. Tan, C. Jagadish, Y. Kim, J. Zou, L.M. Smith, H.E. Jackson, J.M. Yarrison-Rice, P. Parkinson, M.B. Johnston, III-V semiconductor nanowires for optoelectronic device applications, Prog. Quantum Electron. 35 (2011) 23-75.

[36] S.A. Dayeh, C. Soci, X.Y. Bao, D.L. Wang, Advances in the synthesis of InAs and GaAs nanowires for electronic applications, Nano Today 4 (2009) 347-358.

[37] A. Tanaka, Toxicity of indium arsenide, gallium arsenide, and aluminium gallium arsenide, Toxicol Appl Pharm 198 (2004) 405-411.

[38] M. Ohring, Reliability and failure of electronic materials and devices, Physics and Technology of Thin Films (2004) 171-179.

[39] A.N. Lovik, E. Restrepo, D.B. Muller, The Global Anthropogenic Gallium System: Determinants of Demand, Supply and Efficiency Improvements, Environmental Science & Technology 49 (2015) 5704-5712.

[40] S.J.O. White, H.F. Hemond, The anthrobiogeochemical cycle of indium: a review of the natural and anthropogenic cycling of indium in the environment, Crit Rev Env Sci Tec 42 (2012) 155-186.

[41] USGS, Mineral Commodity Summaries, U.S. Geological Survey (2015), 196 p., http://dx.doi.org/10.3133/70140094.

[42] USDOE, Critical Materials Strategy, U.S. Department of Energy (2011).

[43] J.R. Shaw, S.P. Glaholt, N.S. Greenberg, R. Sierra-Alvarez, C.L. Folt, Acute toxicity of arsenic to Daphnia pulex: Influence of organic functional groups and oxidation state, Environ Toxicol Chem 26 (2007) 1532-1537.

[44] V.K. Sharma, M. Sohn, Aquatic arsenic: Toxicity, speciation, transformations, and remediation, Environ Int 35 (2009) 743-759.

[45] R. Sierra-Alvarez, I. Cortinas, U. Yenal, J.A. Field, Methanogenic inhibition by arsenic compounds, Appl Environ Microb 70 (2004) 5688-5691.

[46] H.V. Aposhian, M.M. Aposhian, Arsenic toxicology: Five questions, Chem Res Toxicol 19 (2006) 1-15.

[47] B.P. Rosen, M.J. Tamas, Arsenic Transport in Prokaryotes and Eukaryotic Microbes, in: T.P. Jahn, G.P. Bienert (Eds.) Mips and Their Role in the Exchange of Metalloids 2010, pp. 47-56.

[48] H.W. Chen, Exposure and health risk of gallium, indium, and arsenic from semiconductor manufacturing industry workers, Bull. Environ. Contam. Toxicol. 78 (2007) 5-9.

[49] M. Nakano, K. Omae, K. Uchida, T. Michikawa, N. Yoshioka, M. Hirata, A. Tanaka, Five-year cohort study emphysematous progression of indium-exposed workers, Chest 146 (2014) 1166-1175.

[50] K. Omae, M. Nakano, A. Tanaka, M. Hirata, T. Hamaguchi, T. Chonan, Indium lung-case reports and epidemiology, Int Arch of Occup Environ Health 84 (2011) 471-477.

[51] P. Hoet, E. De Graef, B. Swennen, T. Seminck, Y. Yakoub, G. Deumer, V. Haufroid, D. Lison, Occupational exposure to indium: what does biomonitoring tell us?, Toxicol. Lett. 213 (2012) 122-128.

[52] C.I. Olivares, J.A. Field, M. Simonich, R.L. Tanguay, R. Sierra-Alvarez, Arsenic (III, V), indium (III), and gallium (III) toxicity to zebrafish embryos using a high-throughput multi-endpoint in vivo developmental and behavioral assay, Chemosphere 148 (2016) 361-368.

[53] J.L. Zurita, A. Jos, A. del Peso, M. Salguero, A.M. Camean, M. Lopez-Artiguez, G. Repetto, Toxicological assessment of indium nitrate on aquatic organisms and investigation of the effects on the PLHC-1 fish cell line, Sci Total Environ 387 (2007) 155-165.

[54] W. Jiang, S.J. Lin, C.H. Chang, Z.X. Ji, B.B. Sun, X. Wang, R.B. Li, N. Pon, T. Xia, A.E. Nel, Implications of the Differential Toxicological Effects of III-V Ionic and Particulate Materials for Hazard Assessment of Semiconductor Slurries, ACS Nano 9 (2015) 12011-12025.

[55] S.A. Wood, I.M. Samson, The aqueous geochemistry of gallium, germanium, indium and scandium, Ore Geol Rev 28 (2006) 57-102.

[56] R.A.P. Thomas, A.J. Beswick, G. Basnakova, R. Moller, L.E. Macaskie, Growth of naturally occurring microbial isolates in metal-citrate medium and bioremediation of metal-citrate wastes, J Chem Technol Biot 75 (2000) 187-195.

[57] A. Jindal, S. Hegde, S.V. Babu, Chemical mechanical polishing of dielectric films using mixed abrasive slurries, J Electrochem Soc 150 (2003) G314-G318.

[58] E. Matijevic, S.V. Babu, Colloid aspects of chemical-mechanical planarization, J Colloid Interf Sci 320 (2008) 219-237.

[59] M. Krishnan, J.W. Nalaskowski, L.M. Cook, Chemical Mechanical Planarization: Slurry Chemistry, Materials, and Mechanisms, Chem Rev 110 (2010) 178-204.

[60] D. Speed, P. Westerhoff, R. Sierra-Alvarez, R. Draper, P. Pantano, S. Aravamudhan, K.L. Chen, K. Hristovski, P. Herckes, X.Y. Bi, Y. Yang, C. Zeng, L. Otero-Gonzalez, C. Mikoryak, B.A. Wilson, K. Kosaraju, M. Tarannum, S. Crawford, P. Yi, X.T. Liu, S.V. Babu, M. Moinpour, J. Ranville, M. Montano, C. Corredor, J. Posner, F. Shadman, Physical, chemical, and in vitro toxicological characterization of nanoparticles in chemical mechanical planarization suspensions used in the semiconductor industry: towards environmental health and safety assessments, Environ Sci-Nano 2 (2015) 227-244.

[61] P.B. Zantye, A. Kumar, A.K. Sikder, Chemical mechanical planarization for microelectronics applications, Mat Sci Eng R 45 (2004) 89-220.

[62] X.D. Feng, D.C. Sayle, Z.L. Wang, M.S. Paras, B. Santora, A.C. Sutorik, T.X.T. Sayle, Y. Yang, Y. Ding, X.D. Wang, Y.S. Her, Converting ceria polyhedral nanoparticles into single-crystal nanospheres, Science 312 (2006) 1504-1508.

[63] R. Manivannan, S. Ramanathan, The effect of hydrogen peroxide on polishing removal rate in CMP with various abrasives, Appl Surf Sci 255 (2009) 3764-3768.

[64] Y. Liu, M. Tourbin, S. Lachaize, P. Guiraud, Nanoparticles in wastewaters: Hazards, fate and remediation, Powder Technol 255 (2014) 149-156.

[65] C.T. Wang, W.L. Chou, L.S. Chen, S.Y. Chang, Silica particles settling characteristics and removal performances of oxide chemical mechanical polishing wastewater treated by electrocoagulation technology, J Hazard Mater 161 (2009) 344-350.

[66] U.S. EPA, Effluent Guidelines and Standards. Part 469. Electrical and electronic components point source category. Effluent limitations representing the degreebof effluent reduction attainable by the application of the best practicable control technology currently available (BPT). Title 40 e-C.F.R. x 469.24, (2015).

[67] R.H. Li, Q. Li, S. Gao, J.K. Shang, Exceptional arsenic adsorption performance of hydrous cerium oxide nanoparticles: Part A. Adsorption capacity and mechanism, Chem Eng J 185 (2012) 127-135.

[68] K. Hristovski, A. Baumgardner, P. Westerhoff, Selecting metal oxide nanomaterials for arsenic removal in fixed bed columns: From nanopowders to aggregated nanoparticle media, J Hazard Mater 147 (2007) 265-274.

[69] J. Hu, D.M. Wang, B.E. Forthaus, J.M. Wang, Quantifying the effect of nanoparticles on As(V) ecotoxicity exemplified by nano-Fe2O3 (magnetic) and nano-Al2O3, Environ Toxicol Chem 31 (2012) 2870-2876.

[70] L.Y. Wang, K.L. Zhang, Z.T. Song, S.L. Feng, Ceria concentration effect on chemical mechanical polishing of optical glass, Appl Surf Sci 253 (2007) 4951-4954.

[71] D.S. Lim, J.W. Ahn, H.S. Park, J.H. Shin, The effect of CeO_2 abrasive size on dishing and step height reduction of silicon oxide film in STI-CMP, Surf Coat Tech 200 (2005) 1751-1754.

[72] T. Gopal, J.B. Talbot, Effects of CMP slurry chemistry on the zeta potential of alumina abrasives, J Electrochem Soc 153 (2006) G622-G625.

[73] H. Lee, S. Joo, H. Jeong, Mechanical effect of colloidal silica in copper chemical mechanical planarization, J Mater Process Tech 209 (2009) 6134-6139.

[74] N.L. Flaherty, A. Chandrasekaran, M.D.S. Pena, G.A. Roth, S.A. Brenner, T.J. Begley, J.A. Melendez, Comparative analysis of redox and inflammatory properties of pristine nanomaterials and commonly used semiconductor manufacturing nano-abrasives, Toxicol Lett 239 (2015) 205-215.

[75] H. Yang, C. Liu, D.F. Yang, H.S. Zhang, Z.G. Xi, Comparative study of cytotoxicity, oxidative stress and genotoxicity induced by four typical nanomaterials: the role of particle size, shape and composition, J Appl Toxicol 29 (2009) 69-78.

[76] M. Bhuvaneshwari, S. Bairoliya, A. Parashar, N. Chandrasekaran, A. Mukherjee, Differential toxicity of Al2O3 particles on Gram-positive and Gram-negative sediment bacterial isolates from freshwater, Environ Sci Pollut R 23 (2016) 12095-12106.

[77] C. Fajardo, M.L. Sacca, G. Costa, M. Nande, M. Martin, Impact of Ag and Al2O3 nanoparticles on soil organisms: In vitro and soil experiments, Sci Total Environ 473 (2014) 254-261.

[78] A. Bour, F. Mouchet, S. Cadarsi, J. Silvestre, E. Chauvet, J.M. Bonzom, C. Pagnout, H. Clivot, L. Gauthier, E. Pinelli, Impact of CeO2 nanoparticles on the functions of freshwater ecosystems: a microcosm study, Environ Sci-Nano 3 (2016) 830-838.

[79] T. Yu, A. Malugin, H. Ghandehari, Impact of Silica Nanoparticle Design on Cellular Toxicity and Hemolytic Activity, Acs Nano 5 (2011) 5717-5728.

[80] W.S. Lin, Y.W. Huang, X.D. Zhou, Y.F. Ma, In vitro toxicity of silica nanoparticles in human lung cancer cells, Toxicology and Applied Pharmacology 217 (2006) 252-259.

[81] B.M. Angel, P. Vallotton, S.C. Apte, On the mechanism of nanoparticulate CeO2 toxicity to freshwater algae, Aquat Toxicol 168 (2015) 90-97.

[82] G. Karunakaran, R. Suriyaprabha, V. Rajendran, N. Kannan, Toxicity evaluation based on particle size, contact angle and zeta potential of SiO_2 and Al_2O_3 on the growth of green algae, Adv Nano Res 3 (2015) 243-255.

[83] J. Mui, J. Ngo, B. Kim, Aggregation and Colloidal Stability of Commercially Available Al_2O_3 nanoparticles in aqueous environments, Nanomaterials-Basel 6 (2016).

[84] C. Fruijtier-Polloth, The toxicological mode of action and the safety of synthetic amorphous silica-A nanostructured material, Toxicology 294 (2012) 61-79.

[85] U.S. EPA, Strategic Diagnostics, Inc. Microtox Rapid Toxicity Testing System Technology Verification Report and Statement., (2003).

[86] K.J. Howe, D.W. Hand, J.C. Crittenden, R.R. Trussell, G. Tchobanoglous, Principles of Water Treatment, Wiley2012.

[87] E. Binaeian, H. Attar, A.A. Safekordi, R. Saber, M.J. Chaichi, Study on toxicity of seven manufactured nano particles and two phenolic compounds to bacteria *Vibrio fischeri* using homemade luminometer, Asian J Chem 24 (2012) 5211-5218.

[88] I. Velzeboer, A.J. Hendriks, A.M.J. Ragas, D. Van de Meent, Aquatic ecotoxicity tests of some nanomaterials, Environ Toxicol Chem 27 (2008) 1942-1947.

[89] R. Doshi, W. Braida, C. Christodoulatos, M. Wazne, G. O'Connor, Nano-aluminum: Transport through sand columns and environmental effects on plants and soil communities, Environ Res 106 (2008) 296-303.

[90] H. Basu, R.K. Singhal, M.V. Pimple, A. Kumar, A.V.R. Reddy, Association and migration of uranium and thorium with silica colloidal particles in saturated subsurface zone, J Radioanal Nucl Ch 303 (2015) 2283-2290.

[91] A.L. Noell, J.L. Thompson, M.Y. Corapcioglu, I.R. Triay, The role of silica colloids on facilitated cesium transport through glass bead columns and modeling, J Contam Hydrol 31 (1998) 23-56.

[92] H.P. Jarvie, H. Al-Obaidi, S.M. King, M.J. Bowes, M.J. Lawrence, A.F. Drake, M.A. Green, P.J. Dobson, Fate of Silica Nanoparticles in Simulated Primary Wastewater Treatment, Environ Sci Technol 43 (2009) 8622-8628.

[93] L. Otero-Gonzalez, J.A. Field, I.A.C. Calderon, C.A. Aspinwall, F. Shadman, C. Zeng, R. Sierra-Alvarez, Fate of fluorescent core-shell silica nanoparticles during simulated secondary wastewater treatment, Water Res 77 (2015) 170-178.

[94] Y.V. Li, L.M. Cathles, Retention of silica nanoparticles on calcium carbonate sands immersed in electrolyte solutions, J Colloid Interf Sci 436 (2014) 1-8.

[95] E. Vitorge, S. Szenknect, J.M.F. Martins, J.P. Gaudet, Size- and concentration-dependent deposition of fluorescent silica colloids in saturated sand columns: transport experiments and modeling, Environ Sci-Proc Imp 15 (2013) 1590-1600.

[96] C. Wang, A.D. Bobba, R. Attinti, C.Y. Shen, V. Lazouskaya, L.P. Wang, Y. Jin, Retention and transport of silica nanoparticles in saturated porous media: effect of concentration and particle size, Environ Sci Technol 46 (2012) 7151-7158.

[97] C. Morlay, J.P. Joly, Contribution to the textural characterisation of Filtrasorb 400 and other commercial activated carbons commonly used for water treatment, J Porous Mat 17 (2010) 535-543.

[98] H.H. Salih, C.L. Patterson, G.A. Sorial, R. Sinha, R. Krishnan, The fate and transport of the SiO2 nanoparticles in a granular activated carbon bed and their impact on the removal of VOCs, J Hazard Mater 193 (2011) 95-101.

[99] J.K. Jiang, G. Oberdorster, P. Biswas, Characterization of size, surface charge, and agglomeration state of nanoparticle dispersions for toxicological studies, J Nanopart Res 11 (2009) 77-89.

[100] A.M. El Badawy, T.P. Luxton, R.G. Silva, K.G. Scheckel, M.T. Suidan, T.M. Tolaymat, Impact of environmental conditions (pH, ionic strength, and electrolyte type) on the surface charge and aggregation of silver nanoparticles suspensions, Environ Sci Technol 44 (2010) 1260-1266.

[101] S.W. Bian, I.A. Mudunkotuwa, T. Rupasinghe, V.H. Grassian, Aggregation and Dissolution of 4 nm ZnO Nanoparticles in aqueous environments: Influence of pH, ionic strength, size, and adsorption of humic acid, Langmuir 27 (2011) 6059-6068.

[102] R.W. Miles, K.M. Hynes, I. Forbes, Photovoltaic solar cells: An overview of state-of-the-art cell development and environmental issues, Prog Cryst Growth Ch 51 (2005) 1-42.

[103] T. Butcher, T. Brown, Critical Metals Handbook, Wiley2014.

[104] S.P.M. Ventura, C.S. Marques, A.A. Rosatella, C.A.M. Afonso, F. Goncalves, J.A.P. Coutinho, Toxicity assessment of various ionic liquid families towards *Vibrio fischeri* marine bacteria, Ecotoxicology and Environmental Safety 76 (2012) 162-168.

[105] S. Parvez, C. Venkataraman, S. Mukherji, A review on advantages of implementing luminescence inhibition test (*Vibrio fischeri*) for acute toxicity prediction of chemicals, Environ Int 32 (2006) 265-268.

[106] D.A. Rubinos, V. Calvo, L. Iglesias, M.T. Barral, Acute toxicity of arsenic to *Aliivibrio fischeri* (Microtox® bioassay) as influenced by potential competitive-protective agents, Environ Sci Pollut R 21 (2014) 8631-8644.

[107] X.S. Zhu, L. Zhu, Y.S. Chen, S.Y. Tian, Acute toxicities of six manufactured nanomaterial suspensions to *Daphnia magna,* J. Nanopart. Res. 11 (2009) 67-75.

[108] X.S. Zhu, Y. Chang, Y.S. Chen, Toxicity and bioaccumulation of TiO_2 nanoparticle aggregates in *Daphnia magna*, Chemosphere 78 (2010) 209-215.

[109] V.M. Gamez, R. Sierra-Alvarez, R.J. Waltz, J.A. Field, Anaerobic degradation of citrate under sulfate reducing and methanogenic conditions, Biodegradation 20 (2009) 499-510.

[110] EPA, Aquatic Invertebrate Acute Toxicity Test, Freshwater Daphnids, 1996.

[111] W.H. Fan, J.Q. Ren, X.M. Li, C.Y. Wei, F. Xue, N. Zhang, Bioaccumulation and oxidative stress in Daphnia magna exposed to arsenite and arsenate, Environ. Toxicol. Chem. 34 (2015) 2629-2635.

[112] X.H. Wang, R.J. Qu, A.A. Allam, J. Ajarem, Z.B. Wei, Z.Y. Wang, Impact of carbon nanotubes on the toxicity of inorganic arsenic [As(III) and As(V)] to *Daphnia magna*: The role of certain arsenic species, Environ. Toxicol. Chem. 35 (2016) 1852-1859.

[113] T.H. Le, E.S. Lim, N.H. Hong, S.K. Lee, Y.S. Shim, J.R. Hwang, Y.H. Kim, J. Min, Proteomic analysis in Daphnia magna exposed to As(III), As(V) and Cd heavy metals and their binary mixtures for screening potential biomarkers, Chemosphere 93 (2013) 2341-2348.

[114] Q. He, R.J. Qu, X.H. Wang, Z.B. Wei, P. Sun, Z.Y. Wang, Toxicity of arsenic to *Photobacterium phosphoreum, Daphnia magna*, and *Danio rerio* at different pH Levels, Clean-Soil Air Water 44 (2016) 72-77.

[115] E. Fulladosa, J. Debord, I. Villaescusa, J.C. Bollinger, J.C. Murat, Effect of arsenic compounds on *Vibrio fischeri* light emission and butyrylcholinesterase activity, Environ Chem Lett 5 (2007) 115-119.

[116] A.K. Dunn, *Vibrio fischeri* Metabolism: Symbiosis and Beyond, Adv Microb Physiol 61 (2012) 37-68.

[117] A. Mariscal, M.T. Peinado, M. Carnero-Varo, J. Fernandez-Crehuet, Influence of organic solvents on the sensitivity of a bioluminescence toxicity test with *Vibrio harveyi*, Chemosphere 50 (2003) 349-354.

[118] A.N. Septer, J.L. Bose, A. Lipzen, J. Martin, C. Whistler, E.V. Stabb, Bright luminescence of *Vibrio fischeri* aconitase mutants reveals a connection between citrate and the Gac/Csr regulatory system, Mol Microbiol 95 (2015) 283-296.

[119] L. Rodriguez-Freire, S.E. Moore, R. Sierra-Alvarez, J.A. Field, Adaptation of a methanogenic consortium to arsenite inhibition, Water Air Soil Poll 226 (2015).

[120] F.S. Islam, A.G. Gault, C. Boothman, D.A. Polya, J.M. Charnock, D. Chatterjee, J.R. Lloyd, Role of metal-reducing bacteria in arsenic release from Bengal delta sediments, Nature 430 (2004) 68-71.

[121] S. Fendorf, B.D. Kocar, Biogeochemical processes controlling the fate and transport of arsenic: Implications for South and Southeast Asia, Adv Agron 104 (2009) 137-164.

[122] A.S. Stasinakis, N.S. Thomaidis, A.S. Giannes, T.D. Lekkas, Effect of arsenic and mercury speciation on inhibition of respiration rate in activated sludge systems, Environ Sci Pollut R 10 (2003) 177-182.

[123] B.W. Schmitz, M. Kitajima, M.E. Campillo, C.P. Gerba, I.L. Pepper, Virus Reduction during Advanced Bardenpho and Conventional Wastewater Treatment Processes, Environmental Science & Technology 50 (2016) 9524-9532.

[124] J.L. Yang, H.C. Chen, Effects of gallium on common carp (*Cyprinus carpio*): acute test, serum biochemistry, and erythrocyte morphology, Chemosphere 53 (2003) 877-882.

[125] N. Onikura, A. Nakamura, K. Kishi, Acute toxicity of gallium and effects of salinity on gallium toxicity to brackish and marine organisms, Bull. Environ. Contam. Toxicol. 75 (2005) 356-360.

[126] K.T. Kin, H.S. Tang, S.F. Chan, S. Raghavan, S. Martinez, Treatment of chemical-mechanical planarization wastes by electrocoagulation/electro-Fenton method, Ieee T Semiconduct M 19 (2006) 208-215.

[127] W.H. Kuan, C.Y. Hu, Chemical evidences for the optimal coagulant dosage and pH adjustment of silica removal from chemical mechanical polishing (CMP) wastewater, Colloid Surface A 342 (2009) 1-7.

[128] S.E. Lehman, A.S. Morris, P.S. Mueller, A.K. Salem, V.H. Grassian, S.C. Larsen, Silica nanoparticle-generated ROS as a predictor of cellular toxicity: mechanistic insights and safety by design, Environ Sci-Nano 3 (2016) 56-66.

[129] N.J. Rogers, N.M. Franklin, S.C. Apte, G.E. Batley, B.M. Angel, J.R. Lead, M. Baalousha, Physico-chemical behaviour and algal toxicity of nanoparticulate CeO_2 in freshwater, Environ Chem 7 (2010) 50-60.

[130] A. Thill, O. Zeyons, O. Spalla, F. Chauvat, J. Rose, M. Auffan, A.M. Flank, Cytotoxicity of CeO_2 nanoparticles for *Escherichia coli*. Physico-chemical insight of the cytotoxicity mechanism, Environ Sci Technol 40 (2006) 6151-6156.

[131] L.C.J. Thomassen, A. Aerts, V. Rabolli, D. Lison, L. Gonzalez, M. Kirsch-Volders, D. Napierska, P.H. Hoet, C.E.A. Kirschhock, J.A. Martens, Synthesis and characterization of stable monodisperse silica nanoparticle sols for in vitro cytotoxicity testing, Langmuir 26 (2010) 328-335.

[132] H.F. Zhang, X.A. He, Z.Y. Zhang, P. Zhang, Y.Y. Li, Y.H. Ma, Y.S. Kuang, Y.L. Zhao, Z.F. Chai, Nano-CeO_2 exhibits adverse effects at environmental relevant concentrations, Environ Sci Technol 45 (2011) 3725-3730.

[133] M. Bosi, C. Pelosi, The potential of III-V semiconductors as terrestrial photovoltaic devices, Prog Photovoltaics 15 (2007) 51-68.

[134] K. Torrance, H. Keenan, Management of arsenic-rich waste streams in III-V foundries, Semiconductor Today 4 (2009) 66-68.

[135] X.Y. Bi, P. Westerhoff, Adsorption of III/V ions (In(III), Ga(III) and As(V)) onto SiO_2, CeO_2 and Al_2O_3 nanoparticles used in the semiconductor industry, Environ Sci-Nano 3 (2016) 1014-1026.

[136] Y. Arai, E.J. Elzinga, D.L. Sparks, X-ray absorption spectroscopic investigation of arsenite and arsenate adsorption at the aluminum oxide-water interface, J Colloid Interf Sci 235 (2001) 80-88.

[137] Q.Z. Feng, Z.Y. Zhang, Y.H. Ma, X. He, Y.L. Zhao, Z.F. Chai, Adsorption and desorption characteristics of arsenic onto ceria nanoparticles, Nanoscale Res Lett 7 (2012) 1-8.

[138] L.K. Limbach, P. Wick, P. Manser, R.N. Grass, A. Bruinink, W.J. Stark, Exposure of engineered nanoparticles to human lung epithelial cells: Influence of chemical composition and catalytic activity on oxidative stress, Environ Sci Technol 41 (2007) 4158-4163.

[139] N. Ke, X.B. Wang, X. Xu, Y.A. Abassi, The xCELLigence System for real-time and label-free monitoring of cell viability, Methods Mol Biol 740 (2011) 33-43.

[140] M. Fisichella, H. Dabboue, S. Bhattacharyya, M.L. Saboungi, J.P. Salvetat, T. Hevor, M. Guerin, Mesoporous silica nanoparticles enhance MTT formazan exocytosis in HeLa cells and astrocytes, Toxicol in Vitro 23 (2009) 697-703.

[141] L. Otero-Gonzalez, R. Sierra-Alvarez, S. Boitano, J.A. Field, Application and validation of an impedance-based real time cell analyzer to measure the toxicity of nanoparticles impacting human bronchial epithelial cells, Environ Sci Technol 46 (2012) 10271-10278.

[142] W.Q. Feng, J.J. Guo, H.Y. Huang, B. Xia, H.Y. Liu, J. Li, S.L. Lin, T.Y. Li, J.J. Liu, H. Li, Human normal bronchial epithelial cells: A novel in vitro cell model for toxicity evaluation, Plos One 10 (2015).

[143] B. Forbes, A. Shah, G.P. Martin, A.B. Lansley, The human bronchial epithelial cell line 16HBE14o-as a model system of the airways for studying drug transport, Int J Pharm 257 (2003) 161-167.

[144] C. Ehrhardt, C. Kneuer, M. Laue, U.F. Schaefer, K.J. Kim, C.M. Lehr, 16HBE14o- human bronchial epithelial cell layers express P-glycoprotein, lung resistance-related protein, and caveolin-1, Pharmaceut Res 20 (2003) 545-551.

[145] C.L. Sherwood, R.C. Lantz, S. Boitano, Chronic arsenic exposure in nanomolar concentrations compromises wound response and intercellular signaling in airway epithelial cells, Toxicol Sci 132 (2013) 222-234.

[146] G. Cornelis, B. Ryan, M.J. McLaughlin, J.K. Kirby, D. Beak, D. Chittleborough, Solubility and batch retention of CeO_2 nanoparticles in soils, Environ. Sci. Technol. 45 (2011) 2777-2782.

[147] A.N. Flynn, D.V. Tillu, M.N. Asiedu, J. Hoffman, J. Vagner, T.J. Price, S. Boitano, The Protease-activated Receptor-2-specific Agonists 2-Aminothiazol-4-yl-LIGRL-NH2 and 6-Aminonicotinyl-LIGRL-NH2 stimulate multiple signaling pathways to induce physiological responses in vitro and in vivo, J Biol Chem 286 (2011) 19076-19088.

[148] R. Limame, A. Wouters, B. Pauwels, E. Fransen, M. Peeters, F. Lardon, O. De Wever, P. Pauwels, Comparative analysis of dynamic cell viability, migration and invasion assessments by novel real-time technology and classic endpoint assays, Plos One 7 (2012).

[149] S. Rakers, F. Imse, M. Gebert, Real-time cell analysis: sensitivity of different vertebrate cell cultures to copper sulfate measured by xCELLigence(A (R)), Ecotoxicology 23 (2014) 1582-1591.

[150] M.R. Moniri, A. Young, K. Reinheimer, J. Rayat, L.J. Dai, G.L. Warnock, Dynamic assessment of cell viability, proliferation and migration using real time cell analyzer system (RTCA), Cytotechnology 67 (2015) 379-386.

[151] M.J. Akhtar, M. Ahamed, S. Kumar, H. Siddiqui, G. Patil, M. Ashquin, I. Ahmad, Nanotoxicity of pure silica mediated through oxidant generation rather than glutathione depletion in human lung epithelial cells, Toxicology 276 (2010) 95-102.

[152] H.Y. Zhang, D.R. Dunphy, X.M. Jiang, H. Meng, B.B. Sun, D. Tarn, M. Xue, X. Wang, S.J. Lin, Z.X. Ji, R.B. Li, F.L. Garcia, J. Yang, M.L. Kirk, T. Xia, J.I. Zink, A. Nel, C.J. Brinker, Processing pathway dependence of amorphous silica nanoparticle toxicity: colloidal vs pyrolytic, J Am Chem Soc 134 (2012) 15790-15804.

[153] Z.C. Wei, L.M. Chen, D.M. Thompson, L.D. Montoya, Effect of particle size on in vitro cytotoxicity of titania and alumina nanoparticles, J Exp Nanosci 9 (2014) 625-638.

[154] Y.H. Leung, M.M.N. Yung, A.M.C. Ng, A.P.Y. Ma, S.W.Y. Wong, C.M.N. Chan, Y.H. Ng, A.B. Djurisic, M.Y. Guo, M.T. Wong, F.C.C. Leung, W.K. Chan, K.M.Y. Leung, H.K. Lee, Toxicity of CeO_2 nanoparticles - The effect of nanoparticle properties, J.Photochem. Photobiol., B 145 (2015) 48-59.

[155] S. Hussain, F. Al-Nsour, A.B. Rice, J. Marshburn, B. Yingling, Z.X. Ji, J.I. Zink, N.J. Walker, S. Garantziotis, Cerium dioxide nanoparticles induce apoptosis and autophagy in human peripheral blood monocytes, Acs Nano 6 (2012) 5820-5829.

[156] S.W. Bennett, A.A. Keller, Comparative photoactivity of CeO_2, gamma-Fe_2O_3, TiO_2 and ZnO in various aqueous systems, Appl. Catal., B 102 (2011) 600-607.

[157] L. Rubio, B. Annangi, L. Vila, A. Hernandez, R. Marcos, Antioxidant and anti-genotoxic properties of cerium oxide nanoparticles in a pulmonary-like cell system, Arch. Toxicol. 90 (2016) 269-278.

[158] L.Z. Li, P. Qiu, B.L. Chen, Y.J. Lu, K. Wu, C. Thakur, Q.S. Chang, J.Y. Sun, F. Chen, Reactive oxygen species contribute to arsenic-induced EZH2 phosphorylation in human bronchial epithelial cells and lung cancer cells, Toxicol. Appl. Pharmacol. 276 (2014) 165-170.

[159] C.L. Sherwood, R.C. Lantz, J.L. Burgess, S. Boitano, Arsenic alters ATP-dependent Ca^{2+} signaling in human airway epithelial cell wound response, Toxicol. Sci. 121 (2011) 191-206.

[160] J. Hu, D.M. Wang, J.T. Wang, J.M. Wang, Toxicity of lead on *Ceriodaphnia dubia* in the presence of nano-CeO_2 and nano-TiO_2, Chemosphere 89 (2012) 536-541.

[161] A. Baun, S.N. Sorensen, R.F. Rasmussen, N.B. Hartmann, C.B. Koch, Toxicity and bioaccumulation of xenobiotic organic compounds in the presence of aqueous suspensions of aggregates of nano-C-60, Aquat Toxicol 86 (2008) 379-387.

[162] N.B. Hartmann, F. Von der Kammer, T. Hofmann, M. Baalousha, S. Ottofuelling, A. Baun, Algal testing of titanium dioxide nanoparticles-Testing considerations, inhibitory effects and modification of cadmium bioavailability, Toxicology 269 (2010) 190-197.

[163] A.A. Koelmans, M.T.O. Jonker, G. Cornelissen, T.D. Bucheli, P.C.M. Van Noort, O. Gustafsson, Black carbon: The reverse of its dark side, Chemosphere 63 (2006) 365-377.

[164] X.Y. Cui, F. Jia, Y.X. Chen, J. Gan, Influence of single-walled carbon nanotubes on microbial availability of phenanthrene in sediment, Ecotoxicology 20 (2011) 1277-1285.

[165] E.J. Petersen, R.A. Pinto, P.F. Landrum, W.J. Weber, Influence of carbon nanotubes on pyrene bioaccumulation from contaminated soils by earthworms, Environ Sci Technol 43 (2009) 4181-4187.